

# UC Santa Barbara

## UC Santa Barbara Electronic Theses and Dissertations

### Title

Genetic Determinants of Retinal Cell Development

### Permalink

<https://escholarship.org/uc/item/5sw538k6>

### Author

Kautzman, Amanda Grace

### Publication Date

2017

Peer reviewed|Thesis/dissertation

UNIVERSITY OF CALIFORNIA

Santa Barbara

Genetic Determinants of Retinal Cell Development

A dissertation submitted in partial satisfaction of the  
requirements for the degree Doctor of Philosophy  
in Psychological and Brain Sciences

by

Amanda Grace Kautzman

Committee in charge:

Professor Benjamin E. Reese, Chair

Professor Skirmantas Janušonis

Professor Tod E. Kippin

Professor Carol A. Vandenberg

September 2017

The dissertation of Amanda Grace Kautzman is approved.

---

Skirmantas Janušonis

---

Tod E. Kippin

---

Carol A. Vandenberg

---

Benjamin E. Reese, Chair

September 2017

Genetic Determinants of Retinal Cell Development

Copyright © 2017

by

Amanda Grace Kautzman

## ACKNOWLEDGEMENTS

*“...but it’s no use going back to yesterday, because I was a different person then”*

*- Lewis Carrol*

This dissertation would truly not be possible without the encouragement and support from many special people. I wish I could name you all.

First and foremost, to my PhD advisor, Ben Reese. Your support, meticulousness, and passion have been inspiring and have made me a better scientist in many ways, and I am very thankful to you for that.

To my committee, who provided many helpful suggestions and comments on the work compiled in this dissertation. To all of the talented technicians, undergrads, and high school students who have made the experimental nature of this research possible.

To my family, who have been an unwavering source of support throughout my entire academic career. Especially to my parents, Philip Kautzman and Mary Ann Ferolito, who have encouraged me to follow my passions since I was a little girl. To my brother, Philip Kautzman III, who refuses to acknowledge that “I’m not that kind of doctor”. And to my grandmother, Mary Ferolito, whose daily phone calls have allowed me to disconnect from the often stressful nature of graduate school and laugh a little.

To my dearest friends, both near and far, who have kept me sane during this process, including but not limited to Kate Keeley, Tyson Halseth, Lika Walker, Roxanne Croze, Sarah Benbow, and Lauren Vucovich.

And last, but most certainly not least, to the greatest friend, office-mate and colleague anyone could ask for, Patrick Keeley. You have made my time in graduate school (and in Santa Barbara) not only manageable, but wildly enjoyable as well.

# VITA OF AMANDA GRACE KAUTZMAN

August 2017

## EDUCATION

**Doctor of Philosophy** 2012 –2017 (expected)

Department of Psychological and Brain Sciences  
Research Training Area: Neuroscience and Behavior  
University of California at Santa Barbara – Santa Barbara, CA  
Advisor: Benjamin Reese, Ph.D.  
Dissertation Title: *Genetic Determinants of Retinal Cell Development*

**Master of Arts** 2012 –2014

Department of Psychological and Brain Sciences  
Research Training Area: Neuroscience and Behavior  
University of California at Santa Barbara – Santa Barbara, CA  
Advisor: Benjamin Reese, Ph.D.  
Dissertation Title: *Transcriptional Activation by Islet1 Isoforms*

**Bachelor of Science**

Northeastern University – Boston, MA 2004 – 2008  
Major: Behavioral Neuroscience

University of Alicante – Alicante, Spain May – Aug 2007

## PROFESSIONAL EMPLOYMENT

**University of California Santa Barbara, CA - Psychological and Brain Sciences**  
Graduate Student Researcher 2012 – Present

**Stanford University, CA - Neurology and Neurological Sciences**  
Research Assistant and Laboratory Manager 2011 –2012

**Children's Hospital Boston, MA – Neurobiology/ Neuroimmunology Laboratory**  
Research Technician and Laboratory Manager 2008 –2011

## PUBLICATIONS

**Kautzman, AG**, Keeley, PW, Nahmou, MM, Luna, G, Fisher, SK & Reese, BE. *Sox2 Regulates Astrocytic and Vascular Development in the Retina*. (2017). *Glia*. In Review.

\*Whitney, IE, A, \***Kautzman, AG**, & Reese, BE. *Alternative Splicing of the LIM-Homeodomain Transcription Factor Isl1 in the Mouse Retina*. (2015). *Molecular and Cellular Neuroscience* 65:102-113. [\*co-first authorship]

Whitney, IE, Keeley, PW, St. John, A, **Kautzman, AG**, Kay, JN, & Reese, BE. *Sox2 Regulates Cholinergic Amacrine Cell Positioning Between the INL and GCL*. (2014). *Journal of Neuroscience* 34(30):10109-21.

Kautzman, AG. (2014). *Transcriptional Activation by Islet1 Isoforms*. (Master's Thesis). Available from ProQuest Dissertations and Theses Database. (UMI No. 1565422).

Pujh, TJ, Weeraratne, SD, Archer, TC...**Kautzman, AG** (33/43)...Cho, YJ. *Medulloblastoma exome sequencing uncovers subtype-specific somatic mutations*. (2012). *Nature* 488(7409):106-10.

Schafer, DP, \*Lehrman, EL, \***Kautzman, AG**, Koyama, R, Mardinly, A, Yamasaki R, Ransohoff RM, Greenberg, ME, Barres, BA & Stevens, B. *Microglia Prune Developing Synaptic Circuits by Complement-Mediated Phagocytosis*. (2012). *Neuron* 74(4):691-705  
Manuscript recognized by *Neuron* (2013): most influential paper of 2012

## PRESENTATIONS

**Kautzman, AG**, Keeley, PW, Nahmou, MN, Luna, G, Fisher, SK & Reese, BE. (2017). Sox2 deficiency leads to the abnormal development of retinal astrocytes and vasculature in the mouse. *Association for Research in Vision and Ophthalmology*.

**Kautzman, AG**, Keeley, PW, Nahmou, MN, Luna, G, Fisher, SK & Reese, BE. (2017). Sox2 deficiency leads to the abnormal development of retinal astrocytes and vasculature in the mouse. *Functional Interactions Among Glia and Neurons Gordon Research Conference*.

**Kautzman, AG**. (2017). A role for Sox2 in the astrocytic and vascular networks of the retina. *Neuroscience and Behavior Seminar Series, University of California Santa Barbara*.

**Kautzman, AG**, Keeley, PW, Nahmou, MN, Luna, G, Fisher, SK & Reese, BE. (2016). Sox2 deficiency leads to the abnormal development of retinal astrocytes in the mouse. *Glia in Health and Disease Meeting, Cold Spring Harbor*.

**Kautzman, AG**, Keeley, PW, Ackley, CR, & Reese, BE. (2016). Xkr8 Modulates Bipolar Cell Number in the Mouse Retina. *Association for Research in Vision and Ophthalmology*.

**Kautzman, AG**. (2015). The Contribution of Xkr8 and Sox2 in Retinal Cell Development. *Neuroscience and Behavior Seminar Series, University of California Santa Barbara*.

**Kautzman, AG**. (2015). Genetic Determinants of Retinal Cell Development. *Neuroscience and Behavior Seminar Series, University of California Santa Barbara*.

**Kautzman, AG**. (2014). Islet1 Isoforms in the Retina. *Neuroscience and Behavior Seminar Series, University of California Santa Barbara*.

**Kautzman, AG.** (2014). Transcriptional Activation of Islet1 Isoforms. *Psychological and Brain Sciences Graduate Student Mini-Convention, University of California Santa Barbara.*

**Kautzman, AG.** (2013). In-Vivo Retinal Electroporation. *Neuroscience and Behavior Seminar Series, University of California Santa Barbara.*

**Kautzman, AG,** Whitney, IE & Reese, BE. (2013). Transcriptional Activation Differs Significantly Between Two Isoforms of Isl1. *Association for Research in Vision and Ophthalmology.*

## AWARDS

**Graduate Division Dissertation Fellowship** April 2017  
Graduate Division, University of California at Santa Barbara

**Art of Science competition** March 2017  
Honorable Mention in Center for Science and Engineering Partnerships competition for visually communicating the beauty inherent in scientific investigations.

**Neuroscience Research Institute Travel Award** February 2017  
To attend 2017 Functional Interactions Among Glia and Neurons Gordon Research Conference

**Academic Senate Travel Grant** May 2016  
To attend 2016 annual Association of Research in Vision and Ophthalmology Meeting

**Knights Templar Eye Travel Grant** May 2016  
To attend 2016 annual Association of Research in Vision and Ophthalmology Meeting

**University of California at Santa Barbara Grad Slam** April 2016  
Semi-finalist for best three minute presentation by graduate student

**Graduate Research Mentorship Program Fellowship** May 2015  
Graduate Division, University of California at Santa Barbara

**Harry J. Carlisle Memorial Award** June 2015  
For outstanding graduate student in Neuroscience and Behavior Division in Psychological & Brain Sciences, University of California at Santa Barbara

**Dean's List** 2004-2008  
Northeastern University, MA



## COMMITTEE SERVICE AND MEMBERSHIPS

<b>Graduate Executive Committee</b> Representative	2012-2017
<b>Women in Science and Engineering (WiSE) Organization</b> Officer and Member	2012-2017
<b>Association for Research in Vision and Ophthalmology</b> Member	2013-2017
<b>Graduate Organization in Psychological &amp; Brain Sciences</b> President and Founder	2014-2017
<b>Beyond Academia Conference</b> Programming Committee Member	2017
<b>Collaboration in Neuroscience Undergraduate Club</b> Graduate Advisor	2016
<b>Tech Savvy</b> Workshop Facilitator	2015, 2016
<b>Graduate School Workshop</b> Invited panelist	2014, 2015

## SCIENTIFIC TRAINING

<b>Discipline-based Education Research in Science Course</b> University of California at Santa Barbara, CA Molecular, Cellular and Developmental Biology Department	Spring 2015
<b>Introduction to Microscopy for the Bio-Sciences Course</b> University of California at Santa Barbara, CA Molecular, Cellular and Developmental Biology Department	Fall 2013

## TEACHING EXPERIENCE

### **Teaching Assistant, Lecture classes**

Department of Psychological and Brain Sciences, University of California at Santa Barbara	
Psychopharmacology of Therapeutic Drugs	Winter 2017
Learning and Conditioning	Winter 2015
Biological Basis of Psychology	Spring 2015
Visual Neuroscience	Spring 2015
Development and Plasticity of the Brain	Winter 2014, 2015
Retinal Development	Spring 2014, 2015

Neuropharmacology  
Complex Systems in Brain Sciences

Winter 2014  
Spring 2014

**Teaching Assistant, Section Leader, Laboratory class**

Department of Psychological and Brain Sciences, University of California at Santa Barbara  
Laboratory in Neuroanatomy

Fall 2014, 2015, 2016; Spring 2017

**Mentor**

CONDOR TECHS Mentorship Program  
UCSB Summer Research Mentorship Program

July 2016  
June 2015 – July 2015

# ABSTRACT

## Genetic Determinants of Retinal Cell Development

by

Amanda Grace Kautzman

The central nervous system, is composed of several complex tissues that serve a wide variety of critical functions. One of these tissues residing in the eye, the retina, serves to convert incoming photons of light to neural signals that aid in the perception of vision. The retina is comprised of various cellular populations that each develop through unique set of mechanisms, many of which remained to be elucidated. In this dissertation, we have examined the genetic mechanisms underlying how specific populations of cells in the retina develop, in order to more fully understand how individual populations arise and therefore gain insight into how these populations may interact with one another in the mature retina. First, we sought to uncover genes that modulate neuronal cell number. Through the use of a forward genetic screen, we were able to study the development of the mouse retina across genetically dissimilar strains and identify genes that modulate retinal development. We uncovered a role for two novel genes, *Xkr8* and *Ggct*, in the modulation of bipolar cell number and pursued an investigation into the genetic variants underlying cell number differences across inbred mouse strains. Secondly, we sought to elucidate novel mechanisms by how the glial population of astrocytes develop. We identified an unknown

function for the gene *Sox2* in the development of astrocytes as well as the retinal vasculature. Taken together, these analyses provide insight into how both neuronal and glial cell populations develop in the mouse retina. Both of these cellular populations are critical to a functioning retina and by understanding the specific mechanisms underlying how they develop, we begin to uncover how the complexity of the central nervous system arises.

## TABLE OF CONTENTS

I. Introduction .....	1-14
A. The Retina as a Model to Study CNS Development .....	1
B. The Cellular Constituents of the Retina .....	2
C. The Stages of Retinal Development.....	7
D. The Mouse as a Model to Study Development.....	10
E. Chapter 2 and 3 Overviews .....	12
1. Establishment of Cell Number.....	12
2. Astrocytic and Vascular Development .....	13
II. Genetic Control of Bipolar Cell Number .....	15-73
A. Abstract.....	15
B. Introduction.....	15
1. Identification and Investigation of Candidate Genes.....	16
2. Bipolar Cell Development .....	20
C. Methods.....	23
D. Results.....	36
1. Selection of Candidate Genes from Cell Number QTL.....	36
2. Rod Bipolar and Type 2 Cone Bipolar Cell Number .....	43
3. Interval Analysis .....	45
4. Candidate Gene Selection: <i>Xkr8</i> .....	47
5. <i>Xkr8</i> Knockout Mice.....	52
6. <i>Xkr8</i> Overexpression via <i>In Vivo</i> Electroporation .....	54

7. <i>Xkr8</i> Regulatory Variants .....	57
8. Candidate Gene Selection: <i>Ggct</i> .....	59
9. <i>Ggct</i> Overexpression via <i>In Vivo</i> Electroporation .....	63
10. <i>Ggct</i> Regulatory Variants .....	63
E. Discussion .....	68
III. Astrocytic and Vascular Development in the Retina.....	74-105
A. Abstract.....	74
B. Introduction.....	74
C. Methods.....	77
D. Results.....	81
1. Characterization of the CKO Retina.....	81
2. Maturation of Sox2-Deficient Astrocytes.....	83
3. GFAP Depletion in Peripheral Retina .....	88
4. Sprouting in CKO Retina.....	90
5. Vascular Abnormalities in CKO Retina .....	97
E. Discussion .....	99
IV. Conclusions .....	106-110
References.....	111-129
Appendix.....	130-144

## LIST OF FIGURES AND TABLES57

Figure 1. Viewing retinas as wholemounds or radial sections .....	3
Figure 2. Schematic of neural retina.....	6
Figure 3. Genetic control of bipolar cell number .....	17
Figure 4. Prioritizing candidate genes at genomic interval .....	19
Table 1. Primary antibodies used in Chapter 2.....	27
Figure 5. Electroporation quantification.....	32
Table 2. Real-time quantitative PCR primers.....	34
Figure 6. QTL mapped for 12 retinal cell types .....	37
Table 3. Candidate genes controlling neuronal cell number .....	38
Figure 7. Quantification of cell number changes in candidate gene knockout and conditional knockout mice.....	40
Figure 8. Candidate genes tested via <i>in vivo</i> electroporation .....	42
Figure 9. Distribution of cell number across recombinant inbred strains.....	44
Figure 10. QTL mapping for rod bipolar and type 2 cone bipolar cells .....	46
Figure 11. <i>Xkr8</i> retinal expression.....	49
Figure 12. <i>Xkr8</i> expression correlates to bipolar cell number .....	51
Figure 13. <i>Xkr8</i> knockout mice .....	53
Figure 14. <i>Xkr8</i> overexpression via <i>in vivo</i> electroporation.....	56
Figure 15. <i>Xkr8</i> promoter activity via luciferase assay .....	58
Figure 16. QTL mapping for rod bipolar cells .....	60
Figure 17. <i>Ggct</i> retinal expression.....	62

Figure 18. <i>Ggct</i> overexpression via <i>in vivo</i> electroporation .....	64
Figure 19. <i>Ggct</i> structural variant .....	66
Figure 20. <i>Ggct</i> promoter activity via luciferase assay .....	67
Table 4. Primary antibodies used in Chapter 3.....	79
Figure 21. Characterization of Sox2 conditional knockout mice .....	82
Figure 22. Retinal histology is unaltered in CKO animals .....	84
Figure 23. Pax2-positive astrocytes at P1 migrate normally in CKO retinas .....	85
Figure 24. CKO retinas exhibit a delayed maturation at P5 and P10.....	87
Figure 25. Peripheral astrocytic abnormalities in CKO retinas.....	89
Figure 26. GFAP depletion is pervasive in peripheral regions of CKO retinas .....	91
Figure 27. GFAP processes sprout into the inner retina in CKO animals.....	92
Figure 28. CKO retinas rarely exhibit extreme abnormalities.....	94
Figure 29. Microglia density is not significantly increased in CKO retinas in GCL	95
Figure 30. CKO depleted regions are Sox9-negative .....	96
Figure 31. Retinal vasculature develops abnormally in CKO retinas .....	98



## **I. Introduction**

The function of the mammalian central nervous system (CNS), comprised of the brain and spinal cord, is to process information gathered from the environment and generate motor signals in response, in order to ultimately influence behavior. This processing is remarkably quick and efficient, in part due to the variability and complexity of the many specialized cells that comprise the CNS. As the CNS develops, its cellular constituents mature and diversify into an extensive network of neurons and glial cells working alongside one another. Indeed, it is estimated that the human brain is composed of more than 100 billion neurons. Likewise, there are roughly the same number of glial cells in the brain (Azevedo et al., 2009), which communicate extensively with neurons. To further complicate matters, both the neuronal and glial residents of the CNS exist as heterogeneous populations, made up of many different subtypes of cells with highly specialized functions. This specialization is not only influenced by the genetic makeup of each cell, but also by the complex connectivity amongst cells. The overall focus of this dissertation is to elucidate novel cellular and molecular mechanisms by which this complex organization is achieved. The remainder of this introduction will overview the model system used to dissect mechanisms of CNS development and will provide an introduction into major developmental events that shape how this mature tissue is established. The specific cell types of interest for this dissertation, and their developmental mechanisms, will be discussed in greater detail in the introductions to each subsequent chapter.

### ***A. The Retina as a Model to Study CNS Development***

We have employed the retina, a thin light-sensitive tissue that lines the back of the eye,

as a model tissue to study mechanisms of CNS development. There are many well-established advantages to using this model. Although the retina lies anatomically outside the brain, it originates as an embryonic outpocket of the forebrain and therefore is developmentally related to other CNS tissue. Like other CNS tissue, some cells within the retina, such as the retinal ganglion cells that project directly to the brain, display a typical CNS neuronal morphology comprised of a cell body, dendrites, and an axon. Their axons within the optic nerve are myelinated and fire action potentials, not unlike those fired by neurons within the brain. The retina also has a laminar organization, comprised of five neuronal cell classes residing in discrete positions, similar to that of many brain structures, like the cerebral cortex. This lamination allows for the viewing of cellular populations and synaptic localization in either the horizontal or vertical dimensions. Figure 1 shows both a real and cartoon version of a retinal wholemount and radial section, depicting the retina viewed in the horizontal and vertical dimensions, respectively, when dissected from a whole eye. Given the common features between the retina and the remaining CNS, findings from retinal research can be applicable to other CNS tissues, benefiting further from the fact that the eye is a relatively accessible tissue, unlike the remainder of the CNS, lending itself to experimental manipulations. For these combined reasons the proposed studies employ the retina as a model system to study neuronal development.

### ***B. The Cellular Constituents of the Retina***

The overall function of the retina is to process incoming photons of light into electrical and chemical signals that are then communicated to the visual centers of the brain. This is achieved by a diverse set of retinal cells that form complex circuits. The retina is composed

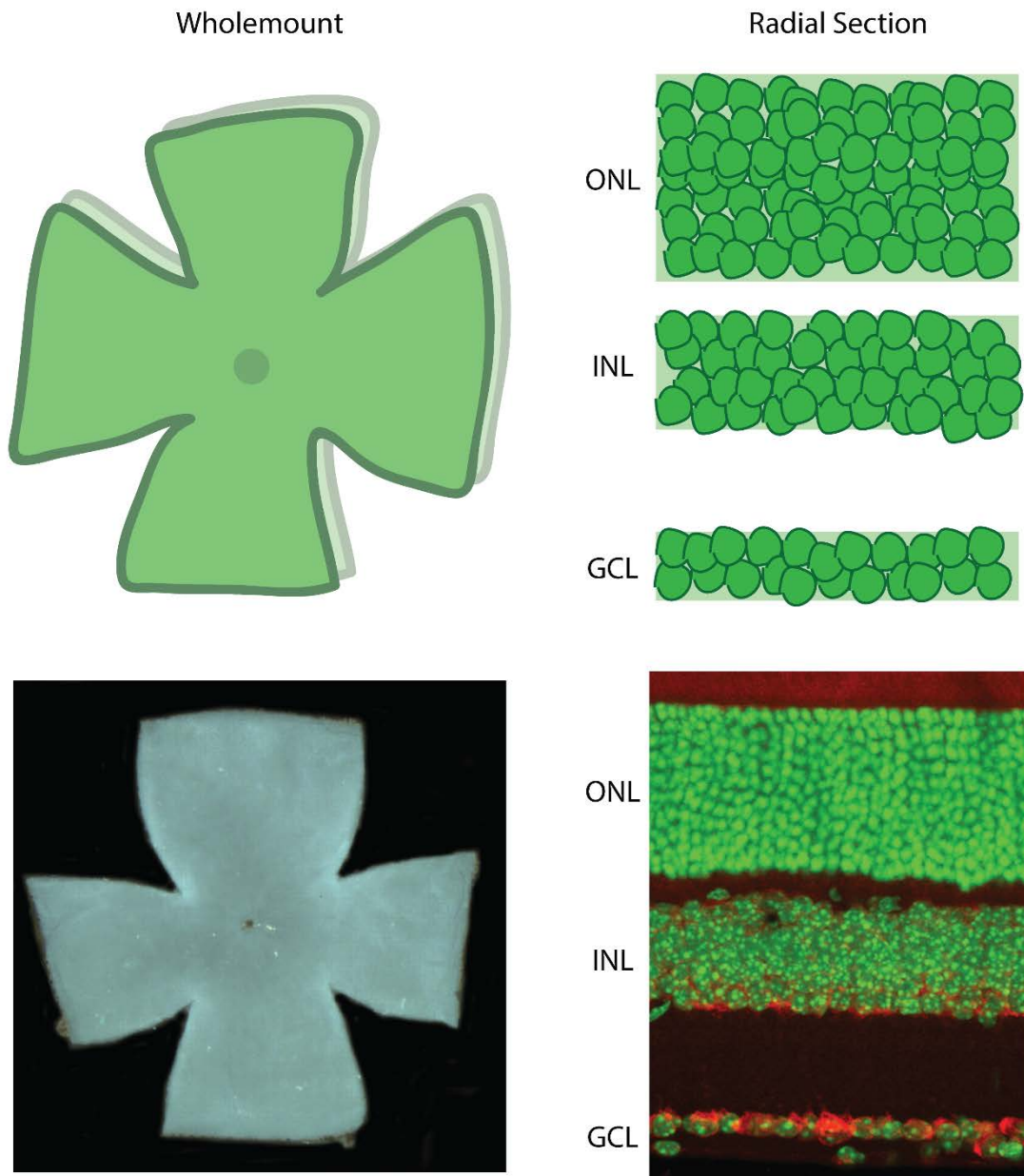


**Figure 1. Viewing retinas as wholemounds or radial sections.** Retinas are microdissected from the eye and given four relieving cuts, permitting the visualization of the layered cytoarchitecture in the horizontal plane (left column). Retinas can also be cut into sections, allowing one to view all retinal layers simultaneously in the vertical plane (right column). ONL = outer nuclear layer, INL = inner nuclear layer, GCL = ganglion cell layer.

of five major classes of neuron, each with a distinct role. Photoreceptors reside in the outer nuclear layer (ONL) and detect incoming photons of light. These cells pass information to bipolar cells in the inner nuclear layer and then the information is transmitted to retinal ganglion cells whose axons exit the eye through the optic nerve and convey this signal to visual nuclei in the brain. There are also two classes of interneuron, the amacrine and horizontal cells, located in the INL alongside bipolar cells that modulate the radial transfer of information. To add to the complexity, each class of neuron is composed of multiple types, totaling at least 85 different types of retinal neurons (Sanes & Masland, 2015), each with its own unique contribution to the processing of visual information.

Additionally three classes of glial cells, being the Müller cells, the astrocytes, and the microglia, reside in the retina and are situated amongst the millions of neurons. These cells, like retinal neurons, have similarities to other CNS glial cells. Müller cells arise from the same progenitor pool as all retinal neurons and are therefore developmentally related. Astrocytes and microglia conversely are both immigrants to the retina; astrocytes are born from ventricular zone cells in the brain and migrate into the retina via the optic nerve during late embryonic development (Ryan, 1989), while microglia are derived from the yolk sac and invade the retina during early embryogenesis (Harry, 2013). All of these cell types interact with neurons in many ways to influence neuronal development. For example, astrocytes are known to promote maturation of neuronal cells by stimulating synaptogenesis and axon growth (Allen et al., 2012; Barker & Ullian, 2008; Christopherson et al., 2005; Ullian, Sapperstein, Christopherson, & Barres, 2001).

In the adult retina, these subsets of glial cells serve distinct functions. Müller cells provide structural support to the retina by extending their processes across the entire depth

of the retina. They have a wide range of functions that help maintain retinal homeostasis including, but not limited to, the breakdown and buffering of extracellular ions like glutamate (Pow & Robinson, 1994). Astrocytes also contribute to ionic homeostasis by buffering extracellular ions such as potassium. They serve an important developmental role by aiding in synaptic pruning (Chung, Welsh, Barres, & Stevens, 2015; Stevens et al., 2007), but also play a protective role by promoting glial scar formation following injury (Bushong, Martone, Jones, & Ellisman, 2002; Watanabe & Raff, 1988). In addition, they are critical for vascularization of the retina, being a primary concern of one of the experimental chapters in this dissertation. Microglia, on the other hand, play a critical role in protecting the retina from invasion or injury; microglia respond by phagocytizing debris in order to facilitate tissue repair (Chen, Yang, & Kijlstra, 2002). They have also recently been demonstrated to participate in the sculpting of synaptic connectivity by engulfing synaptic material in an activity-dependent manner, through complement-mediated phagocytosis (Bialas & Stevens, 2013; Paolicelli et al., 2011; Schafer et al., 2012; Stevens et al., 2007; Tremblay, Lowery, & Majewska, 2010).

Figure 2 illustrates the cellular components in a radial section, showing the close interaction between neurons and glia in the mouse retina. Müller glia (gray) are large cells that span the entire retinal depth and come in close contact with cells in all layers in addition to blood vessels in the inner and outer retina. Astrocytes (cyan) conversely, are confined to the innermost portion of the retina in the nerve fiber layer, physically contacting only blood vessels and Müller glia endfeet. This interaction between astrocytes and blood vessels will be relevant to the data discussed in Chapter 3. Lastly, microglia are highly motile cells that are found in all retinal layers in the mouse, except the ONL.

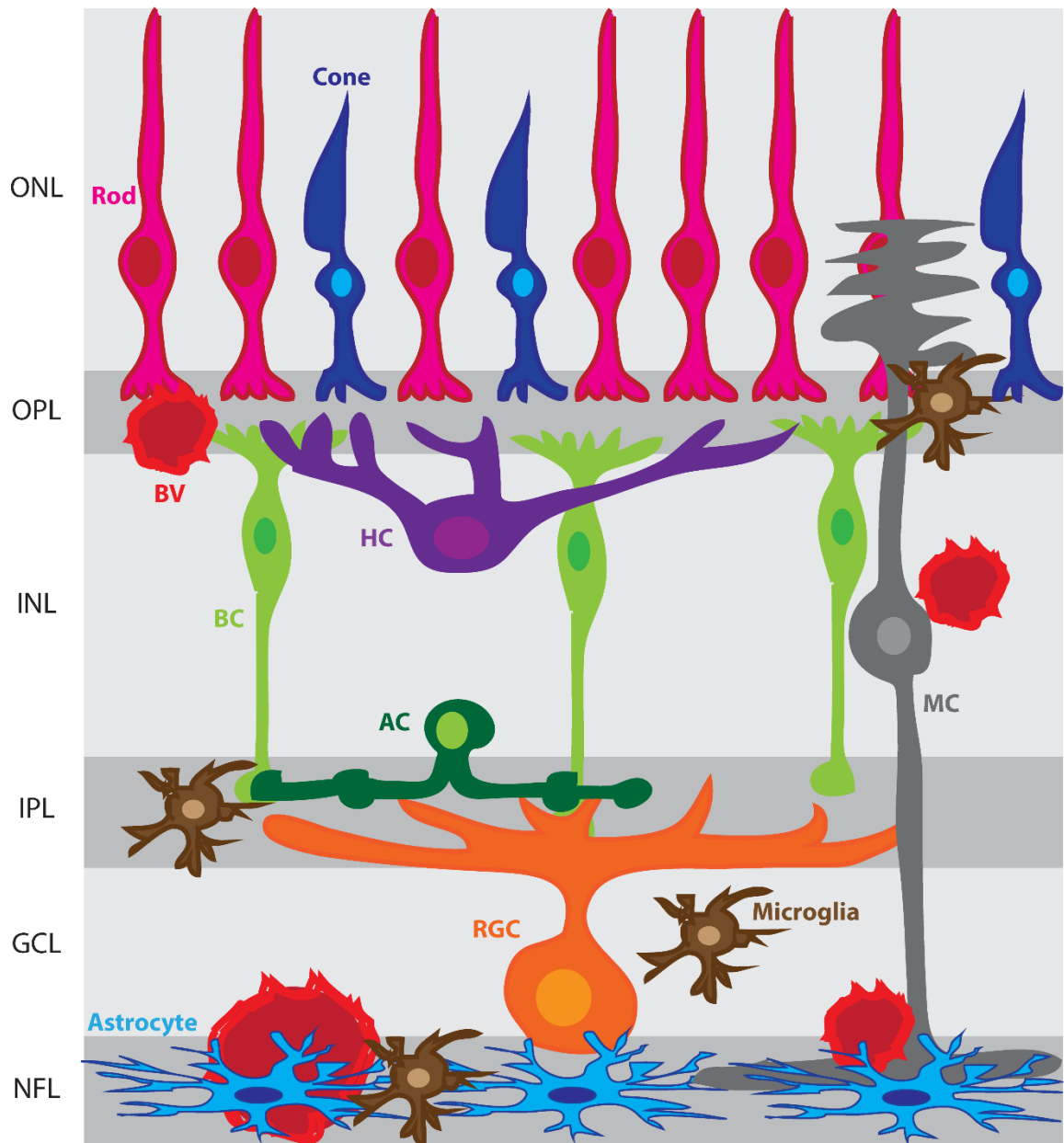


**Figure 2. Schematic of neural retina.** Retinal layers from outer to inner retina consist of the outer nuclear layer (ONL), outer plexiform layer (OPL), inner nuclear layer (INL), inner plexiform layer (IPL), ganglion cell layer (GCL), and nerve fiber layer (NFL). Retinal neurons include rod and cone photoreceptors, horizontal cells (HC), bipolar cells (BC), amacrine cells (AC), and retinal ganglion cells (RGC). Glial cells include microglia, astrocytes, and Müller cells (MC). Blood vessels (BV) are also shown.

### ***C. The Stages of Retinal Development***

The manner by which the retina develops and how these specific cellular traits are determined is tightly regulated by genetic factors (X. Zhang, Serb, & Greenlee, 2011). The last fifty years of research have observed an expansion in our understanding of the genetic mechanisms by which retinal cells are born, acquire their fates, migrate, differentiate their dendritic and axonal morphologies, and communicate with neighboring cells. These processes are not unique to retinal tissue, rather all CNS cells undergo the same broad set of processes when progressing from a progenitor cell into a mature cell. However, for the purpose of this dissertation I will focus the present developmental overview upon retinal tissue, being immediately relevant to the experimental chapters to follow.

Retinal progenitor cells (RPCs) are multipotent cells that give birth to all neuronal cells of the retina, in addition to Müller cells, through intrinsically defined expression of transcription factors as well as by responding to extrinsic cues (Godinho et al., 2005; Mumm & Lohmann, 2006; Reese, 2011). Some transcription factors, such as Rax, are vital to retinal formation, given that Rax knockout mice are born with anophthalmia, or no eyes (Mathers, Grinberg, Mahon, & Jamrich, 1997). Others are critical later in development for formation of specific cell types, for instance Nrl, which regulates photoreceptor fate specification; Nrl knockout mice fail to produce rod photoreceptors, generating cone photoreceptors instead (Mears et al., 2001). Examples of environmental regulators of cell fate determination, by contrast, include ciliary neurotrophic factor (CNTF) and leukemia inhibitory factor (LIF), two factors known to inhibit rod photoreceptor fate and promote differentiation to bipolar and Müller cells (Ezzeddine, Yang, DeChiara, Yancopoulos, & Cepko, 1997; Rhee & Yang, 2010).

Retinal neurogenesis proceeds in an established histogenetic order from roughly embryonic (E) day 11 to postnatal (P) day 10 in the mouse (Marquardt & Gruss, 2002; X. Zhang et al., 2011). This process whereby cells acquire their fates occurs first by retinal ganglion cells (RGCs), followed sequentially by horizontal cells, cone photoreceptors, amacrine cells, rod photoreceptors, bipolar cells, and Müller glia (Bassett & Wallace, 2012; C. L. Cepko, Austin, Yang, Alexiades, & Ezzeddine, 1996; Rapaport, 2006). Each cell type is born over a limited neurogenic period, and while those windows of neurogenesis partially overlap, their sequence of production is conserved.

Following fate determination, cells migrate to their appropriate layer within the retina, which is critical for them to make proper synaptic connections and function normally. The earliest born cells, the RGCs, migrate further distances than all other six cell types. As RGCs leave the cell cycle, they migrate out of the ventricular zone and travel to the ganglion cell layer (GCL). The next progenitor cells to become postmitotic are those fated to be horizontal cells, cone photoreceptors, and amacrine cells. These cell types are all destined for different retinal locations in the INL and ONL, and therefore migrate varying distances. The bipolar cells and Müller glia are the final cells generated and migrate to the INL postnatally. Rod photoreceptors are unique in that their window of neurogenesis overlaps with nearly all cell types, as they are generated over a long period of time. These cells, along with cone photoreceptors, travel very little distance given that the proliferative zone in which they are born becomes the future ONL. As each cell migrates to the prospective layer where it will reside in maturity, these cells are believed to respond to physical and/or environmental cues that guide their movement. However, little is known about the specific mechanisms and genes involved in the migration of individual cell types (C. Cepko, 2014;



Godinho & Link, 2006).

Once cells migrate to the location they will ultimately reside, all retinal cells elaborate their morphology following both intrinsic differentiation instructions and communication with neighbors (Reese, 2011). Cells extend processes to form contacts with specific pre- and post-synaptic targets. For example, different subtypes of bipolar cells preferentially make synaptic targets with subtypes of photoreceptors; rod bipolar cells only receive input from rod photoreceptors, while the 10 or more subtypes of cone bipolar cells receive synaptic input selectively from cone photoreceptors (reviewed in Euler, Haverkamp, Schubert, & Baden, 2014). In addition, each cell type is thought to exhibit a specific axonal and dendritic branch pattern, that overlaps some amount, or not at all, with their neighbors of the same subtype. Two cell types that fall on either end of this spectrum are horizontal cells and cone bipolar cells. Horizontal cells extend their dendrites into the territories occupied by other horizontal cell dendrites, thus having a large amount of overlap. Cone bipolar cells conversely do not overlap with the dendritic arbors of neighboring cone bipolar cells of the same subtype, in a phenomenon known as tiling (reviewed in Reese & Keeley, 2015). These subtype-specific patterns can be influenced by many different factors, including physical contact with neighboring cells and detection of environmental cues. Each cell therefore has its own unique combination of intrinsic and/or extrinsic cues that guide the development of pre- and post-synaptic processes.

In addition to these aforementioned developmental events, some populations of cells within the developing mouse retina are overproduced, namely retinal ganglion cells, most bipolar cells, and some amacrine cells. These populations subsequently undergo the process of programmed cell death, leading to a reduction in the number of cells residing in the

mature retina (Pequignot et al., 2003; Reese & Keeley, 2015; Young, 1984). Apoptosis is accompanied by morphological changes that facilitate recognition and removal by phagocytic cells, such as translocation of phosphatidylserine to the surface of dying cells. Over the course of development, partially overlapping phases of cellular production, followed by programmed cell death, participate in determining the total number of cells with a population in maturity. Taken together, retinal complexity is achieved through a combination of these intricate developmental processes that occur concurrently during the late embryonic and early postnatal mammalian life.

Despite this understanding of the major developmental processes that lead to a mature retina, all of the contributing genes and mechanisms have yet to be elucidated. The focus of this dissertation is to gain knowledge about novel genes that influence how different retinal cells develop. This is important because the genes and operations that direct formation of the retina often guide development of tissues in the body and the brain as well. For example, the transcription factor *Bhlhb5* is known to influence specification of a single type of bipolar cell in the retina (Feng et al., 2006), but also plays a critical role in neocortical development (Joshi et al., 2008).

#### ***D. The Mouse as a Model to Study Development***

The mouse is a great model organism for discovering the mechanisms by which genes influence development. Most importantly, the mouse genome has been fully sequenced and shares more than 95% homology with humans, therefore making experimental findings applicable to human biology. Indeed, the mouse shares many anatomical and physiological similarities to humans, being based on the same fundamental vertebrate plan. The CNS of

mice, like humans, contains the same cellular components of both neurons and glial cells, albeit in different proportions. The human brain is estimated to have about an equal number of neurons and glial cells, while the mouse is made up of about 65% neurons and 35% glia (Herculano-Houzel, Mota, & Lent, 2006). In addition, thousands of genetically modified and inbred strains of mice are available to researchers for a low cost, making the study of complex diseases or phenotypes feasible.

In addition to the hundreds of inbred mouse strains, there are also a wide variety of knockout mice and conditional knockout mice that aid researchers studying development. Many strains are available that express *Cre* recombinase under different cell type-specific promoters. If these mice are bred with mice carrying conditional, or floxed, alleles of a gene of interest, recombination occurs and removes the gene from a specific cell type or tissue, thereby creating conditional knockout mice. For example, if bred with a mouse expressing *LoxP* sites flanking a gene of interest, *Rx-Cre* will excise the target gene from most retinal cells, given that *Rx* is a gene expressed in all retinal progenitor cells. These genetically engineered mice provide a means to study the specific role that candidate genes play in retinal development. Other advantages to using mice as a model organism are that they reproduce quickly (about every 21 days) and can give birth to large litters (up to 14 pups). In addition, mice are inexpensive to house and care for, compared to many other vertebrate species.

Although mice are a commonly used model organism, they have limitations as well. While mice share a high percentage of genetic homology with humans, it is often difficult to mimic human diseases in mouse models. One reason is that human diseases are caused by a complex mixture of both genetic and environmental factors. Laboratory mice are housed in

facilities that are designed to minimize the influence environmental factors, which could result in an overrepresentation of individual genetic factors. In addition, many human diseases and disorders are diagnosed by self-report and behaviors that are difficult to mimic in rodents, such as depressed mood and suicidal tendencies. For this reason, many therapeutic drugs that pass preliminary trials in rodents fail to produce the same effects when introduced to the human population in clinical trials.

Despite limitations in precisely mimicking the human condition, mice remain a widespread model organism. Due to their popularity, many antibodies and murine-specific reagents are readily available to researchers, which are critical to the types of studies this dissertation has employed. In addition, direct manipulation of the mouse genome is available through a wide variety of genetic tools and resources, including *in vivo* electroporations, which will be discussed in detail in Chapter 2. For these reasons in addition to those discussed above, we have used the mouse retina as a model to study genetic mechanisms of development.

### ***E. Chapter 2 and 3 Overviews***

This dissertation will consist of two parts, each of which explores different genetic underpinnings of retinal cell development.

#### **1. Establishment of Cell Number**

The size of cell populations within the retina varies greatly, ranging from greater than six million rod photoreceptors (Jeon, Strettoi, & Masland, 1998) to less than one thousand dopaminergic amacrine cells (Whitney, Raven, Ciobanu, Williams, & Reese, 2009).

Chapter 2 will focus upon the genetic mechanisms by which the sizes of specific neuronal populations are determined. It will describe the methodology by which we identify candidate genes and subsequently test their function. It will then describe a number of candidate genes modulating retinal cell number, ultimately focusing upon the role of two specific genes, *Xkr8* and *Ggct*, in the control of retinal bipolar cell number. Specifically, by using a forward genetic screen to map genomic loci correlated to these cell number phenotypes, I identified *Xkr8* and *Ggct* as novel genes involved in this process, neither of which had previously been identified as playing a role during retinal development.

## **2. Astrocytic and Vascular Development**

Astrocytes are immigrants to the retina, migrating from the optic stalk into the developing retina in the perinatal period (Dorrell, Aguilar, & Friedlander, 2002). In maturity, these cells interact closely with the neuronal populations of the retina, being critical for their function. For decades it was believed that glial cells only played a supportive role in the CNS, yet it is becoming increasingly clear that these cells play many active roles and serve a wide range of functions (Barres, 2008) that will be discussed in Chapter 3.

Astrocytes play an important role in the vascularization of the retina (Fruttiger et al., 1996). As astrocytes enter the retina at the optic nerve head, they provide a template for blood vessels to follow as they move across the inner surface of the retina (Fruttiger et al., 1996). That they are critical for blood vessel formation is supported by the observation that possum retinas lack almost all retinal astrocytes and are avascular. In addition, blood vessels in the rabbit retina are confined to a small region that corresponds to the precise location where astrocytes are present (Stone & Dreher, 1987). Chapter 3 seeks to elucidate

mechanisms controlling the development of retinal astrocytes and the corresponding vasculature, specifically via the gene *Sox2*. *Sox2* has been previously shown to play various roles in later stages of retinal development (Lin, Ouchi, Satoh, & Watanabe, 2009; Surzenko, Crowl, Bachleda, Langer, & Pevny, 2013; Whitney et al., 2014), but its role in astrocytes has not been explored.

The overall goal of this dissertation is to further our understanding of the mechanisms by which specific classes of cells develop within the mouse retina. Information about the specific morphology, connectivity, and molecular identity of each class of cells better informs researchers as to how those cells may function. The research in the following two chapters directly addresses these questions by exploring the developmental mechanisms by which two distinct classes of cells, that of bipolar cells and astrocytes, develop. While having very different lineages and functions, both of these cell types communicate directly with retinal ganglion cells, the sole output neurons of the retina that send information via the optic nerve to the brain. Understanding how each of these individual cell types develop is critical towards our knowledge of how those populations operate to form a mature and functioning nervous system.

## **II. Genetic Control of Bipolar Cell Number**

### ***A. Abstract***

The specification of neuronal number in the retina is under precise genomic control, but the underlying genetic mechanisms regulating population size are still relatively unknown. Through a previous forward genetic screen using recombinant inbred mouse strains, we identified genomic loci that correlate to the variation in cell number for many retinal cell populations. Genes at these loci were interrogated using bioinformatic tools and top candidates were prioritized. Two genes in particular, *Xkr8* and *Ggct*, were identified as top candidates and were found to play a novel role in the modulation of bipolar cell number through *in vivo* electroporation strategies, whereby both genes were found to alter the proportion of bipolar cells in the mature retina when overexpressed in early postnatal development. Furthermore, we identified and investigated genetic variants within regulatory regions for both genes that are likely to influence gene expression and consequently alter cell number. These results implicate *Xkr8* and *Ggct* as two novel genes involved in the establishment of bipolar cell number in the developing mouse retina.

### ***B. Introduction***

The mature retina contains over 85 subtypes of neurons, ranging from millions of rod photoreceptors to less than one thousand dopaminergic amacrine cells. We have recently shown that neuronal number for any one subtype exhibits minimal variation within an inbred laboratory strain of mice, such as the C57BL/6J (B6/J) and A/J strain, suggesting that cell number is under precise genetic control. Across inbred strains however, like those generated from crossing the B6/J and A/J strains, we observe conspicuous variability in cell

number, strongly indicating the presence of genetic variants that contribute to the modulation of this trait (Keeley, Whitney, et al., 2014). Such variants may alter the size of these cell populations by acting through one or several of the developmental events previously discussed, such as proliferation, fate determination, or cell death. The studies carried out within this chapter seek to address the genetic underpinnings that establish neuronal number within the retina. To do so, we have utilized data from many forward genetic screens to identify novel genes playing a role in the development of retinal cell number, specifically focusing on the population of bipolar cells (Figure 3).

### **1. Identification and Investigation of Candidate Genes**

Previous work used a commercially available panel of recombinant inbred (RI) strains derived from two parental mouse strains, A/J and B6/J, to map quantitative traits of interest to specific regions of the genome. Each of these 26 RI strains has a unique combination of the two parental genomes due to recombination during meiosis followed by extensive inbreeding to drive every genomic locus to homozygosity. The genomes of the two parental strains have been fully sequenced, and each of the RI strains has been genotyped at high density for single nucleotide polymorphisms (SNPs) and microsatellite markers (Williams, Gu, Qi, & Lu, 2001). Variation in strain data for any quantifiable trait can therefore be mapped to discrete genomic locations, called quantitative trait loci (QTL), revealing regions where there must be allelic variants discriminating the parental genomes and contributing to some of the variation in the trait of interest.

QTL identification is the first step in an exercise to uncover the genetic participants in the regulation of a trait. QTL contain genes which are causal to variations in a trait of interest across RI strains. Using QTL already generated in our lab, I narrowed the list of



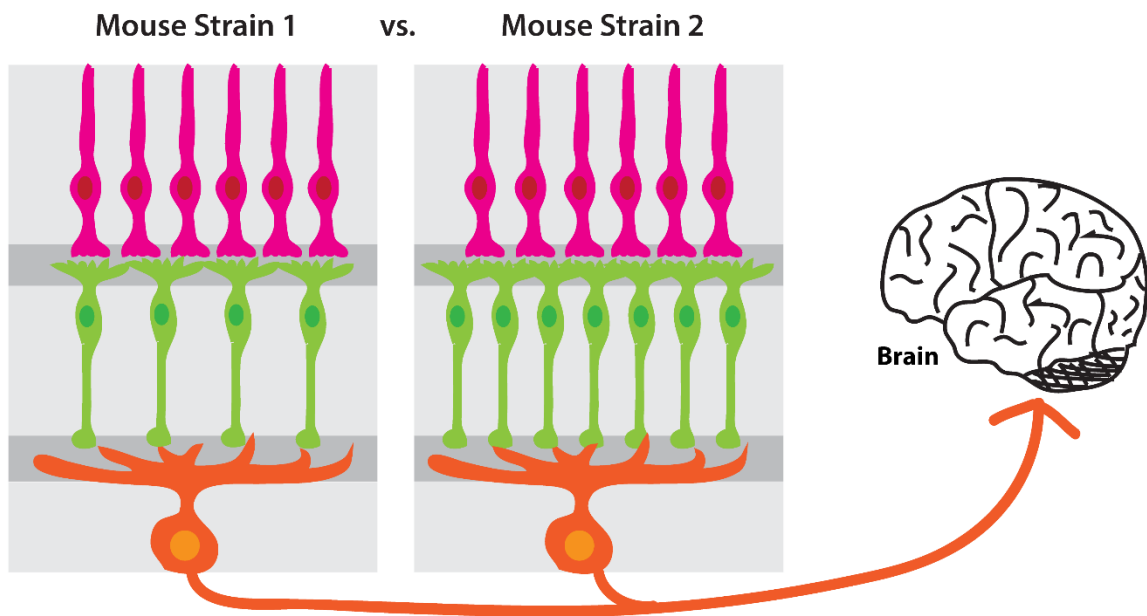


**Figure 3. Genetic control of bipolar cell number.** Bipolar cells play a role in the transferring of information from photoreceptors (pink) to retinal ganglion cells (orange) on their way to the visual enters of the brain. Across different mouse strains, bipolar cell number varies, suggesting that genetic variants between these strains modulate the development of these cells. Identifying these variants will shed light on the genetic mechanisms by which bipolar cell number is specified.

potential candidate genes at each genomic interval, consulting several bioinformatic databases for a set of criteria (reviewed in Figure 4). First, the gene must have allelic variants that discriminate the two parental strains from one another. A gene with no variants and therefore identical A/J and B6/J strain DNA sequences cannot be a source of the phenotypic differences seen across RI strains derived from these mice. The specific variants, either coding or regulatory, were interrogated to address how the gene may be functioning or regulated. Second, the gene must be expressed in the retina, either during development or in maturity. Genes with retinal expression and variants discriminating parental strains were then subjectively ranked based upon a review of known gene function. Every candidate gene was ranked hierarchically based on all information gathered (Figure 4).

Once a list of candidate genes was determined, the preferred method to test gene function was via knockout or conditional knockout mouse, if available commercially or through another lab willing to provide us with the animal and/or tissue. These methods enable us to determine whether elimination of the gene alters the trait of interest. However, removal of the gene from the entire animal, or even from a subset of cells, can have off-target consequences as well. For example, the candidate gene of interest may also be expressed in a tissue from a vital organ, thereby rendering a knockout animal not-viable if removed. In some instances, CKO mice can mitigate these potential off-target effects due to the gene removal from a specific population of cells, yet these mice are often unavailable.

An alternative, or in some cases complementary, approach we employed was to modulate gene expression via *in vivo* electroporation. Electroporation is a technique by which delivery of a short electrical pulse causes temporary pores to form in the plasma

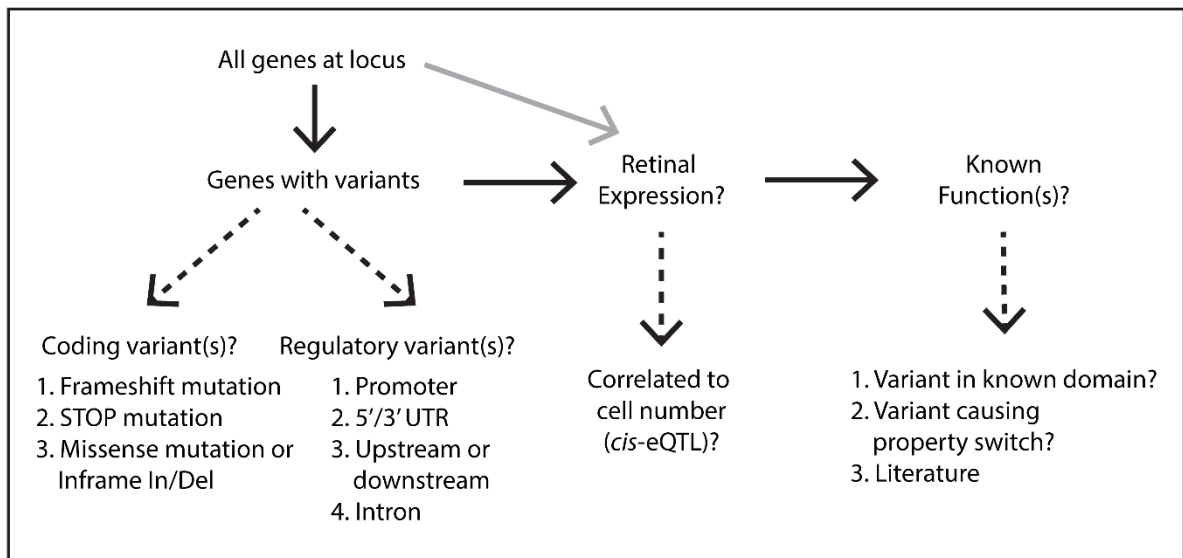


**Figure 4: Prioritizing candidate genes at genomic interval.** All genes at a locus are first prioritized by the presence of genetic variants and retinal expression. Genetic variants are further ranked according to disruptions of the coding or regulatory sequence, listed from highest to lowest priority. Known information about retinal expression in development and maturity is uncovered, and genes are further assessed for a correlation to the trait of interest, i.e. cell number. Lastly, known gene functions are researched and those with predicted deleterious variants or interesting functions are ranked higher. Black arrows indicate the first level of screening done on all candidate genes and dashed arrows indicate further methods of inquiry that aid in the prioritization of those genes.

membrane of a cell allowing charged molecules like plasmids, or small DNA molecules, to enter. Dividing cells acquire these foreign plasmids in their nuclei while their nuclear membranes are disrupted during mitosis (Goldstein, Fordis, & Howard, 1989; Saito, 2006), thereby allowing the plasmid DNA to be introduced into the progenitor cell and its descendent neurons, and become expressed. This method allowed us to abnormally express a gene of interest in the developing retina and determine the consequence on cell number.

We also employed methods to test genetic variants or gene regulation in a highly targeted manner via luciferase expression assays. These experiments test whether a particular variant that discriminates the mouse parental strains alters the level of gene expression, presumably contributing to the variation in the trait across RI strains. For our purposes, this assay was used to test regulatory variants in gene promoters that could differentially affect gene expression between A/J and B6/J mice. This *in vitro* assay consists of engineering plasmids that use a specific gene promoter to drive expression of a luciferase gene in a maintained cell line. Transcription and translation of this gene produces a luciferase enzyme that undergoes an enzymatic reaction in the presence of a luciferin substrate, yielding the production of light. Gene expression is therefore directly correlated to the measured output of light produced by the luciferase reaction.

To date, our lab has mapped QTL for cell number for 12 subtypes of retinal neurons (Keeley, Whitney, et al., 2014). This chapter reports 11 genes that I have tested from QTL generated for 6 different cell types, focusing upon two genes in particular, *Xkr8* and *Ggct*, which were candidates for controlling bipolar cell number.

## **2. Bipolar Cell Development**

Bipolar cells are the latest generated retinal neurons, with their window of neurogenesis

from E17 to P6, and the majority of the cells being born after birth around P3 (Morrow, Chen, & Cepko, 2008; Young, 1985). At least 15 subtypes of bipolar cells have been documented, each of which is believed to have a unique neurogenetic window during which that subtype is produced (Macosko et al., 2015). While largely overlapping in their neurogenetic windows, the order of subtype production is preserved so that rod bipolar cells are born last, following that of the many subtypes of cone bipolar cells (Morrow et al., 2008). Many genes are known to participate in the establishment of bipolar cell populations. For example, members of the basic helix-loop-helix (Bhlh) transcription factor family have been identified to play a role in the specification of bipolar cells, including *Ascl1* (*Mash1*) and *Neurod4* (*Math3*). Removal of *Ascl1* and *Neurod4* in double-mutant retinas causes a complete loss of bipolar cells, with a consequent increase in Müller cells (Tomita, Moriyoshi, Nakanishi, Guillemot, & Kageyama, 2000; Tomita, Nakanishi, Guillemot, & Kageyama, 1996). In addition, the homeobox gene *Vsx2* (*Chx10*), is required for bipolar cell specification (Hatakeyama, Tomita, Inoue, & Kageyama, 2001). *Vsx2* knockout mice show a complete loss of bipolar cells, and *Vsx2* has been shown play a role in the choice between bipolar and photoreceptor fate specification (Burmeister et al., 1996). Additionally, *Blimp1* (*Prdm1*) has been shown to be required for determining the ratio of bipolar cells to photoreceptors, as *Blimp1* removal generates more bipolar cells and fewer rods (Brzezinski, Lamba, & Reh, 2010; Brzezinski, Uoon Park, & Reh, 2013; Katoh et al., 2010; Wang, Sengel, Emerson, & Cepko, 2014). Other *Bhlh* family members have been described to play a role in the development of specific bipolar cell subtypes. For example, *Bhlhb23* (*Bhlhb4*) knockout mice show a near complete loss of rod bipolar cells by P12, although these cells are born, acquire their fate, and differentiate into PKC-positive rod

bipolar cells in early development (Bramblett, Pennesi, Wu, & Tsai, 2004).

While many genes that influence bipolar cell genesis and fate determination have been identified, less is known about those that specify cell number through other mechanisms, like that of cell death. As is true in many CNS tissues, it is known that some retinal populations are overproduced during development. Through cell-intrinsically defined programs, these cells undergo apoptosis leading to an overall reduction in the number of cells present in the mature retina from that in development (Linden, 2000; Linden, Martins, & Silveira, 2005; Pequignot et al., 2003; Young, 1984). Indeed, some bipolar cell subtypes undergo programmed cell death, including the rod bipolar and type 2 cone bipolar cells (Keeley, Madsen, St John, & Reese, 2014; Strettoi & Volpini, 2002).

Candidate genes controlling bipolar cell number therefore could play a role in many different developmental processes, including those of fate determination and/or cell death. Being that bipolar cells are the main relay cells between photoreceptors and ganglion cells, a change in their number could potentially cause a change in how information is processed in the retina. In the present study, I have sought to identify and test genes that modulate the number of bipolar cells. After first reviewing in detail our strategy for parsing a genomic region into a list of promising candidate genes, and then discussing the pursuit of a number of candidates participating in the control of cell number for a variety of subtypes, I will then focus in greater detail on two specific candidate genes that each contribute to the establishment of bipolar cell number.

### ***C. Methods***

#### **Bioinformatic Databases**

Chromosomal locations of candidate genes are found using NCBI gene (<https://www.ncbi.nlm.nih.gov/gene>). Variants within a genomic region are found using the Sanger Institute Mouse Genomes Project database (Keane et al., 2011; Yalcin et al., 2011), including coding variants like single nucleotide polymorphisms (SNPs) or small insertions/deletions (InDels) that fall within coding regions of the gene, thereby causing frameshift mutations, STOP mutations, missense mutations, or inframe InDels. Missense mutations are then run through the SIFT database, which predicts whether specific amino acid substitutions will be deleterious to protein function (Ng & Henikoff, 2003). This database is also used to identify regulatory variants that fall within 1 kilobase (kb) upstream of the transcriptional start site (TSS), which we have defined as the size of a putative promoter region, in addition to variants in 5' or 3' untranslated regions (UTR), downstream regions, or introns. In some instances, variants up to 5 kb upstream of the TSS are considered if they are predicted to be deleterious to gene expression, by creating or destroying transcription factor binding sites.

Retinal gene expression is first assessed using microarray expression data derived from whole eye mRNA across RI strains (GeneNetwork, BXD and AXB/BXA datasets). For genes that show promise as a candidate for further study, we can look for variation in the pattern of adult gene expression over time by using the mouse retina SAGE library (Blackshaw, Croix, Polyak, Kim, & Cai, 2007). Microarray expression data derived from whole retina mRNA (Siegert et al., 2012) can also be used to show expression differences relative to all genes expressed in maturity (hereinafter referred to as the Roska database).

Gene expression in postnatal development is assessed using microarray data from purified populations of retinal neurons at P6 (Kay, Chu, & Sanes, 2012). Variation in gene expression can also be correlated to phenotypic variation in cell number using the microarray data derived from ocular mRNA of the same RI strain-sets (Gene Network). Additionally, we can map QTL by using variation in gene expression as a trait and identify genomic loci for investigation, referred to as an expression-QTL or eQTL (GeneNetwork).

Known gene and protein functions were assessed via PubMed (<https://www.ncbi.nlm.nih.gov/pubmed/>) and UniProt ([www.uniprot.org](http://www.uniprot.org)) searches. Of particular interest are genes that have a documented role in developmental mechanisms such as fate determination, proliferation, differentiation, migration, or apoptosis. We also search the literature for known expression in the retina or other CNS tissue, as well as any information about protein expression and/or localization. Genes at all previously identified QTL intervals were subjectively ranked as described in Figure 4, while considering gene expression, genetic variants, and known function.

## **Mice**

*Lrrk1* knockout mice (FVB.Cg-*Pde6b*<sup>+</sup> *Lrrk1*<sup>tm1.1Mjff</sup> *Tyr*<sup>c-ch</sup>/J; #022880) were obtained from the Jackson Laboratories (Bar Harbor, ME). *Rbfox1* conditional knockout mice (B6.129S2-*Rbfox1*<sup>tm1.1Dbk</sup>/J; Jackson Laboratories, Bar Harbor ME; #014090) were provided by the laboratory of Dr. Thomas Cooper at Baylor College of Medicine in Houston, TX. Eyes from *Xkr8* knockout mice were provided by the laboratory of Dr. Shigekazu Nagata at Kyoto University in Japan (described in Suzuki, Denning, Imanishi, Horvitz, & Nagata, 2013). Eyes from *Hmgn 1/2/3* triple knockout mice (unpublished) were provided by the laboratory of Michael Bustin at the National Institutes of Health and



National Cancer Institute in Bethesda, MD (Hmgn2 single knockout mice were unavailable). Smad4 conditional knockout mice (*Smad4<sup>lox/lox</sup>;Tg-Six3Cre*) were provided by the laboratory of Dr. Yasuhide Furuta at the RIKEN Center for Developmental Biology in Kobe, Japan (described in Murali, Kawaguchi-Niida, Deng, & Furuta, 2011).

Electroporation studies were performed on CD1 mice (CrI:CD1; #022) obtained from Charles River Laboratories (Wilmington, MA). All imported mice were maintained in the UCSB Animal Resource Center. Experiments on them were conducted under the authorization of the Institutional Animal Care and Use Committee at UCSB, following guidelines outlined in the NIH *Guide for the Care and Use of Laboratory Animals*.

### **Tissue Preparation**

Animals were given a lethal dose of sodium pentobarbital or Euthasol (120 mg/kg, i.p.; Virbac, Fort Worth, TX). When unresponsive via tail-pinch, animals underwent an intracardial gravity perfusion with 2 ml of 0.9% sodium chloride followed by ~75mls of 4% paraformaldehyde (PFA) dissolved in 0.1M sodium phosphate buffer pH 7.2 for 15 minutes. Eyes were then removed from each mouse and left in the same fixative for an additional 15 minutes at room temperature. Eyes from animals P12 or younger, in addition to all electroporated animals, were immersed in fixative for 30 minutes in lieu of perfusion. Retinas were subsequently dissected in phosphate buffered saline (PBS) and given four radial cuts to allow them to lay flat. Retinas were then either immunostained as wholemounts or embedded in 5% agarose and sectioned perpendicular to the plane of the retina at a thickness of 150  $\mu$ m on a Vibratome.

### **Immunostaining**

Wholemount retinas or radial sections were immersed in PBS with 5% normal donkey

serum for three hours, rinsed three times in PBS (10 minutes per rinse), and then transferred to primary antibody for a duration of 72 hours. Retinas were then rinsed again for 30 minutes in PBS and transferred to a solution of secondary antibodies for a duration of 16 hours. After a final rinse with PBS for 30 minutes, samples were mounted onto glass slides using Fluoro-Gel with DABCO (Electron Microscopy Sciences, Hatfield, PA). All solutions were prepared in sodium phosphate buffer with 1.0% triton-X and were performed at 4°C under agitation. Table 1 lists the primary antibodies used for quantification of cell types of interest in Chapter 1. All secondary antibodies were raised in donkey and conjugated to AlexaFluor dyes (Jackson ImmunoResearch Laboratories, West Grove, PA; 1:200). Radial sections were also stained with Hoechst (Invitrogen, Eugene, OR; 1:1000) to label cell nuclei.

### **Image Acquisition and Quantification**

All micrograph images used for cell counts and measurements were acquired on an Olympus FV1000 scanning laser confocal microscope, with the exception of TH-positive cells that were counted using BioQuant Nova Software (BIOQUANT Image Analysis).

Total cell number counts for ChAT-positive cells in Rbfox1 mice were quantified from 8 fields per retina, at 4 central and 4 peripheral locations. Z-stack images were taken using either a 20× or 40× objective yielding field sizes of 0.4 mm<sup>2</sup> and 0.1 mm<sup>2</sup>, respectively. Total cell number counts were made by multiplying the average density of cells by the retinal area to yield animal averages. Cholinergic amacrine cells were identified by ChAT labeling within the cell soma for populations within the INL and GCL, while type 2 cone bipolar cells were identified by Syt2-positive axon stalks. All cells were manually counted from projection images so as to include all cells within a nuclear layer. Given their low

<b>Antibody</b>	<b>Abbreviation</b>	<b>Target</b>	<b>Supplier</b>	<b>Catalog Number</b>	<b>Dilution</b>
Mouse $\alpha$ Synaptotagmin2	Syt2	Type 2 cone bipolar cells	Santa Cruz Biotechnologies (Santa Cruz, CA)	SC6026	1:250
Mouse $\alpha$ Protein Kinase C	PKC	Rod bipolar cells	Millipore (Temecula, CA)	05-983	1:500
Sheep $\alpha$ Tyrosine Hydroxylase	TH	Dopaminergic amacrine cells	Millipore (Temecula, CA)	AB152	1:10,000
Goat $\alpha$ Choline Acetyltransferase	ChAT	Cholinergic amacrine cells	Millipore (Temecula, CA)	AB144P	1:50
Goat $\alpha$ Xkr8	-	-	Santa Cruz Biotechnologies (Santa Cruz, CA)	SC249360	1:100
Rabbit $\alpha$ Green Fluorescent Protein*	GFP	-	Molecular Probes (Waltham, MA)	A21311	1:1,000

\* conjugated to Alexa Fluor 488

**Table 1.** Primary antibodies used in Chapter 2.

density compared to other retinal cells, dopaminergic amacrine cell number was acquired by counting all TH-positive cells across the INL in the entire whole-mounted retinas from *Lrrk1* mice.

To quantify the thickness of retinal layers for *Hmgn1/2/3* and *Lrrk1* mice, two 40× magnification images were taken per retinal section, each about 0.7 mm from optic nerve head in either direction. Using Fiji software (<https://fiji.sc/>), images were then divided into 10 equal portions whereby the thickness of the outer nuclear layer, outer plexiform layer, inner nuclear layer, inner plexiform layer, and ganglion cell layer was measured at each location to account for any variability within a section. All 10 measurements were then averaged to yield mean thickness measurements per retinal layer and were added together to get a total retinal thickness measurement.

### ***In Vivo* Overexpression via Electroporation**

Electroporation studies were performed on CD1 mice obtained from Charles River Laboratories (Wilmington, MA). Experimental conditions were adapted from Matsuda & Cepko (2004) with adjustments made to optimize plasmid concentration (~1500 ng/μl) and injection volume (0.6-0.8 μl per retina). We performed our surgeries on P2 animals, in order to maximize the likelihood of bipolar cell transfection, given that this age directly coincides with the peak of bipolar cell neurogenesis. For construction of overexpression plasmids, cDNA clones were acquired from the mammalian gene collection (MGC) from GE Healthcare Dharmacon (Lafayette, CO). The MGC clone identification numbers for each gene were: *Dhdds* – 3493585; *Egfr* – 5351807; *Urgcp* – 5696000; *Dtx4* – 6405881; *Ccm2* – 4952288; *Zmiz2* – 30354393; *Xkr8* – 5698137; *Ggct* – 30286931. Coding regions from genes of interest were amplified via PCR and cloned into a pCAGIG backbone

(Addgene plasmid, Cambridge, MA; # 11159), which was also used as a control plasmid, and driver by a CAG promoter. The bicistronic pCAGIG vector also has an IRES site that drives GFP. All gene inserts were ligated into the EcoRI and NotI restriction sites (except Dtx4, which used EcoRV and NotI given that an EcoRI site is present in the coding region) in the pCAGIG multiple cloning site using the Instant Sticky-end Ligase Master Mix (New England BioLabs Inc., Ipswich, MA; #M0370L). The genetic sequences that were amplified and cloned into the pCAGIG vector are listed in Appendix A.

Electroporations are carried out on P2 animals. Pups are placed on ice for 3 minutes to induce hypothermia, after which pressure is applied to the tail to confirm a cessation of movement. The fused skin of the presumptive eyelid is cleaned with a sterile cotton-swap of 70% ethanol and severed with a sterile sharp 27.5 gauge needle. This needle is then used to puncture a small hole in the sclera of the eye, near the limbus, to allow for entry of the injection needle. A 32 gauge Hamilton syringe is then inserted into this hole and once resistance is felt from the inside wall of the retina, the plasmid is injected into the sub-retinal space, between the retinal pigment epithelium and the retina. The plasmid solution is pre-mixed with 0.1% of fast-green dye tracer to aid in visualizing placement of the plasmid solution. The needle is then slowly removed from the eye and electroporation paddles, coated with PBS to increase conductivity, are then placed on either side of the head with the positive electrode on the side in which an injection was made. Five 50 ms square wave pulses with 950 ms intervals of 80V is delivered via foot switch (BTX ECM 830, Holliston, MA). The current flows in a negative to positive direction and creates temporary pores in the plasma membrane of diving cells, through which the plasmid can enter, so that only cells undergoing division are effectively electroporated. Previously published research using this

approach has been ineffective at transfecting post-mitotic cells that have already been born such as retinal ganglion cells and horizontal cells. Rather, the plasmid is only effectively delivered into dividing progenitor cells, and then passed along to their progeny and all cells descending from them, generating mostly bipolar cells and photoreceptors at this age (Matsuda & Cepko, 2004). Following the electroporation, two drops of 0.5% proparacaine (Henry Schein Animal Health, Reno, NV; #035908) are then applied to the injected eye and animals are placed on a platform resting in a 42°C water bath. Pups are then immediately returned to their mother upon regaining ambulation and vocalization.

At P21, mice were euthanized with a lethal dose of 120 mg/kg of Euthasol via intraperitoneal injection and their eyes were subsequently dissected from the orbits, and then immersed in 4% paraformaldehyde for 30 minutes as previously described. About 30% of all electroporated retinas appeared small and underdeveloped, presumably due to mechanical damage during surgery, and were not used for quantification. The remaining retinas were dissected and immunostained as wholemounts with an  $\alpha$ GFP antibody and Hoechst. Retinas were then scanned for GFP-positive regions ensuring an efficient electroporation. Those retinas exhibiting GFP-positive (GFP+) regions were sectioned and all sections exhibiting GFP immunofluorescence were quantified. An average of 10 sections were quantified per retina, with each retina containing an average of 910 GFP-positive cells and all sections were counted blind to genotype.

We observed GFP-positive cells in the ONL and INL only (but not the GCL), as expected given the windows of neurogenesis for cells occupying these layers. Recognizing that we are unable to count absolute numbers of GFP-positive cells between conditions due to variability in transfection efficiency, instead we documented the relative frequency of

cells in three retinal subdivisions, the ONL (photoreceptors), outer INL (bipolar cells), and inner INL (amacrine cells). GFP-positive Müller cells, residing in the middle of the INL, were binned into outer INL or inner INL categories based upon subjective determination of the side in which more than 50% of their soma was positioned (see Figure 5).

Consequently, our intended strategy has been to see if we can affect the proportion of GFP+ cells that are bipolar cells. We consider in further detail in the discussion section what biological processes may be altered by this overexpression strategy to yield such a change.

### **Real-time quantitative PCR (qPCR)**

A minimum of 6 retinas were collected from 3 separate litters of A/J and B6/J animals at P1, P5, and P10 in RNase-free conditions. RNA was extracted using an RNeasy Plus Mini Kit (Qiagen, Hilden, Germany) and single-stranded cDNA was synthesized using the iScript cDNA synthesis kit (Bio-Rad, Hercules, CA). Expression levels of *Xkr8* and *Ggct* were measured using the CFX96 Touch Real-Time PCR detection system in conjunction with the SsoAdvanced Universal SYBR Green Supermix (Bio-Rad, Hercules, CA), using the recommended product protocol and empirically determined annealing temperatures for each primer set. Each primer set was run on a separate plate and all samples were run in triplicate (outliers, defined as samples more than two standard deviations from the triplicate mean, were removed). RNA abundance was corrected for product size, primer melting temperature, and primer efficiency, which was determined by creating a standard curve for each primer pair. Levels of *Xkr8* and *Ggct* expression were normalized to the geometric mean of three control genes, Glyceraldehyde 3-phosphate dehydrogenase (*Gapdh*), TATA-

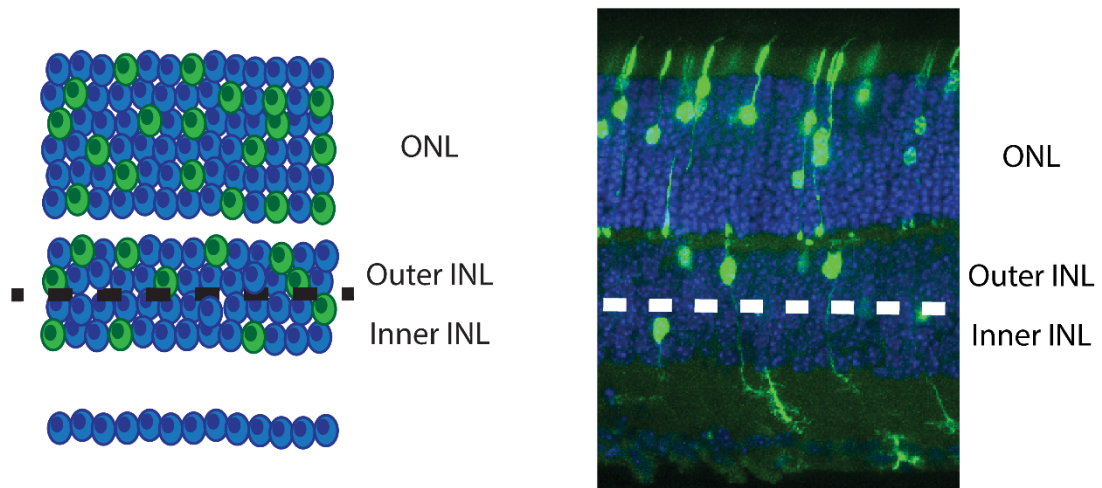


**Figure 5. Electroporation quantification.** Schematic representation (left) and real micrograph (right) depicting the three retinal layers from which we quantified GFP-positive cells. The INL is subjectively divided in half and cells are placed into the category for which more than 50% of their soma resides. ONL = outer nuclear layer, INL = inner nuclear layer, GFP = green fluorescent protein.



binding protein (TBP), and  $\beta$ -2 microglobulin ( $\beta$ 2M). The primer sequence, product size, annealing temperature, and calculated efficiency for each primer set are listed in Table 2.

### **Luciferase Assay**

Plasmid inserts were made by amplifying the A/J or B6/J sequence of interest from DNA isolated from tail tissue samples. The following PCR primers were used to amplify *Xkr8* and *Ggct* promoter sequences, including adapters and restriction enzyme sequences listed 5' to 3' (*Xkr8* forward: TAAGCACTCGAGGCAGTCGTCCGGGAGGCTGG; *Xkr8* reverse: GTGCTCGATGCGGCAGCTGGGTACCTAAGCA; *Ggct* forward: TAAGCAGAGCTCGAACTCACAGAGAACTGCCTGCCTC; *Ggct* reverse: TAAGCAAAGCTTCAGAGAAGCCGGACTAGCGCTG). *Xkr8* ligations were performed using the Instant Sticky-end Ligase Master Mix (New England BioLabs Inc., Ipswich, MA; #M0370L) with a three-fold molar excess of insert to backbone. A seven-fold molar excess of insert was ligated into the backbone using T4 ligase for *Ggct* ligations. The *Xkr8* fragment was cloned into the multiple cloning site using *KpnI* and *XhoI* restriction sites, while *Ggct* used *SacI* and *HindIII*. Following ligation, all plasmids were transformed into One Shot MAX Efficiency DH5 $\alpha$ -T1 chemically competent *E. coli* (Life Technologies, Carlsbad, CA; #12297016). The destination vector, also used as a control, was the pGL3-basic vector (Promega, Madison, WI; #E175A).

Experimental plasmids, in addition to a control plasmid expressing only GFP with no gene of interest inserted, were transiently transfected into HEK293T cells. The cells were grown in high glucose (4.5 g/L) DMEM media plus 10% FBS, with penicillin (100 U/mL) and streptomycin (100  $\mu$ g/mL), in a T75 tissue culture flask. When the cells reached 80% confluence they were passaged, and plated in 12-well tissue culture plates at  $1.5 \times 10^5$  cells

<b>Gene</b>	<b>Forward Primer Sequence (5' to 3')</b>	<b>Reverse Primer Sequence (5' to 3')</b>	<b>Product Size (basepairs)</b>	<b>Annealing Temperature (°C)</b>	<b>Calculated Efficiency</b>
<i>Ggct</i>	CGTTTGCGAA CAGGAGTCTG	GTCTAAGCCCA TCCCCATTCC	130	63	101%
<i>Xkr8</i>	CGGCTCAGAA GATCACTTCC	ACCCATTGTTC CAGTGAAGG	105	63	94%
<i>Gapdh</i>	AACTTTGGCA TTGTGGAAGG	GGATGCAGGGA TGATGTTCT	132	60	98%
<i>TBP</i>	CTCAGTTACA GGTGGCAGCA	CAGCACAGAGC AAGCAACTC	120	61.5	94%
<i>β2M</i>	GAGCCCAAGA CCGTCTACTG	GCTATTTCTTT CTGCGTGCAT	134	61.5	97%

**Table 2.** Real-time quantitative PCR primer sequences, product sizes, annealing temperatures, and calculated efficiencies.

per well. Media was changed 24 h after plating, and cells were transfected 48 h after plating, with the proprietary transfection reagent TurboFect (Thermo Scientific, Carlsbad, CA; #R0531). 400 ng of *experimental* or control plasmid was transfected into each well, with 20 ng of  $\beta$ -galactosidase ( $\beta$ -gal), and the transfectant was removed within 16 h. Cell lysates were collected 24 h from the start of transfection using 100  $\mu$ l per well of cold 1X Passive Lysis Buffer (Promega, Madison, WI; #E1941).

Cell lysates were assayed for luciferase (Promega) and  $\beta$ -Gal activity on a Perkin-Elmer plate reader, and 3 wells of the same condition were assayed and averaged to serve as internal experimental replicates. Luciferase units were corrected by subtraction of untransfected well units, and then were normalized using  $\beta$ -Gal. *Xkr8* results are representative of three independent experiments. Each independent *Ggct* experiment yielded similar results, although the magnitude of the change exhibited high variability, and therefore only one experiment is represented in Figure 20c (averages of three transfected wells per condition are shown).

### **Statistics**

Comparisons between *Xkr8* KO and Het conditions were tested for statistical significance using a Student's two-tailed t-test. In addition, *Xkr8* overexpression versus control quantification was tested for statistical significance using a Student's two-tailed t-test. Results from qPCR experiments were tested for statistical significance between strains of mice, across developmental ages, and for an interaction between strain and age using a two-way ANOVA. All statistical analyses were performed using SPSS Statistics (IBM, Armonk, NY).

## ***D. Results***

### **1. Selection of Candidate Genes from Cell Number QTL**

As previously described, our lab has collected cell number estimates for twelve different retinal populations and mapped QTL for each of these traits, thereby defining genomic intervals where potential genes controlling these traits reside (Keeley, Whitney, et al., 2014). These QTL are depicted in Figure 6, whereby red arrows denote the location of QTL that were investigated in this dissertation.

Using either gene knockout, conditional knockout, or overexpression strategies, we tested the function of 11 genes that were hypothesized to play a role in the establishment of neuronal cell number after determining their expression in the retina in development and/or maturity, the presence of genetic variants discriminating A/J and B6/J strains, and a relevant biological function. Nine of these genes, the criteria used to select them, and the method by which they were tested are described in Table 3. The remaining two genes will be subsequently described in detail.

*Lrrk1*, *Rbfox1*, and *Hmgn2* candidates were tested via knockout or conditional knockout strategies due to the availability of mice or tissue. For each gene, we employed a slightly different analysis strategy for assessing changes to cell number due to tissue availability, condition, and the cell type in question. When applicable, total cell number estimates were made from wholemounts. Total cell number estimates were acquired for dopaminergic amacrine cells in *Lrrk1*-KO mice, and cholinergic amacrine cells in *Rbfox1*-CKO mice. In some instances we can use the relative thickness of each retinal layer as an indication of major alterations in the number of cells residing therein, if cell-type-specific counts cannot be completed. These measurements of retinal thickness in sectioned tissue were assessed in

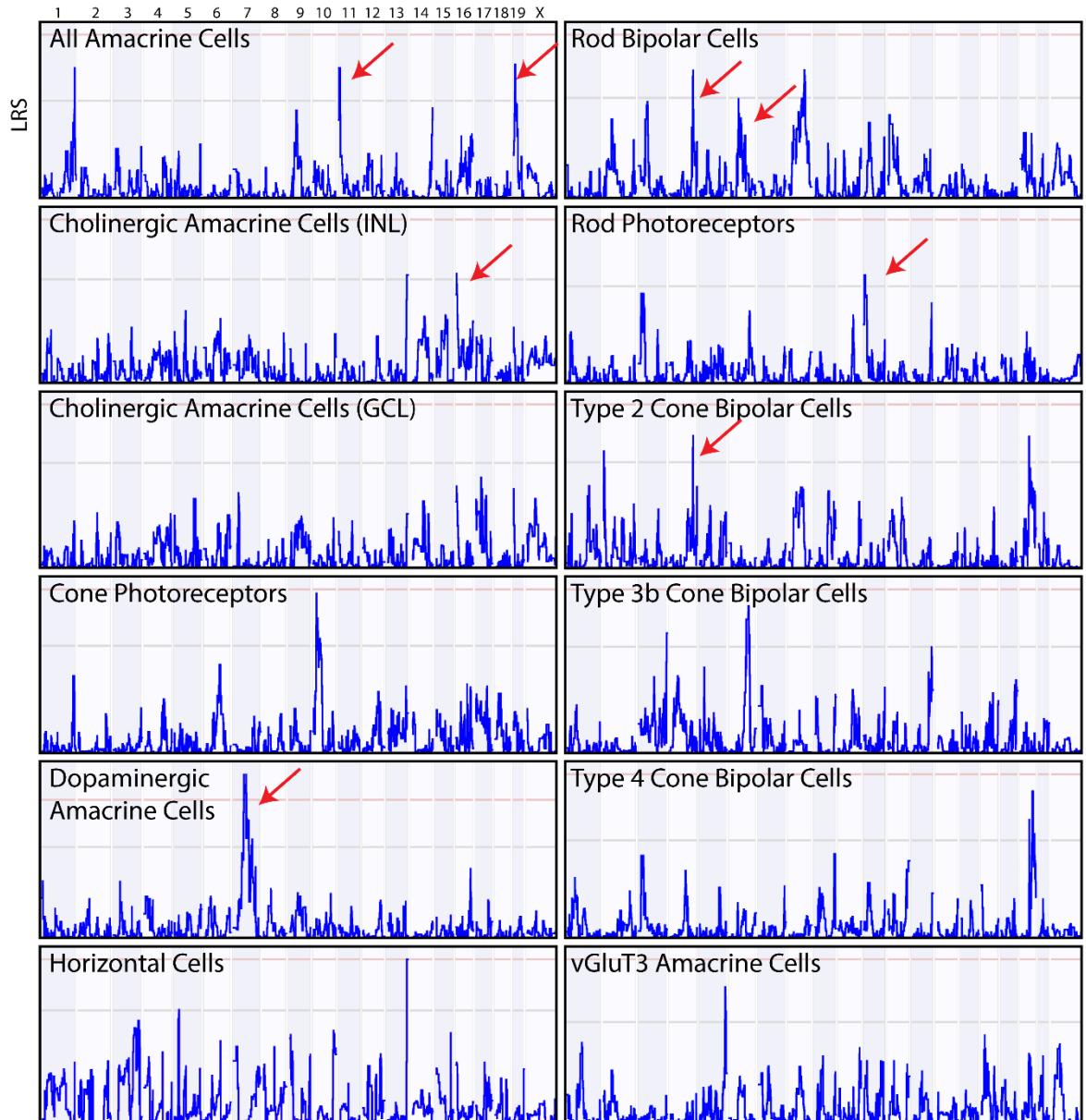


**Figure 6. QTL mapped for 12 retinal cell types.** Blue traces represent LRS scores, across the genome from left to right, for each of the 12 cell number traits quantified. Red arrows denote QTL that were examined in this study. LRS = likelihood ratio statistic.

Gene	Trait	Chr	Retinal Expression	Variants	Relevant Literature / Function	Method of Testing
<i>Lrrk1</i>	Dopaminergic amacrine cell number	7	X	X	Variants implicated in Parkinson's disease pathogenesis (Biskup et al., 2007; Taylor et al., 2007)	Knockout mouse
<i>Rbfox1</i>	INL cholinergic amacrine cell number	16	X	X	Regulates alternative splicing events in neurodevelopmental disorders (Fogel et al., 2014)	Conditional knockout mouse
<i>Hmgn2</i>	Rod bipolar cell number and type 2 cone bipolar cell number	4	X	X	Unfolds chromatin and enhances DNA replication (Kulkeaw 2012)	Knockout mouse
<i>Dhdds</i>	Rod bipolar cell number and type 2 cone bipolar cell number	4	X	X	Knockdown causes photoreceptor degeneration in zebrafish (Wen et al., 2014)	<i>In vivo</i> electroporation
<i>Egfr</i>	Rod and AII cell number	11	X	X	Leads to cell proliferation by binding to epidermal growth factor (Fraguas 2011)	<i>In vivo</i> electroporation
<i>Urgcp</i>	Rod and AII cell number	11	X	X	May contribute to cell growth and survival in cancer models (Dodurga 2002)	<i>In vivo</i> electroporation
<i>Dtx4</i>	AII cell number	19	X	X	Regulator of Notch signaling (Endo 2003)	<i>In vivo</i> electroporation
<i>Ccm2</i>	Rod and AII cell number	11	X	X	May function as a scaffold protein for MAP2K3-MAP3K3 signaling (Fong et al 2007)	<i>In vivo</i> electroporation
<i>Zmiz2</i>	Rod and AII cell number	11	X	X	Increases transcriptional activity of nuclear hormone receptors (Peng 2010), Regulates Wnt/ $\beta$ -catenin signaling (Lee et al 2013)	<i>In vivo</i> electroporation

**Table 3.** Traits, chromosomal location, selection criteria, and method of investigation for candidate genes controlling neuronal cell number.

*Hmgn1/2/3*-KO and additionally in *Lrrk1*-KO mice.

*Lrrk1* was a particularly promising candidate gene at the peak of the QTL on Chr 7 for dopaminergic amacrine cell number, because a related gene, *Lrrk2*, has been shown to play a role in Parkinson's disease (reviewed in Cookson, 2010). Upon counting the total number of dopaminergic amacrine cells in littermate KO and control retinas, however, no significant differences were detected (Figure 7a), and subsequent analysis of retinal histology confirmed no changes in the thickness of the various retinal layers nor changes on retinal histology (Figure 7b).

*Rbfox1* stood out as a strong candidate gene at the peak of the QTL on Chr 16 for cholinergic amacrine cell number in the INL, being the only gene present at this narrow interval. It is heavily expressed in cholinergic amacrine cells, making it particularly attractive (Roska database). In addition, it has been shown to play a role in neurodevelopmental disorders by regulating alternative splicing events (Fogel et al., 2012). We generated conditional KO mice, by excising *Rbfox1* from cholinergic amacrine cells exclusively, yet found no effect upon the size of the population of cholinergic amacrine cells in the INL, nor those situated in the GCL (Figure 7c).

*Hmgn2* was a top candidate at the Chr 4 locus for controlling rod bipolar cell number, given that it maps a significant *cis*-eQTL (LRS = 25.7), has high expression in the developing and adult retina across many cell types (Roska database, SAGE database, and Lucey, Wang, Bustin, & Duncan, 2008), and is known to play a role in the enhancement of DNA replication and regulates transcription (Kulkeaw et al., 2012). *Hmgn2* belongs to a family of five proteins that all share a similar structure and are thought to have some functional redundancy (Hock, Furusawa, Ueda, & Bustin, 2007; Rochman et al., 2011).

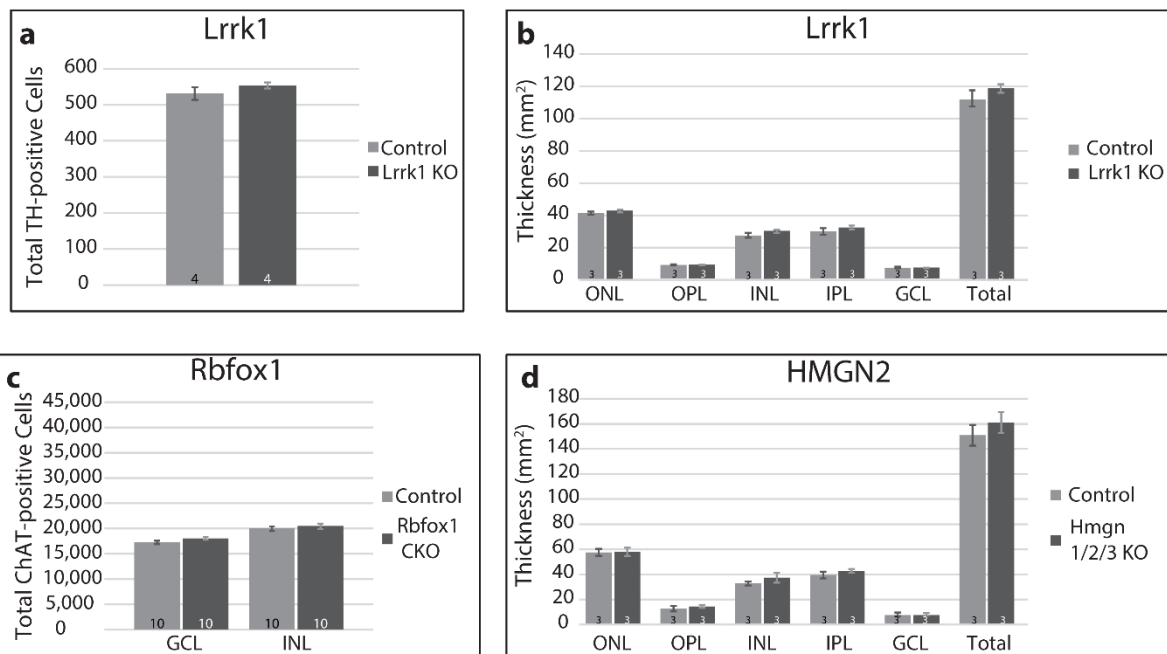


**Figure 7. Quantification of cell number changes in candidate gene knockout and conditional knockout mice.** The total number of TH-positive dopaminergic amacrine cells (a) and retinal thickness (b) is unaltered in *Lrrk1*-KO mice compared to controls. *Rbfox1*-CKO mice exhibit no change in the number of ChAT-positive cholinergic amacrine cells in the GCL or INL (c). Retinal thickness in *Hmgn 1/2/3*-KO mice appears normal, compared to control animals (d). ONL = outer nuclear layer, IPL = inner plexiform layer, INL = inner nuclear layer, IPL = inner plexiform layer, and GCL = ganglion cell layer.



*Hmgn2*-KO mice were unavailable but given the potential redundancy amongst family members, we assessed changes to the retinal architecture in *Hmgn1/2/3* triple KO mice that were available, and detected no change to retinal thickness between KO and control conditions (Figure 7d).

*Dhdds*, *Egfr*, *Urgcp*, *Dtx4*, *Ccm2*, and *Zmiz2* are candidate genes that were examined by overexpression via *in vivo* electroporation, given the lack of available KO and/or CKO mice. We adopted the strategy of *in vivo* electroporation as a way to screen potentially interesting genes for a role in influencing cell number. Our strategy was to overexpress genes of interest, and to assess their effects upon the relative number of cells in the ONL versus the INL, as well as between the inner (amacrine cell) and outer (bipolar cells) divisions of the INL. We first targeted five different promising candidate genes that were positioned at the QTL on Chrs 4, 11, and 19 for rod and type 2 cone bipolar cells, rod and AII amacrine cells, and AII amacrine cells, respectively, focusing on these because each of them had prospective regulatory or coding variants and retinal expression. In addition, *Ccm2* and *Dtx4* expression levels map a *cis*-eQTLs. None of them, however, affected the relative frequency of GFP-positive cells in the ONL, outer INL, or inner INL compared to that of all combined control animals. Given that these three retinal layers include the target cells of interest and were unaltered post-electroporation, we concluded that these genes do not significantly play a role in the modulation of retinal cell number and were therefore not pursued further. These results are summarized in Figure 8.

While this degree of negative results was initially discouraging and led us to wonder whether the electroporation strategy might be suffering some other technical difficulty preventing us from seeing any clear effect using this overexpression strategy, two

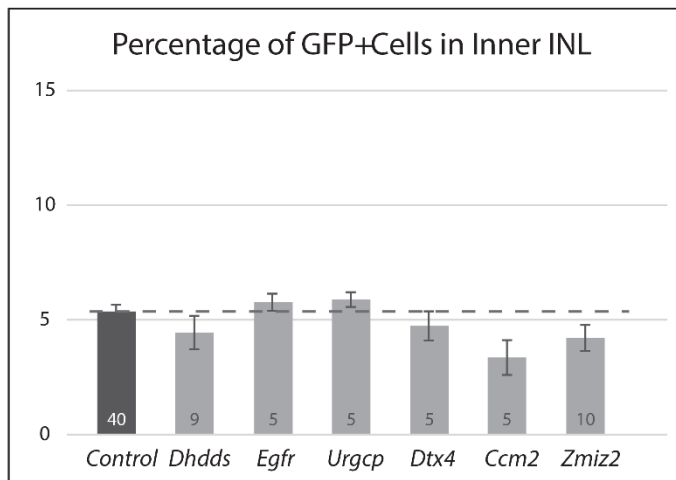
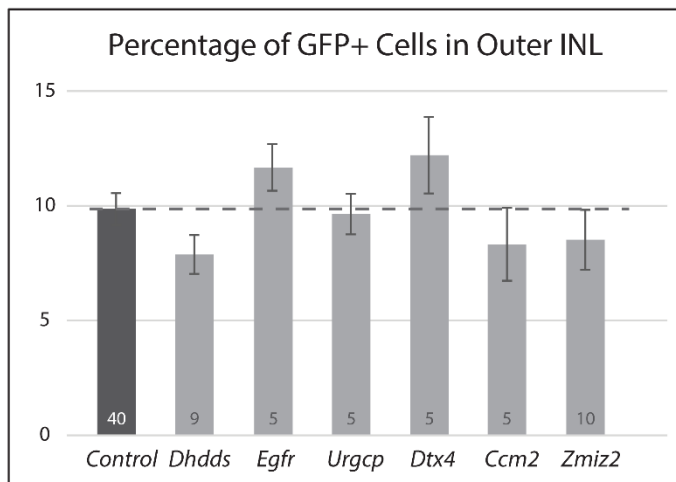
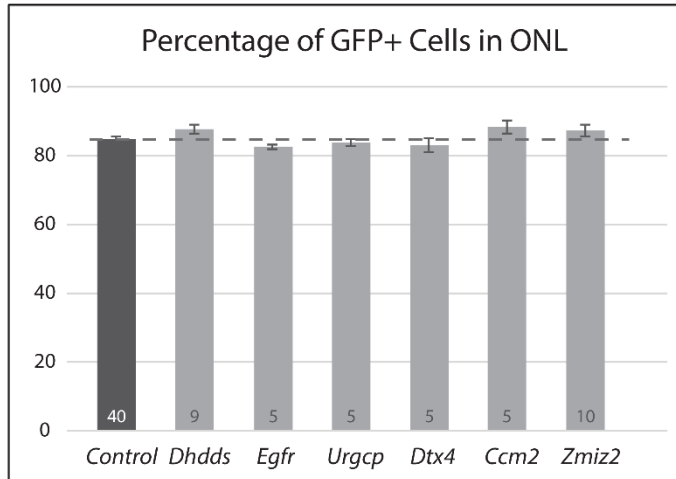


**Figure 8. Candidate genes tested via *in vivo* electroporation.** The percentage of GFP-positive cells in the ONL, outer INL (bipolar cell layer), and inner INL (amacrine cell layer) is unchanged between *Dhdds*, *Egfr*, *Urgcp*, *Dtx4*, *Ccm2*, and *Zmiz2* overexpression retinas and control retinas. Dashed line represents average percentage for control retinas. Histograms = mean +/- s.e.m.

subsequent genes did in fact generate striking effects using this approach. These negative results therefore lend credence to the specificity of the effects for these two genes, which will be described next in far greater detail, including subsequent studies to explore their expression across the tissue and through time during development, as well as to test particular variants directly through luciferase expression assays.

## **2. Rod Bipolar and Type 2 Cone Bipolar Cell Number**

Previous research examining 12 different retinal subtypes observed minimal covariation in cell number (Keeley, Whitney, et al., 2014). Interestingly, this was true of both developmentally related genes as well as synaptically connected genes. For example, cell number was not significantly correlated between the two developmentally-related subtypes of photoreceptor cells. Furthermore, rod photoreceptor cell number is not significantly correlated to rod bipolar cell number across RI strains, although these subtypes are synaptically coupled. These data indicate that cell number may be modulated differentially across individual populations of cells. One of the few exceptions to this lack of covariation exists between two subtypes of bipolar cell; the rod bipolar and type 2 cone bipolar cell number are significantly (if not strongly) correlated ( $p = 0.0042$ ) across the RI strains (Figure 9a). This suggests potential co-regulation of their number, whereby one variant may selectively influence cell number in these two types of bipolar cells through a comparable developmental process. For this reason, among others that will be discussed, we specifically focused our efforts towards exploring genes that regulated bipolar cell number.

The number of rod bipolar cells and type 2 cone bipolar cells had been previously determined for the parental strains, A/J and B6/J, and all 26 RI strains (Figure 9b,c) (Keeley, Whitney, et al., 2014). Rod bipolar cell number varied across RI strains from 202,415 cells

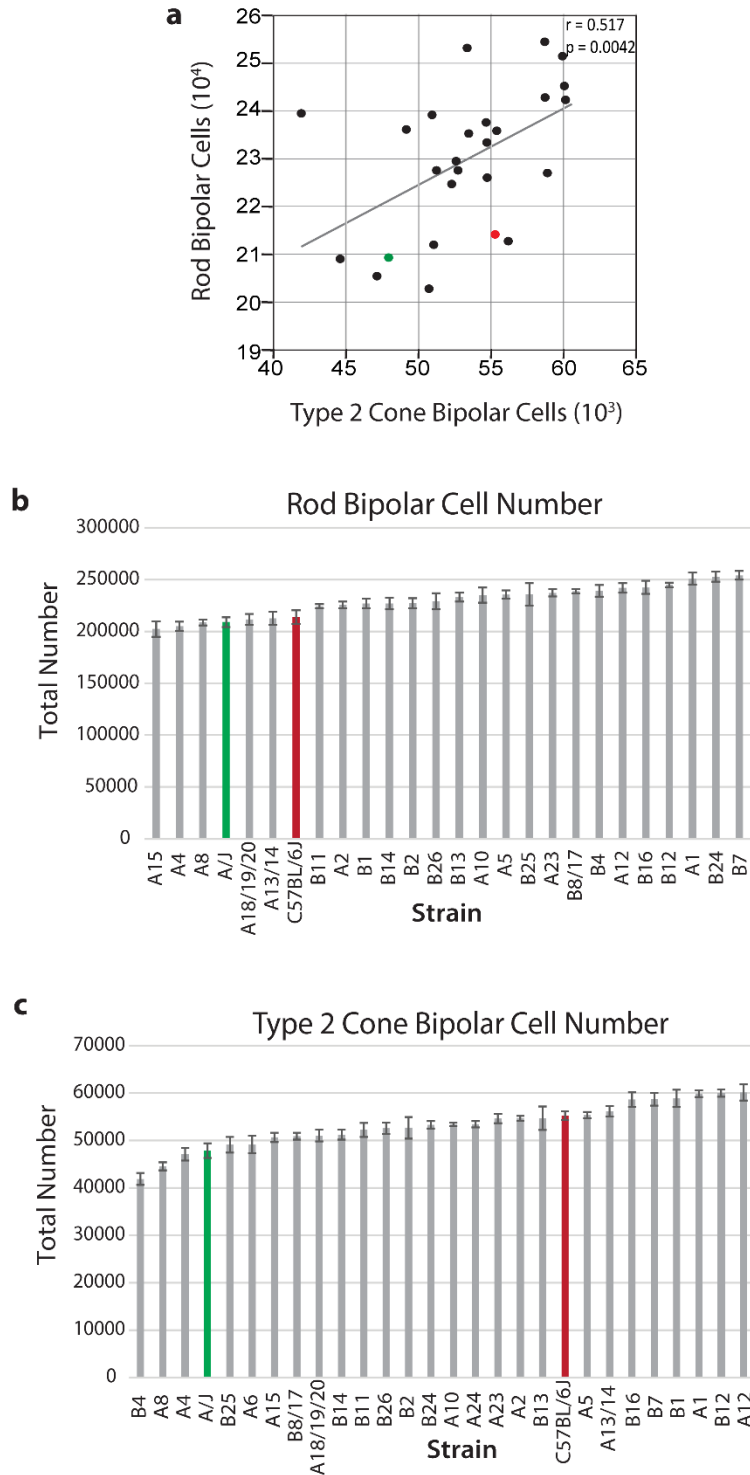


**Figure 9: Distribution of cell number across recombinant inbred strains.** Rod bipolar cell and type 2 cone bipolar cell number are significantly correlated across recombinant inbred and parental strains (a). Rod bipolar cell (b) and type 2 cone bipolar cell number (c) vary across the AXB/BXA recombinant inbred strains (gray bars), plotted here from lowest to highest strain. The A/J (green bars) and B6/J (red bars) parental strains fall at varying positions in each distribution. Histograms = mean  $\pm$  s.e.m.

to 254,176 cells, thereby showing a 26% increase from lowest to highest strains (Figure 9b). As has been shown (Keeley, Whitney, et al., 2014), the coefficient of variation (CoV), measured as the standard deviation divided by the mean, averaged 0.05 across all strains, indicating meager variability within any strain despite the conspicuous variation across the strains. Type 2 cone bipolar cells showed an even larger (45%) increase in cell number across RI strains, ranging from 41,908 to 60,570 cells (Figure 9c). These cell counts showed a similar degree of consistency within each strain, with an average CoV of 0.05.

### **3. Interval Analysis**

The variation in rod bipolar cell number mapped three QTL on Chromosomes (Chr) 4, 6 and 8 (Figure 10a, red arrows). At each QTL, an interval was defined as the region of strongest association between genotype and trait of interest as indicated by the likelihood ratio statistic (LRS, blue traces in Figures 10a-b). The locus on Chr 4 spans a genomic region from 131.5 Megabases (Mb) to 133.5 Mb, containing 55 genes (Figure 10c). The chromosome 6 QTL spanned from 52.1 Mb to 57.1 Mb and contained 70 genes. Lastly, the locus on Chr 8 contained 96 genes between 90.7 Mb and 98.2 Mb.

The variation in type 2 cone bipolar cell number across RI strains mapped three QTL on Chrs 2, 4, and 18 (Figure 10b, red arrows). The intervals on Chrs 2 and 18 each contained a small number of genes, 15 and 20 respectively, with the interval on Chr 2 spanning from 3 Mb to 4.2 Mb and the interval on Chr 18 from 49.9 Mb to 53.5 Mb. Interestingly, the QTL on Chr 4 for type 2 cone bipolar cell fell precisely at the same location as the QTL peak for rod bipolar cell number on Chr 4. The interval on Chromosome 18 is believed to be a potentially spurious one, given that much of that locus on the chromosome was unable to be genotyped, and for that reason was not investigated. The intervals at the remaining rod

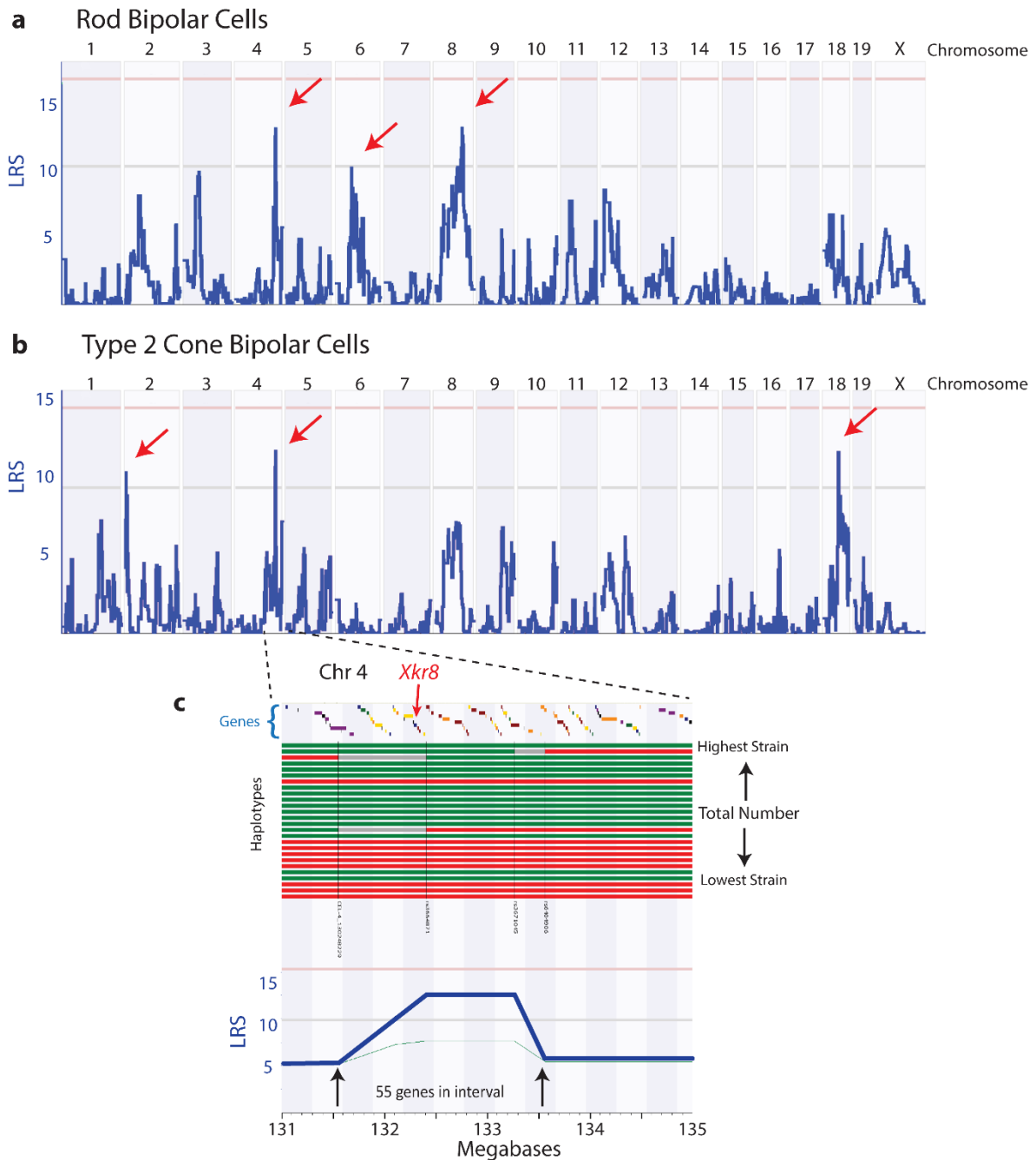


**Figure 10: QTL mapping for rod bipolar and type 2 cone bipolar cells.** Interval mapping of the variation in rod bipolar cell number reveals three QTL (red arrows), one on Chr 4 (likelihood ratio statistic [LRS] = 13.99), one on Chr 6 (LRS = 26.4), and one on Chr 8 (LRS = 12.7), indicated by the blue trace (a). Variation in type 2 cone bipolar cell number maps QTL to Chrs 2 (LRS = 11.05), 4 (LRS = 12.55), and 18 (LRS = 11.7) (b). Horizontal lines indicate suggestive threshold (gray line) and significant thresholds (pink line). Chr 4 map shows QTL in greater detail (c). Haplotype blocks indicate the allele present at each genotyped location (black vertical lines) with green, red, and gray bars indicating A/J, B6/J, and unknown haplotypes, respectively. Colored boxes at the top of the map represent the location of genes across the chromosome. The interval from 131.5 Mb to 133.5 Mb was selected for further investigation and included 55 genes, one of which is *Xkr8*.

bipolar cell and type 2 cone bipolar cell QTL, were interrogated to determine top candidate genes based on criteria described above in Figure 4. Appendices B, C, and D show the analysis that was done on the genes present at the QTL on Chromosomes 4, 6, and 8 respectively, including *Xkr8* and *Ggct* which together will constitute the remaining focus of this chapter. Genes highlighted in green contained coding variants and/or a *cis*-eQTL. Coding variants occur much less frequently than regulatory ones and have the potential to disrupt gene function in a straightforward way, i.e. by rendering a gene non-functional via the creation of an early STOP codon, or by altering protein structure in a manner that alters its functional efficiency. For this reason, we chose to prioritize genes with coding versus regulatory variants for primary investigation. In addition, genes with *cis*-eQTLs are those that likely have one or many variants within the gene itself that alters its own expression. This could provide a direct link between expression of a gene and changes in cell number. The presence of a *cis*-eQTL, therefore, makes a gene a strong candidate for further study. While many of genes highlighted in green at Chrs 4, 6, and 8 deserve future scrutiny, two genes in particular were studied in detail and will constitute the remainder of the experimental studies in this chapter.

#### **4. Candidate Gene Selection: *Xkr8***

The gene *Xkr8*, or X Kell blood group precursor related family member 8 homolog, was identified as a top candidate gene at the Chr 4 QTL, for rod bipolar cell and type 2 cone bipolar cell number. *Xkr8* belongs to a large family of evolutionarily conserved XK proteins the functions of which are not well understood (Calenda et al., 2006). Interestingly however, *Xkr8* has recently been shown to play a role in promoting phosphatidylserine exposure on the surface of dying cells (Suzuki et al., 2013; Suzuki, Imanishi, & Nagata,

2014). In addition, recent studies suggest that rod bipolar and type 2 cone bipolar cells undergo substantial apoptosis, given that cell number is increased in both of these populations in *Bax* KO mice that lack the pro-apoptotic gene *Bax*. (Keeley, Madsen, et al., 2014). This role in the apoptotic pathway provides a potential mechanism for how *Xkr8* expression may influence bipolar cell number in the retina

There is no recognized role for *Xkr8* in the retina but microarray data shows it is expressed throughout development and into adulthood (Retina SAGE Database). *In situ* hybridizations performed in our laboratory confirm it is heavily expressed in the ONL and INL in adult mouse retinal tissue (Figure 11a,b). *Xkr8* immunohistochemistry performed on wildtype B6/J sections at P3, P6, and P11 confirmed expression in the developing retina as well (Figure 11c-e). *Xkr8* is expressed in migrating progenitor cells in the neuroblastic layer at P3 but then becomes localized to inner portions of the retina at later developmental ages, with the densest labeling detected in the INL by P11 (Figure 11c-e). Adult tissue shows a similar pattern, however the protein appears to be expressed throughout the entire cell in adulthood, while it appears localized to nuclei in development (Figure 11f-i). This may be biologically relevant given that *Xkr8* is known to play a role in trafficking proteins to the cellular membrane, yet this hypothesis remains to be determined. *Xkr8* protein appears to be expressed differentially within populations where some cells are more brightly stained than others in the GCL, inner INL (amacrine cell layer), and outer INL (bipolar cell layer) (Figure 11f-h). We confirmed the specificity of the antibody using retinal sections from *Xkr8* knockout animals, where we detected a complete loss of staining in all retinal layers, minus some non-specific staining seen on the retinal surface (Figure 11i,j). Taken together, these data indicate that *Xkr8* is expressed in both the developing and mature retina



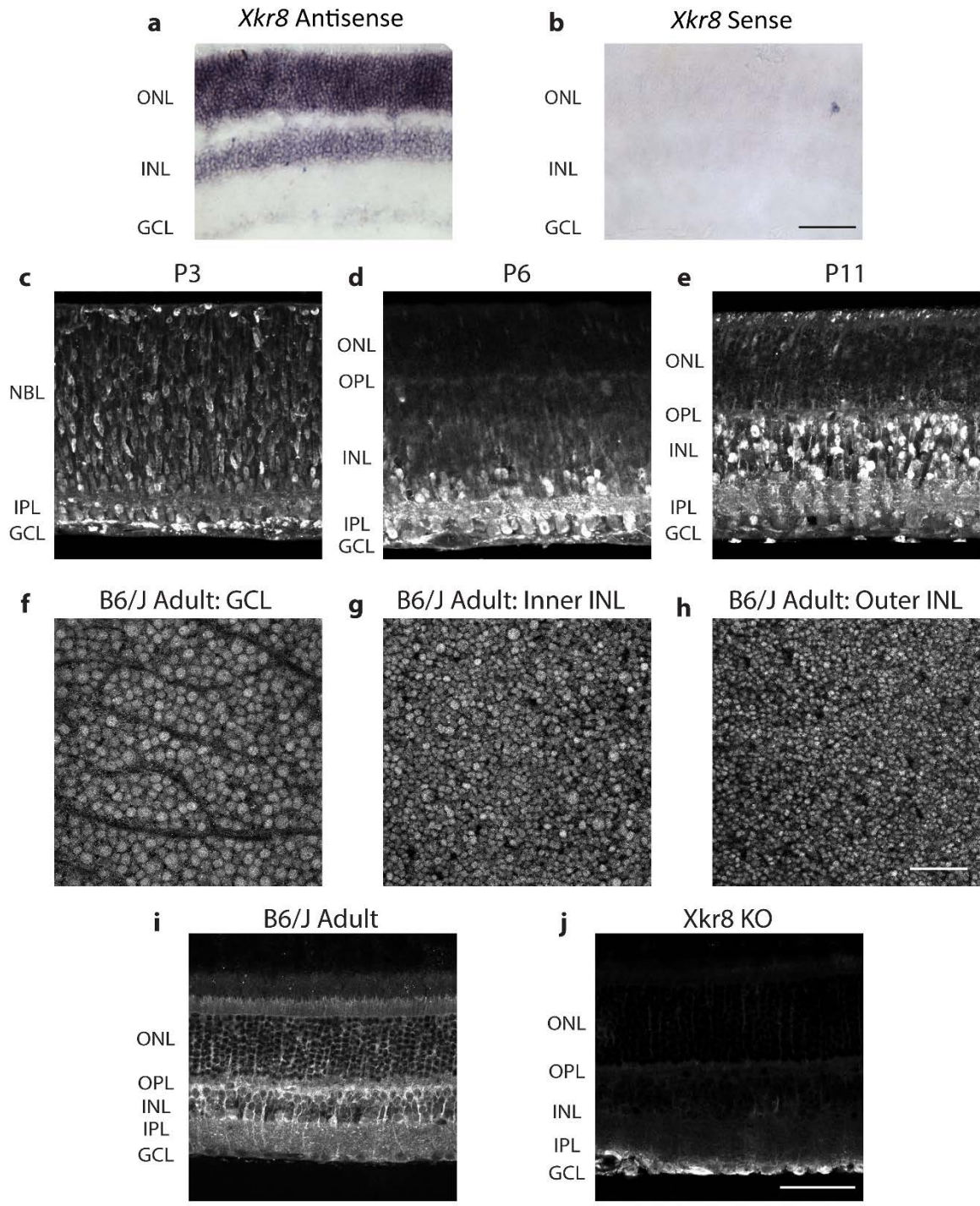


**Figure 11: *Xkr8* retinal expression.** *In situ* hybridizations with *Xkr8*-specific probes in adult retinas show that *Xkr8* mRNA is detectable in all three nuclear layers, as indicated by the purple precipitate in the antisense condition (a) and a lack of precipitate in sense controls (b). A stronger signal was observed in the ONL and the INL than the GCL. *Xkr8* protein is detected in migrating cells in the NBL at P3 (c) yet becomes localized to the inner retina at later timepoints, with heavy labeling in the INL and IPL at P6 (d) and P11 (e). Wholemount staining indicates that *Xkr8* is expressed in cells in the GCL (f) and INL (g,h) yet seems to be expressed in some cells more than others (f-h). Adult B6/J radial sections confirm that *Xkr8* is detectable in all layers, with the strongest staining observed in cells in the INL (i). Adult *Xkr8* knockout retinas show an almost complete loss of staining, confirming the specificity of the antibody (j). Scale bars = 50µm.

and does not seem to be restricted from any cell types.

Microarray expression data collected from adult mouse whole eyes show a significant negative correlation between expression of *Xkr8* and rod bipolar as well as type 2 cone bipolar number (GeneNetwork AXB/BXA Whole Eye Expression Microarray Database, Figure 12a,b). Additionally, this microarray data was used to correlate the variation in *Xkr8* expression to the variation in genotype, and mapped a significant expression-QTL (eQTL), i.e. a genomic locus where a variant must contribute to the variation in gene expression itself (Figure 12c). The fact that this variation in expression maps to the very location of the gene suggests that it is *cis*-regulated, i.e. that the variant lies in a regulatory sequence for *Xkr8* gene that is modulating its expression across the strains. Indeed, those strains with the A/J haplotype at this locus all have lower levels of expression relative to those with the B6/J haplotype (Figure 12a,b).

Developmental expression of *Xkr8* reflects the same strain difference observed in adulthood (Figure 12d). A two-way ANOVA of the real time RT-PCR (qPCR) analysis reveals a main effect of strain, where *Xkr8* is significantly increased in B6/J animals compared to A/J animals ( $p = .020$ ). We did not, however, observe a significant effect of age ( $p = .073$ ) nor any significant interaction between age and strain ( $p = 0.078$ ), although the increase in B6/J retinas appears to be most prominent at P5. This age coincides with the period of maximal programmed cell death for neurons in the bipolar cell layer of the INL, suggesting that a variant in *Xkr8* leading to greater expression in B6/J might produce greater cell death in the strains carrying this B6/J allele, thereby modulating bipolar cell number.

*Xkr8* does not have variants within the coding regions of the gene but has many potential regulatory variants, including 8 in the 3' UTR, 7 upstream, 2 downstream, and 14 in intronic

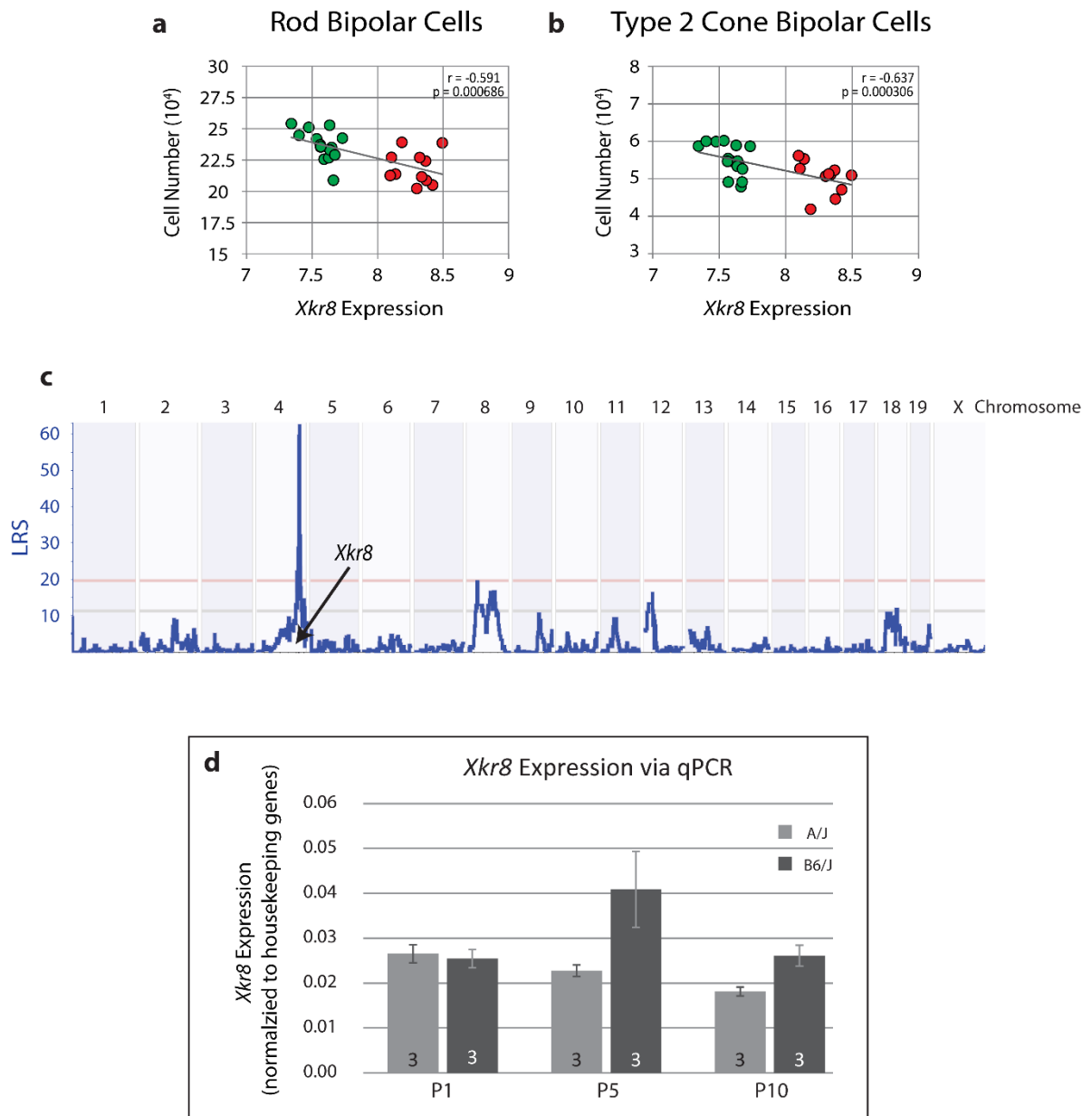


**Figure 12: *Xkr8* expression correlates to bipolar cell number.** Rod bipolar cell (a) and type 2 cone bipolar cell (b) number show a significant negative correlation with expression of *Xkr8*. For both cell types, gene expression is lower in the A/J strains (green circles) than B6/J strain (red circles). Variation in *Xkr8* expression across recombinant inbred strains map a significant QTL (LRS = 63) at the location of the *Xkr8* gene, indicating a cis-eQTL (c). Expression levels of *Xkr8* at P1, P5, and P10 for A/J and B6/J retinas via qPCR are shown normalized to housekeeping genes GAPDH, TBP, and  $\beta 2M$ . LRS = likelihood ratio statistic. n = number of litters analyzed.

regions (Appendix B). In addition, one InDel is located 374 base pairs (bp) upstream from the transcriptional start site, within the presumed promoter region. Given the presence of many putative regulatory variants, expression during retinal development, and described role in the apoptotic pathway, *Xkr8* was chosen as a top candidate for further investigation.

## 5. *Xkr8* Knockout Mice

*Xkr8*-knockout (*Xkr8* KO) and *Xkr8* heterozygous control (*Xkr8* Het) mice were obtained from the Suzuki laboratory and analyzed for changes to cell number (*Xkr8* wildtype controls were unavailable). *Xkr8* KO animals were genetically engineered to lack ubiquitous *Xkr8* expression (Suzuki et al., 2013). Given that *Xkr8* expression is negatively correlated to rod bipolar cell and type 2 cone bipolar cell number (Figure 12a,b), we would have predicted that a decrease in *Xkr8* expression in *Xkr8* KO animals would cause an increase in cell number. Retinal wholemount area ( $p = 0.8713$ ), total retinal thickness ( $p = 0.1339$ ), and thickness of all individual retinal layers were no different between *Xkr8* Het versus KO eyes (ONL:  $p = 0.1358$ ; OPL:  $p = 0.8784$ ; INL:  $p = 0.2499$ ; IPL:  $p = 0.2042$ ; GCL:  $p = 0.2450$ ), implicating that no gross morphological changes or cell loss is occurring in knockout animals compared to controls (Figure 13a,b).

To assess if rod bipolar and/or type2 cone bipolar cell number was altered in KO animals, we counted the number of Syt2-positive type 2 cone bipolar cells and the number of PKC-positive rod bipolar cells from Het and KO sectioned retinas. Rod bipolar cell number appeared unchanged between conditions ( $p = 0.5909$ ) and type 2 cone bipolar cell number showed a slight but nonsignificant increase ( $p = 0.2571$ ) in *Xkr8* KO animals compared to *Xkr8* Hets (Figure 13c,d). In order to get more accurate cell number counts, we used the remaining tissue to count Syt2-positive profiles in wholemount retinas, yet

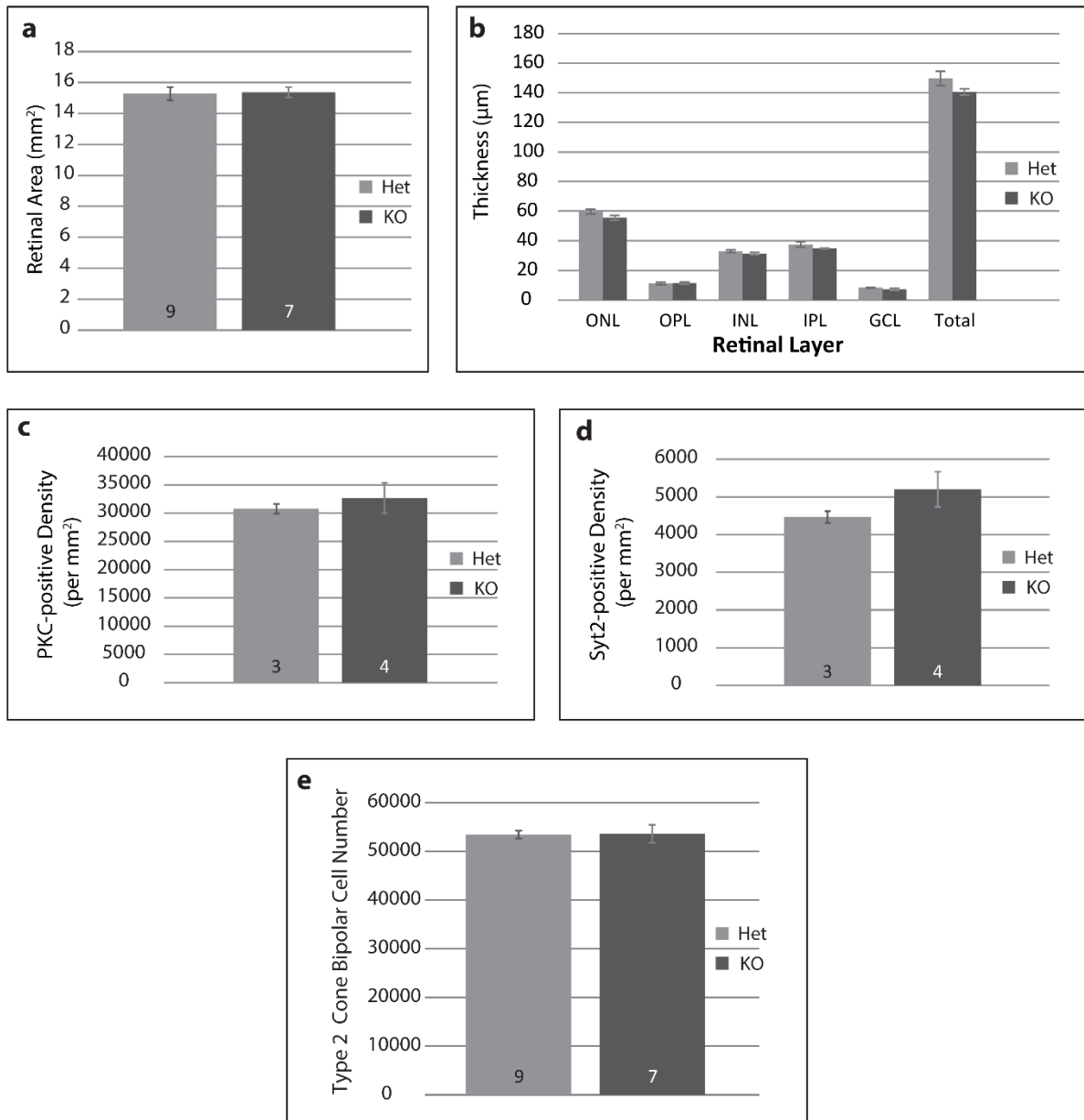


**Figure 13: Xkr8 knockout mice.** Retinal area (a) and thickness of all retinal layers (b) are unchanged between control (Het) and Xkr8 knockout (KO) animals. The density of PKC-positive rod bipolar cells (c) and Syt2-positive type 2 cone bipolar cells (d) are non-significantly different than controls. In addition, the total number of cone bipolar cells does not differ from controls when counted from wholemount preparations (e). n = number of animals. Histograms = mean +/- s.e.m.

observed no difference between groups ( $p = 0.8698$ , Figure 13e; due to the lack of available samples, we were unable to do the same quantification for PKC-positive cells). Taken together, these data imply that the complete removal of *Xkr8* (e.g. Figure 11j) does not affect retinal histology or the number of bipolar cells generated.

## **6. *Xkr8* Overexpression via *In Vivo* Electroporation**

While the above data suggest that complete removal *Xkr8* had minimal effect upon bipolar cell populations, this could however indicate redundancy with other *Xkr8* family members, such as *Xkr4* and *Xkr9*, which have been shown to have a similar function and share common genetic binding motifs (Suzuki et al., 2014). As an alternative approach, we directly modulated *Xkr8* expression via overexpression, in an attempt to uncover a specific effect upon the population of bipolar cells. Given that our surgical manipulations are done on P2 animals, our experimental paradigm targets postnatally generated cells, which include the population of bipolar cells. By limiting the retinal populations susceptible to *Xkr8* overexpression, we were able to assess changes to cell number in a more targeted manner, compared to that of the knockout approach that removes *Xkr8* globally.

Rod bipolar and type 2 cone bipolar cells make up only a small fraction of the cells in the retina; RBCs comprise the largest population of all bipolar cell types, accounting for an estimated 2.5% of cells in the entire B6/J retina (Keeley, Whitney, et al., 2014), while type 2 cone bipolar cells are approximately a quarter of this proportion. Due to their inherent rarity and the limitations of electroporation efficiency, it was not possible to calculate changes in the specific populations of rod bipolar and type 2 cone bipolar cells without utilizing many animals in order to generate a large enough sample size. Instead, we employed a strategy to assess changes in the total bipolar cell population in consideration that cell types in the INL

can be distinguished by virtue of where their cell bodies are positioned. The INL has a natural division near the center where Müller glial cell bodies are positioned, separating the bipolar cells on the scleral side (or outer half) of the INL from amacrine cells situated in the vitreal side (or inner half) of the INL. Horizontal cells also make up a small proportion (about a quarter of one percent of all retinal neurons) of the cells in the outer INL, but given that these cells are all generated prenatally, they cannot incorporate injected plasmids following electroporation postnatally; Indeed, I have never observed any GFP-positive cells with typical horizontal cell morphology in the outer INL. Furthermore, we confirmed that we are able to target bipolar cells via this electroporation method; Figure 14a depicts a GFP-positive bipolar cell (arrowhead) from an electroporated retina, whose soma resides in the bipolar cell layer in the INL and is immunoreactive for PKC, a marker specific to rod bipolar cells.

Figure 14b schematically represents the plasmids used for overexpression and control conditions, illuminating the identical composition of the plasmids, except for the insertion of the *Xkr8* coding sequence (driven by the CAG promoter) upstream of the IRES site that drives GFP. *Xkr8* overexpression resulted in a significant decrease in the proportion of GFP-expressing bipolar cells in the outer INL (Figure 14c,d,f). In addition, overexpression caused an increase in the proportion of GFP-expressing photoreceptors in the ONL and had a minor effect on the amacrine cell population in the inner INL (Figure 14e,g). While we did see an alteration in the percentage of cells in all layers compared to controls, the effect was the most pronounced in the bipolar cell layer, with a 55% decrease in the number of GFP-positive cells when *Xkr8* was overexpressed. Given our experimental methodology we are unable to determine if *Xkr8* overexpression causes a specific fate change or a change in

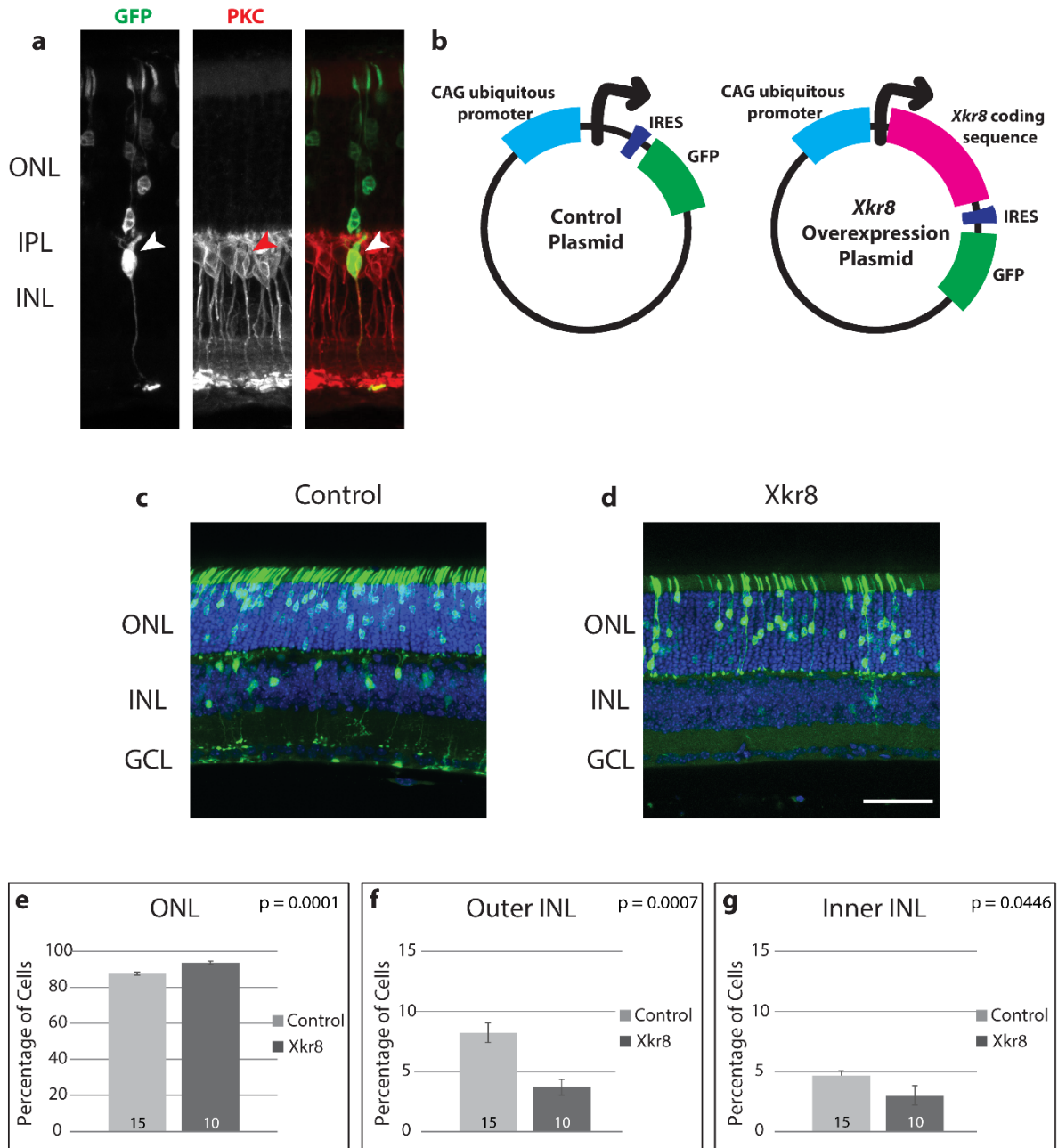


**Figure 14: *Xkr8* overexpression via *in vivo* electroporation.** Bipolar cells are able to be successfully electroporated, as evidenced by GFP-positive cells co-stained with PKC, a marker of rod bipolar cells (a, arrowhead). Control plasmids used for electroporation experiments are identical to overexpression plasmids, except for the insertion of the *Xkr8* coding sequence that is driven by a CAG promoter (schematized in b). Plasmids also make a bicistronic mRNA that makes GFP via an IRES. Exemplary sections of electroporated retinas from control (c) and *Xkr8* overexpression retinas (d). *Xkr8* overexpression causes a significant increase in the proportion of cells in the ONL (e) and decrease in the cells in the outer INL, where bipolar cells reside (f). *Xkr8* overexpression also causes a slight, if significant, decrease in cells in the inner INL (g). IRES = internal ribosome entry site, GFP = green fluorescent protein. n = number of animals. Histograms = mean  $\pm$  s.e.m. Scale bar = 50  $\mu$ m.



the frequency of one cell type, yet our data indicate a significant role for *Xkr8* in the modulation of bipolar cell number, given that its overexpression in retinal progenitor cells causes a decrease in the proportion of bipolar cells present in the adult retina. The robustness of this phenotype is made apparent when comparing *Xkr8* to all other electroporated candidate genes that showed no effect, relative to controls (Appendix E). These results, showing that overexpression of *Xkr8* alters the relative number of bipolar cells in the mouse retina, are consistent with the hypothesis that a regulatory variant participates in modulating transcript levels for *Xkr8*, contributing to the total number of rod and type 2 cone bipolar cells. We next turned our attention to identifying the potential variant itself.

## **7. *Xkr8* Regulatory Variants**

In order to identify the variant or variants between A/J and B6/J mice that could affect *Xkr8* expression, we engineered plasmids to express a luciferase gene under the control of the A/J or B6/J *Xkr8* 1 kb promoter sequence. Figure 15a and 15b show schematics of the plasmid construction. We predicted luciferase activity to increase in B6/J versus A/J constructs given that the presence of B6/J alleles corresponds to higher *Xkr8* expression and fewer bipolar cells (Figure 12a,b). While both the A/J and B6/J promoters increased luciferase expression relative to the  $\beta$ -galactosidase control, albeit weakly, the variant in this region does not appear to yield a difference in *Xkr8* expression (Figure 15c). Interestingly, there are 6 other variants that discriminate A/J and B6/J strains within 5 kb upstream of the TSS, therefore it is plausible that one or more of these could be differentially regulating *Xkr8* expression, but this remains to be determined. Alas, we were unsuccessful in assaying this entire 5 kb sequence, due to technical difficulties with cloning any promoter fragment

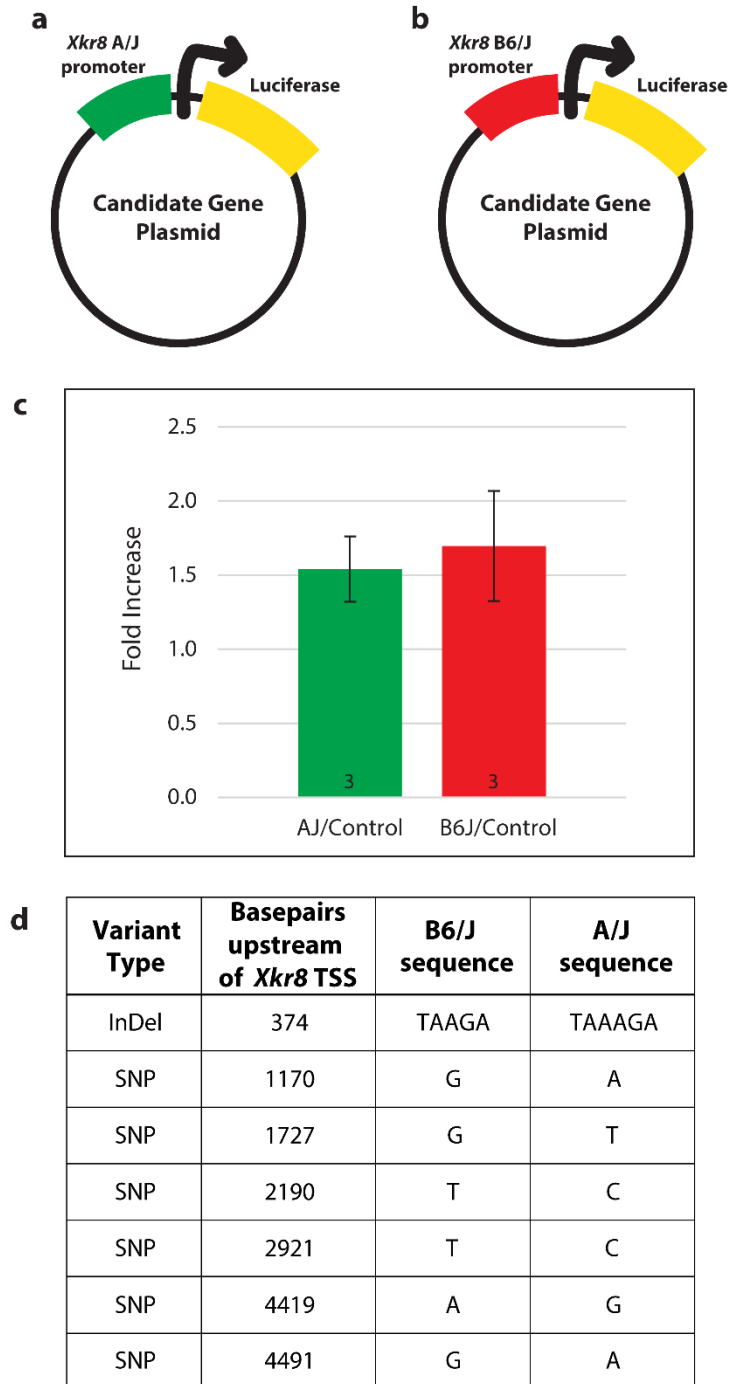


**Figure 15: *Xkr8* promoter activity via luciferase assay.** Schematics of luciferase plasmids demonstrate that either the A/J (a) or B6/J (b) promoter sequence for *Xkr8* was used to drive expression of the luciferase gene. While both the A/J and B6/J 1kb promoters increased luciferase expression relative to control, the InDel variant within 1kb of the TSS does not appear to yield a difference in *Xkr8* expression (c,d). There are 6 more SNPs that discriminate parental stains, whose location and nucleotide change are shown in (d), in addition to the InDel tested in c.

larger than 1.3 kb into the multiple cloning site. Given that the 1.3 kb sequence only varies in 1 SNP from the 1 kb fragment assayed (Figure 15c), we did not pursue this experiment further. Figure 15d describes the location of each of these seven variants relative to the TSS, along with the nucleotide in the A/J versus B6/J sequence, still worthy of future assessment.

## **8. Candidate Gene Selection: *Ggct***

*Ggct* was chosen as a top candidate from the 70 genes present at the chromosome 6 QTL for rod bipolar cell number, in a similar way as previously described for *Xkr8*. Figure 16a shows the QTL map for rod bipolar cell number, with the interval on Chromosome 6, which includes *Ggct*, magnified in 16b. *Ggct*, or gamma glutamylcyclotransferase, is an enzyme that plays a role in glutathione degradation (Oakley et al., 2008) and has been shown to be a contributor to a variety of cancers (reviewed in W. Zhang et al., 2016). Importantly, *Ggct* has been recently shown to play a role in cell proliferation and death, implicated by *Ggct* knockdown experiments that resulted in an inhibition of cell proliferation and an induction of apoptosis in human cancer cells (W. Zhang et al., 2016), which provides a potential mechanism by how *Ggct* could alter cell number.

Bioinformatic resources show that *Ggct* is expressed in the adult retina (Retina SAGE Database, Roska database, and GeneNetwork). Data specifically from the Roska database indicates that the highest expression of *Ggct* is found within photoreceptors and ganglion cells in the adult retina. *Ggct* is also expressed within the developing retina as evidenced by qPCR data acquired from retinas at P1, P5, and P10 (Figure 17a). Expression is significantly different between B6/J and A/J stains, while appearing to be differentially regulated at early postnatal ages. In B6/J mice, *Ggct* expression is low at P1 yet increases

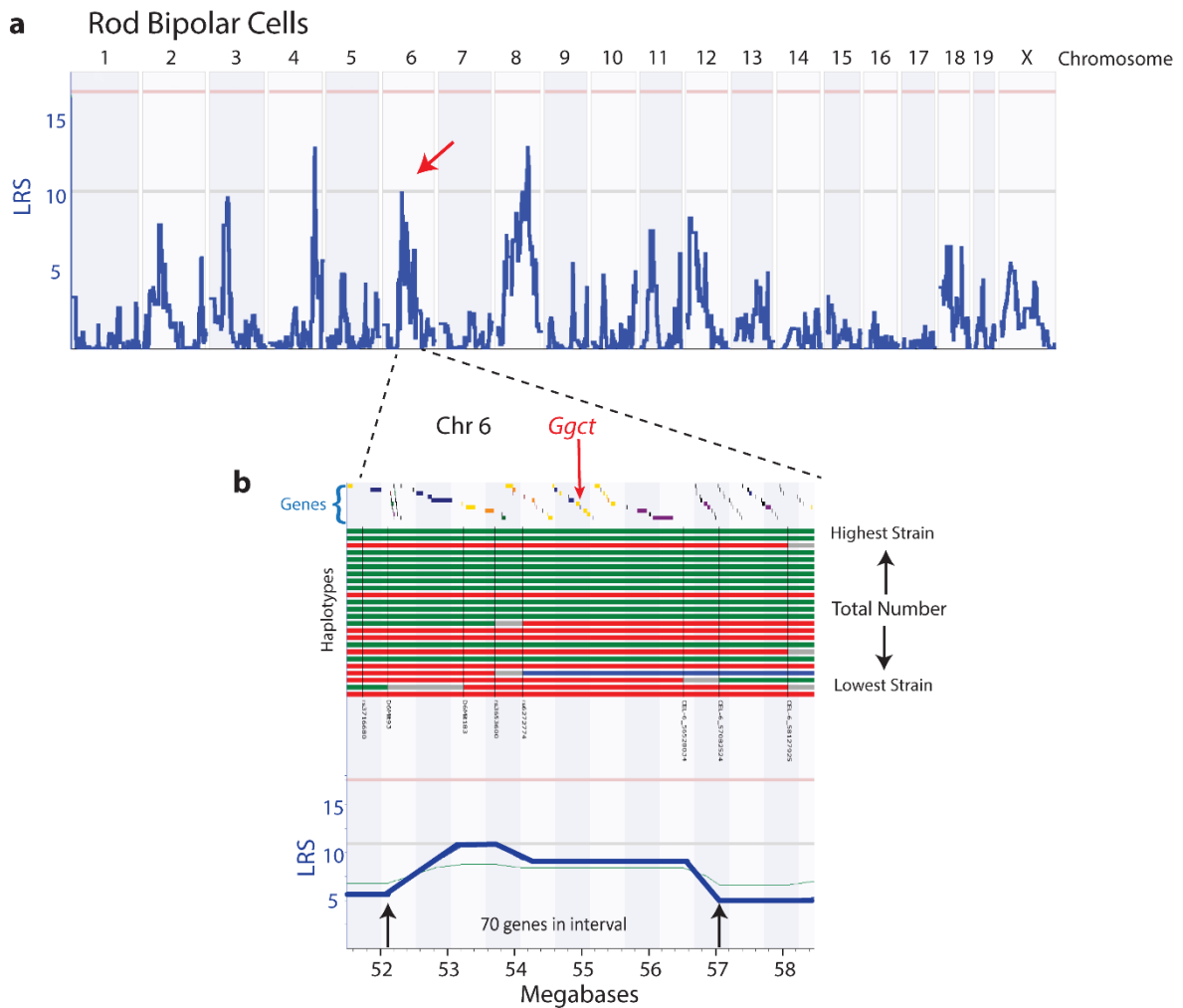


**Figure 16: QTL mapping for rod bipolar cells.** Interval mapping of the variation in rod bipolar cell number reveals three QTL, with the one on Chr 6 (LRS = 26.4) highlighted (red arrow, a). Magnification of interval from 52 to 57 mb (b) includes 70 genes, one of which is *Ggct*. Horizontal lines indicate suggestive threshold (gray line) and significant thresholds (pink line). Haplotype blocks indicate the allele present at each genotyped location (black vertical lines) with green, red, and gray bars indicating A/J, B6/J, and unknown haplotypes, respectively. Colored boxes at the top of the map represent the location of genes across the chromosome, with the location of *Ggct* circled in red.

by P5. In the A/J strain conversely, *Ggct* expression is high at P1 and then decreases by P5, while then returning to levels comparable to those in B6/J at P10 (Figure 17a). A two-way ANOVA revealed no main effect of strain nor developmental age, but did reveal a significant interaction, with post-hoc Tukey tests showing a significant difference between the strains at P1 (favoring A/J) and then reversing at P5 (favoring B6/J). It is possible that the discrepancy between strains at P1 and P5 are a result of differential gene regulation due to one of many of the genetic variants that differ between strains.

*Ggct* expression from the AXB/BXA adult whole eye mRNA database showed it to be negatively correlated with rod bipolar cell number, with lower *Ggct* expression being associated with the presence of A/J alleles (Figure 17b). *Ggct* also has a *cis*-eQTL indicating that a variant in its sequence is likely contributing to modulation of its own expression (Figure 17c), making this a gene of particular interest. *Ggct* has many coding variants in addition to regulatory variants in putative promoter regions. *Ggct* has a total of 55 SNPs and 14 InDels that discriminate A/J and B6/J mice. One of these variants within the coding region creates a missense mutation (R45C) that is predicted to be potentially damaging to function given the change from a basic amino acid to a non-basic one (SIFT database). In addition, the 1kb putative promoter region upstream of *Ggct* has 4 SNPs and 1 InDel that discriminate the A/J and B6/J mouse strains from one another. If one expands this search to 2 kb upstream of the TSS, the number of variants increases to 9 SNPs, 7 InDels, and, even more enticing, 1 structural variant (Sanger Institute Mouse Genomes Project). In general, structural variants are large and complex DNA rearrangements that are known to be pathogenic, causing diseases such as Charcot-Marie Tooth disease (Weischenfeldt, Symmons, Spitz, & Korbel, 2013). Structural variants have been hard to

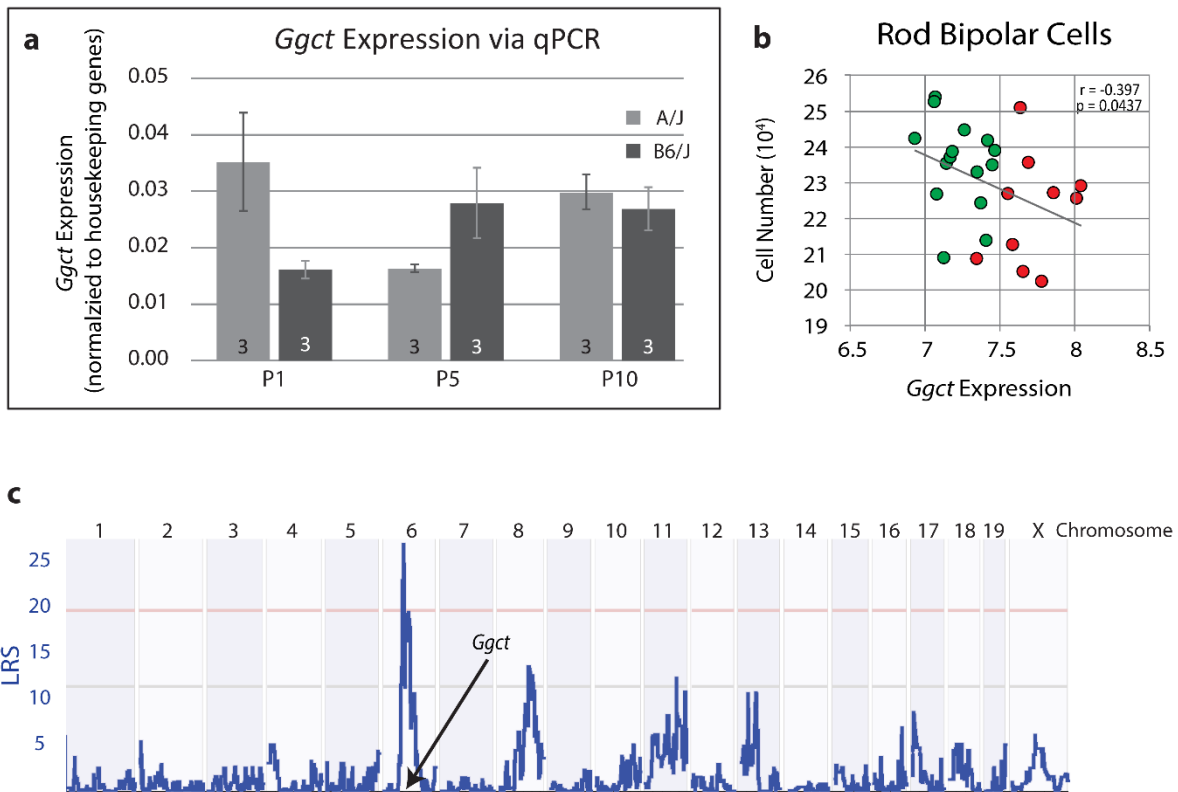


**Figure 17: *Ggct* retinal expression.** *Ggct* expression significantly differs between A/J and B6/J strains, although expression appears to be differentially regulated at P1 and P5 as evidenced by the opposite expression patterns observed in each strain (a). Rod bipolar cell number shows a significant negative correlation with expression of *Ggct*, with the presence of A/J alleles (green circles) corresponding to lower *Ggct* expression and higher rod bipolar cell number, and B6/J alleles (red circles) corresponding to higher *Ggct* expression and lower rod bipolar cell number (b). Variation in *Ggct* expression across recombinant inbred strains map a significant QTL (LRS = 26.2) at the location of the *Ggct* gene, indicating a *cis*-eQTL (c). n = number of litters analyzed.

identify until the recent advances made in sequencing technology, and are now thought to account for roughly 1% of all sequence variation in the mouse genome (Keane et al., 2014; Yalcin et al., 2011). Given its expression in both the developing and mature retina, in addition to the presence of many coding and regulatory variants, *Ggct* became the most promising candidate gene at the QTL on Chromosome 6.

### **9. *Ggct* Overexpression via *In Vivo* Electroporation**

We directly manipulated the expression of *Ggct* within the developing retina via electroporation, as previously described for *Xkr8*, in order to ascertain a role for *Ggct* in the modulation of bipolar cell number. A schematized version of the plasmids used for overexpression and control manipulations are shown in Figure 18a. *Ggct* overexpression resulted in a significant decrease in the proportion of GFP-expressing bipolar cells in the outer INL (Figure 18b,c,e) and a corresponding increase in the proportion of GFP-expressing rods in the ONL (Figure 18d), with a slight change to the population of amacrine cells in the inner INL (Figure 18f). While all changes were significant, the largest percent change was, again, in the outer INL, showing a 38% decrease in GFP-positive cells compared to controls. When viewed alongside *Xkr8* and all other genes we have overexpressed, one can appreciate the magnitude of this effect (Appendix F). These data strongly implicate *Ggct* as a player in the modulation of bipolar cell number in the retina.

### **10. *Ggct* Regulatory Variants**

According to the Sanger database, the structural variant upstream of *Ggct* was predicted to begin about 1,075 kb upstream of the TSS. In order to confirm the presence and size of this variant, we amplified this region of the promoter from genomic DNA extracted from A/J and B6/J mice, using primers to known regions surrounding the predicted structural

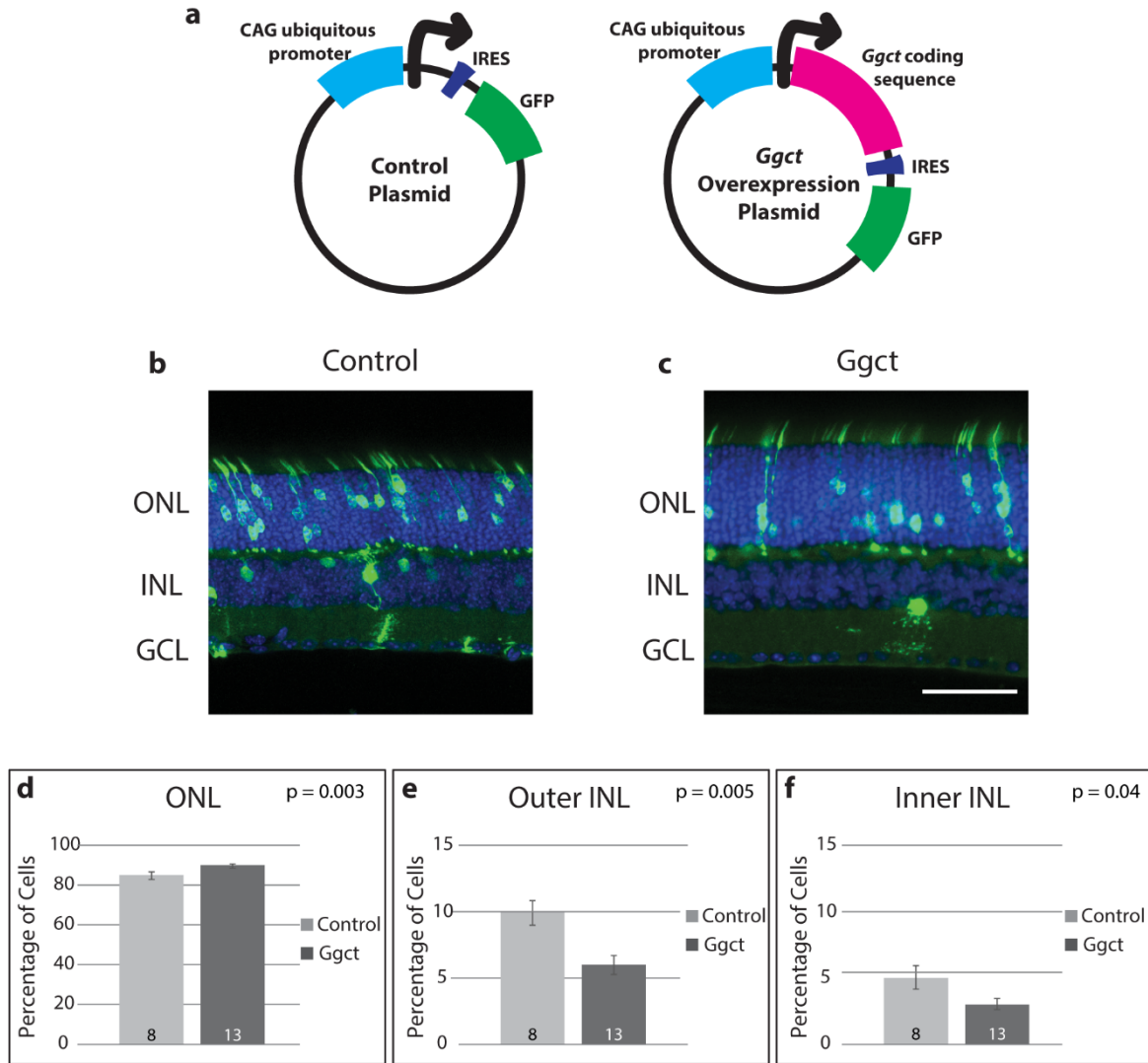


**Figure 18: *Ggct* overexpression via *in vivo* electroporation.** Control plasmids used for electroporation experiments are identical to overexpression plasmids, except for the insertion of the *Ggct* coding sequence that is driven by a CAG promoter (schematized in a). Exemplary sections of electroporated retinas from control (b) and *Ggct* overexpression retinas (c). *Ggct* overexpression causes a significant increase in the proportion of cells in the ONL (d) and decrease in the cells in the outer INL, where bipolar cells reside (e). *Ggct* overexpression also causes a slight, if significant, decrease in cells in the inner INL (g). IRES = internal ribosome entry site, GFP = green fluorescent protein. n = number of animals. Histograms = mean  $\pm$  s.e.m. Scale bar = 50  $\mu$ m.



variant. Figure 19a shows a representation of the *Ggct* gene in red with an arrow denoting the transcriptional start site. The 5 kb region upstream of the gene is represented in blue with the location of the structural variant and the relative location of the forward and reverse primer sequences shown. When amplifying this region, we found the structural insertion in the A/J sequence to be approximately 500 bp in size (Figure 19b). Furthermore, upon sequencing this region, we determined that the insertion in the A/J promoter is precisely 478 bp, relative to B6/J (Figure 19c). The nucleotide sequences for the entirety of the A/J and B6/J promoter regions that were cloned into the luciferase vector are shown in Appendix G. This large discrepancy could feasibly underlie the differential *Ggct* expression observed in the two parental strains of mice, thereby causing an alteration to the number of bipolar cells generated.

In order to test if the presence of this insertion in the A/J sequence could modulate expression of *Ggct*, we performed a luciferase assay. We amplified the promoter region in the A/J sequence that included the structural insertion, and the corresponding B6/J sequence. We cloned these fragments into our luciferase backbone so that these promoter sequences would be used to drive expression of the luciferase gene. The construction of both the A/J and B6/J plasmids are schematized in Figures 20a and 20b. Preliminary results indicate that the A/J structural variant causes a decrease in *Ggct* promoter activity, given that the B6/J sequence was able to sufficiently drive more luciferase activity than that of A/J (Figure 20c). These data indicate that the presence of the structural variant within the A/J sequence is sufficient to hinder promoter activity, relative to B6/J, leading to a decrease in gene expression, being consistent with the correlation between *Ggct* expression and bipolar cell number described in Figure 17a. This structural variant, therefore, may be responsible for

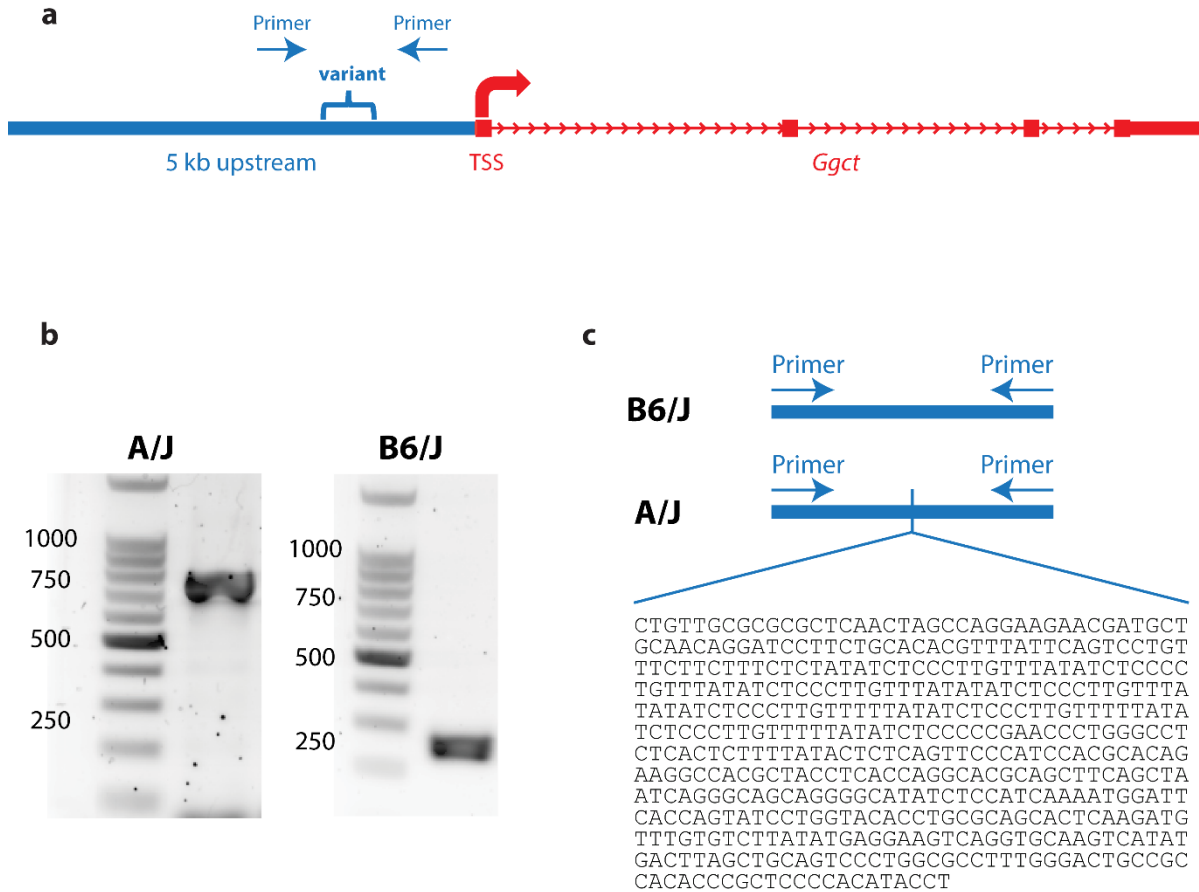


**Figure 19: *Ggct* structural variant.** *Ggct* has 4 exons (red boxes) and 3 introns (red arrows). The location of a predicted structural variant is shown (blue bracket) and located 1,075 bp upstream of the TSS (a). Forward and reverse primers were used to amplify the region surrounding the structural variant and the fragment size was found to be roughly 500 bp larger in the A/J strain than for B6/J (b), shown by the discrepancy in band sizes when PCR fragments were run on an agarose gel. The A/J insertion was confirmed to be 478 bp in size, compared to B6/J (c). The nucleotide sequence is listed 5' to 3'. TSS = transcriptional start site.

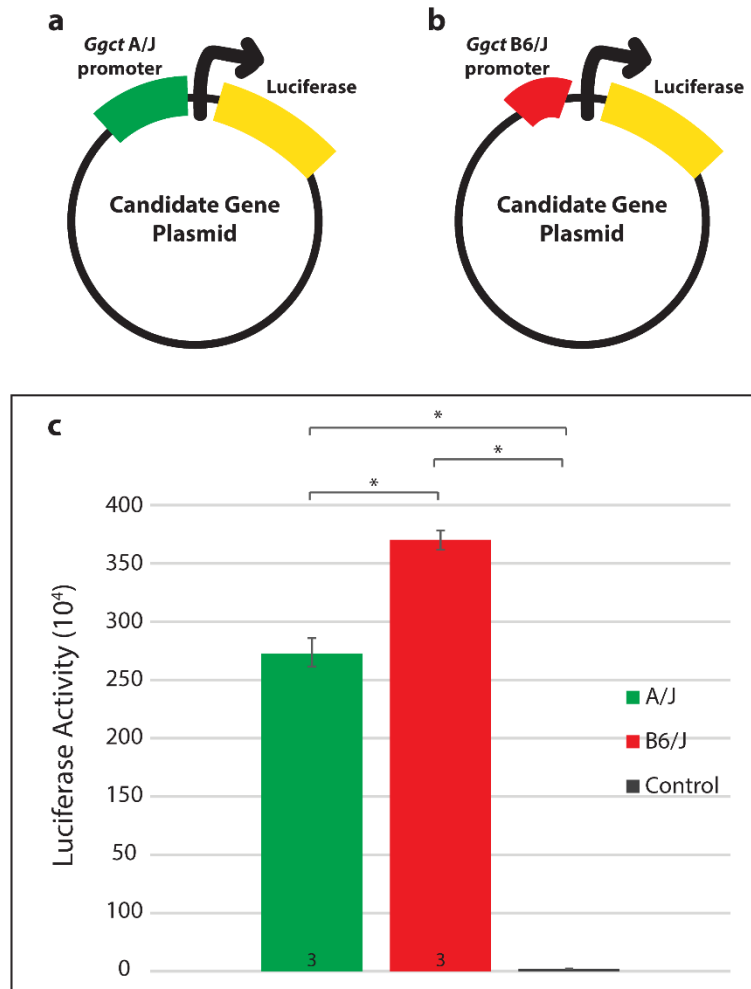


**Figure 20: *Ggct* promoter activity via luciferase assay.** Schematics of luciferase plasmids demonstrate that either the A/J (a) or B6/J (b) promoter sequence for *Ggct* was used to drive expression of the luciferase gene. While both the A/J and B6/J promoters increased luciferase expression relative to control, the structural variant in the A/J sequence significantly decreases promoter activity, relative to the B6/J promoter (c). \* =  $p < 0.005$

the *cis*-eQTL shown in in Figure 17c, and for the QTL on Chr 6 in Figure 16a, i.e. a quantitative trait variant (QTV).

### ***E. Discussion***

The current study sought to discover genes that play a role in establishing neuronal number in the developing retina. We investigated candidate genes residing at specific genomic loci, or QTL, that had previously been identified as locations likely to contain candidates involved in this specification process. These specific genes were further investigated by correlating gene expression data from a panel of recombinant inbred mice (AXB/BXA) with cell number counts across these strains. A large degree of variation in cell number exists between all of the strains, indicating that genetic variants affecting the size of these populations must exist between the A/J and B6/J strains that founded the panel of RI mice. Utilizing this knowledge, this study used a variety of experimental methods to identify these genetic variants and further understand how neuronal population size is established, a necessary step in the formation of an organized and mature retina.

Cell number is a complex trait that is controlled by many genes, and many allelic variants within those genes (Reese & Keeley, 2016). In virtually all instances, QTL map to locations that contain many genes, in which any number of genes may be critical to cell number specification. In cases when the alteration of a candidate gene's expression by gene knockout, conditional knockout, or electroporation strategies (Figure 7) yields no significant change from control conditions, we often do not pursue the candidate further. This does not mean, however, that the gene may not play a role in the modulation of cell number that would perhaps be made evident if tested at a different timepoint or via an alternative

manipulation. In some instances, like that for *Xkr8*, we are able to test candidates by both knockout and overexpression manipulations, although this is atypical due to a lack of available genetically modified mice. Indeed, we did not see an alteration to cell number via *Xkr8* knockout strategies, yet found a significant alteration in the modulation of bipolar cell number via overexpression experiments, indicating that each individual strategy is not always sufficient to identify causal genes. Instead, the forward-genetic approach employed in this chapter was used as a way to identify many candidate genes, of which one or several could modulate the cell number trait. By testing many genes at each locus, we are able to identify those that produce the largest effect upon the trait of interest, and can therefore examine those in the greatest detail.

This current study demonstrates that rod bipolar cell number is indeed a complex trait, which is controlled by several genes at multiple different genomic loci. *Xkr8* and *Ggct* are both candidates for rod bipolar cell number, yet reside at QTL on Chromosomes 4 and 6, respectively. All of the genes that have previously been identified to participate in the establishment of bipolar cell populations, belong to master transcription factor families like those previously discussed, such as *Vsx2*, *Ascl1*, and *Neurod4*. Neither *Xkr8* or *Ggct* belong to transcription factor families, nor have been shown to play a role in the development of the nervous system, making the findings in this dissertation novel while furthering our understanding of how the population of retinal bipolar cells are established.

It remains unclear if *Xkr8* and *Ggct* modulate bipolar cell number through similar mechanisms. *Xkr8* is known to play a role in apoptosis, by causing cells to expose phosphatidylserines on their surface to promote phagocytosis (Suzuki et al., 2013; Suzuki et al., 2014). Very little is known about *Ggct* however, except that is upregulated in many

human cancers and therefore postulated to play a role in apoptosis or cell proliferation (W. Zhang et al., 2016). One study found that silencing GGCT in cultured colorectal cancer cells triggered caspase-3-mediated apoptosis (Dong et al., 2016). It could be true that both *Xkr8* and *Ggct* utilize mechanisms to promote cell death in order to sculpt the number of cells that will make up the total population of bipolar cells. We attempted to address this question by collecting electroporated retinas at P6, during the timepoint when bipolar cells are undergoing programmed cell death, and immunostaining for cell death markers such as caspase-3. We hypothesized that if *Xkr8* or *Ggct* are modulating bipolar cell number by increasing their likelihood to undergo apoptosis, than we would see a higher coincidence of GFP-positive and caspase-3-positive cells compared to control retinas. Unfortunately, these experiments were not able to be completed given that GFP expression is too low to be detected and quantified in retinas at this age. This question remains an interesting one for future studies.

While *Xkr8* is known to influence apoptosis, the mechanism by which it causes apoptosis suggests that the gene is not active until the apoptotic pathway is already underway. *Xkr8* is activated following cleavage at a conserved caspase cleavage site (amino acid sequence DLVD) near the C-terminal end of the protein via caspase-3 or caspase-7. Once cleaved, *Xkr8* then mediates phospholipid scrambling to expose phosphatidylserines on the cell surface that ultimately lead to engulfment (Suzuki et al., 2013; Suzuki et al., 2014). This proposes that perhaps it is not merely *Xkr8* expression that is important but instead a specific level of *Xkr8* expression that impacts neuronal population number. Conceivably, *Xkr8* expression might be tightly controlled in a wildtype animal where regulation of *Xkr8* expression is necessary for programmed cell death to occur; disordered

expression, like that caused by our overexpression manipulations, may therefore lead to alterations in the final number of bipolar cell populations. This could explain why a global knockout of *Xkr8* did not result in the opposite phenotype that we observed in the overexpression studies. Perhaps a knockdown of *Xkr8* might instead shift the expression in the opposite direction as in the overexpression manipulations, and result in an increase in the percentage of bipolar cells yet further studies are needed to confirm this.

Further evidence that *Xkr8* expression levels must be delicately balanced comes from the known interaction between *Xkr8* and the flippase ATP11C (Segawa et al., 2014). ATP11C contains the same caspase cleavage site as *Xkr8* but redirects phosphatidylserine from the outer to inner membrane so that following caspase cleavage, *Xkr8* becomes activated and ATP11C is likewise inactivated (Kimani et al., 2014). Data from this study indicate that expression levels of *Xkr8* and ATP11C proteins must be evenly balanced for the normal process of cell survival to occur. Taken together, these data indicate that *Xkr8*, while important for the specification of retinal bipolar cell number, is likely not working alone, but instead exhibits an expression pattern that may be dependent on the presence of enhancers, cofactors, or other genes in order to modulate cell survival, thereby affecting total cell number.

*Xkr8* and *Ggct* both mapped significant *cis*-eQTLs, which made them very strong candidate genes. Out of the 125 genes analyzed from QTL at Chromosomes 4 and 6, only seven genes mapped *cis*-eQTL, four of which were discussed in this chapter (*Xkr8*, *Ggct*, *Dhdds*, and *Hmgn2*). The presence of a *cis*-eQTL suggests that one or many genetic variants within regulatory regions of those genes alters its own expression, and could therefore result in a change in cell number. The one variant between A/J and B6/J mice that

fell within the putative promoter region of *Xkr8* proved to not be sufficient to drive significant changes in gene expression (Figure 15a-c). One caveat to this experiment is that the promoter activity was weak, being only slightly elevated above the control, therefore might not have been sensitive enough to detect differences between A/J and B6/J promoter activity. However, it is feasible that one or several of the other six variants upstream of *Xkr8* could modulate gene expression. For technical reasons we were unable to clone a larger promoter region to test if any other variant/s might regulate gene expression. It is possible, however, that one of these variants creates or destroys a transcription factor binding site that alters gene expression. In addition, *Xkr8* has many other regulatory variants in introns, the 3' UTR, and downstream of the gene (2 kb beyond the 3' UTR), that could be regulated differentially. MicroRNAs are known to bind to microRNA response elements (MREs) in the 3' UTR of mRNAs to alter gene expression. Given that *Xkr8* has 8 SNPs between B6/J and A/J strains within the 3' UTR, one or many of these could create or destroy an MRE/s resulting in altered gene expression.

Like *Xkr8*, *Ggct* has many regulatory variants that discriminate the A/J and B6/J strains, although in much higher numbers. It has 52 SNPs in the 3' UTR, 7 in the promoter, 81 downstream, and 16 in introns, including the one structural variant previously discussed. Preliminary results indicate that the presence of the large structural variant in the A/J promoter is sufficient to alter its activity, given that the A/J promoter drives less luciferase activity than that of the B6/J. This structural variant may be instrumental in driving differential expression of *Ggct* and/or other downstream processes that modulate neuronal number. Taken together, these data describe two novel genes that participate in the



development of bipolar cells and shed light upon the complex mechanisms involved in building a retina.

### **III. Astrocytic and Vascular Development in the Retina**

#### ***A. Abstract***

*Sox2* is a master transcriptional regulator that is highly expressed in retinal astrocytes, yet its function in these cells has not previously been examined. To understand its role, we conditionally deleted *Sox2* from the population of astrocytes and examined the consequences on retinal development. We found that *Sox2* deletion does not alter the migration of astrocytes, but it impairs their maturation, evidenced by the delayed upregulation of glial fibrillary acidic protein (GFAP) across the retina. Coincident with this temporal delay in GFAP expression, the centro-peripheral gradient of angiogenesis is delayed. In the mature retina, we observed lasting abnormalities in the astrocytic population evidenced by the sporadic loss of GFAP immunoreactivity in the peripheral retina as well as by the aberrant extension of processes into the inner retina. Blood vessels in the adult retina are also under-developed and show a decrease in the frequency of branch points and in total vessel length. The developmental relationship between maturing astrocytes and angiogenesis suggests a causal relationship between the astrocytic loss of *Sox2* and the vascular architecture in maturity. We suggest that the delay in astrocytic maturation and vascular invasion may render the retina hypoxic, thereby causing the abnormalities we observe in adulthood. These studies uncover a novel role for *Sox2* in the development of retinal astrocytes and indicate that its removal can lead to lasting changes to retinal homeostasis.

#### ***B. Introduction***

Astrocytes play many roles in the developing and mature CNS, including the retina.

They promote growth and maturation of neuronal cells by stimulating synaptogenesis and axon growth (Allen et al., 2012; Barker & Ullian, 2008; Christopherson et al., 2005; Ullian et al., 2001), secrete growth factors necessary for neuronal differentiation and survival (Chan-Ling & Stone, 1991; Liesi & Silver, 1988), aid in synaptic pruning (Stevens et al., 2007), and buffer ions in the extracellular space (Newman, 1986). Within the retina, the stellate morphology of the astrocytes forms a web-like network of overlapping processes that use gap-junctions to propagate intracellular signals and establish metabolic homeostasis (Hollander et al., 1991; Ramirez, Trivino, Ramirez, Salazar, & Garcia-Sanchez, 1996). Astrocytes also play an important role in the vascularization of the retina (Dorrell et al., 2002), providing a scaffold for blood vessels to follow as they migrate from the optic nerve head across the inner surface of the retina via the secretion of growth factors such as vascular endothelial growth factor (VEGF).

Astrocytes constitute the majority of cells in the central nervous system (Molofsky et al., 2012), yet surprisingly little is known about the genetic factors that regulate their development. *Sox2* was previously explored by our lab after a QTL mapping exercise, similar to that described in Chapter 2, had identified it as a candidate gene for controlling neuronal positioning (Whitney et al., 2014). This study documented that cholinergic amacrine cells, the only retinal neurons that express *Sox2*, are mis-positioned within the layered architecture of the retina when *Sox2* is deleted specifically from these cells in mice. These *Sox2*-negative amacrine cells also showed conspicuous bistratified morphology, as their dendrites normally stratify in a single synaptic layer. In addition, cholinergic amacrine cells displayed a loss of subtype identity in these conditional knockout animals (Whitney et al., 2014). In this study, we noted that two types of glial cells, astrocytes and Müller glia,

also express *Sox2* in adulthood but little is known about the function of this gene in these cells (Fischer, Zelinka, & Scott, 2010; Whitney et al., 2014).

Transcriptome analysis performed on purified populations of astrocytes derived from mouse cortical tissue found *Sox2* to be within the top 10% of all expressed genes (Cahoy et al., 2008). In addition, *Sox2* expression is enriched in astrocytes, being expressed at higher levels than in cortical neurons and other glial cells (Cahoy et al., 2008; Y. Zhang et al., 2014). *Sox2* belongs to the large SRY-related HMG-box transcription factor family and is best recognized for its role in early development by maintaining embryonic stem cell pluripotency (Matsushima, Heavner, & Pevny, 2011; Taranova et al., 2006). *Sox2* is also a critical gene for eye development as human mutations lead to severe abnormalities in eye formation (Fantès et al., 2003; Schneider, Bardakjian, Reis, Tyler, & Semina, 2009). In addition, it has been suggested that *Sox2* is able to promote glial cell survival in cultures of dorsal root ganglion cells (Koike, Wakabayashi, Mori, Hirahara, & Yamada, 2015). Given these documented roles for *Sox2*, the present study has assessed its role in the development of retinal astrocytes.

Using a conditional deletion strategy to excise *Sox2* from the population of astrocytes, we examined the consequences for retinal astrocytic and vascular development, and for the astrocytic and vascular architecture in maturity. While we found no alteration in the spatio-temporal time-course of astrocyte migration across the retina, we observed a conspicuously delayed expression of glial fibrillary acidic protein (GFAP), a hallmark of their maturation. Coincident with this delayed maturation, vascular invasion across the retinal surface was delayed. These events led to lasting changes in the adult retina consisting of an aberrant distribution of astrocytic processes as well as vascular network abnormalities, yet the overall

architecture of the retina was unaffected. These data identify *Sox2* as an important participant in the development of astrocytes, and suggest a complex interaction with the forming vasculature in the mouse retina.

### ***C. Methods***

#### **Mice**

*GFAP-Cre* (FVB-Tg(GFAP-cre)25Mes/J) mice and *Sox2-flox* mice (*Sox2*<sup>tm1.1Lan/J</sup>) were used to generate conditional knockout mice (CKO) in which GFAP-positive astrocytes lack expression of *Sox2*. Cre activation was characterized by crossing *GFAP-Cre* mice with a reporter mouse carrying a floxed stop-cassette upstream of *EYFP*, under a constitutively active promoter (*Rosa-EYFP*; B6.129X1-Gt(ROSA)26Sor<sup>tm1(EYFP)Cos/J</sup>); Cre is activated in all astrocytes and a subset of Müller glia. All *GFAP-Cre* control animals (CTL) were CKO littermates that lacked *GFAP-Cre* and/or *Sox2-loxP* alleles. All three lines of mice were obtained from The Jackson Laboratories (Bar Harbor, MA; *GFAP-Cre*: #004600; *Sox2-flox*: #013093; *Rosa-EYFP*: #006148). Retinas were examined from post-natal mice, and into maturity, with retinas older than 21 days of age designated adult retinas. All experiments were conducted under authorization by the Institutional Animal Care and Use Committee at the University of California–Santa Barbara and in accordance with the National Institutes of Health *Guide for the Care and Use of Laboratory Animals* and the ARVO Statement for the Use of Animals in Ophthalmic and Vision Research.

#### **Tissue Preparation**

Mice were given a lethal dose of sodium pentobarbital or Euthasol (120 mg/kg, i.p.; Virbac, Fort Worth, TX) and once deeply anesthetized, were intracardially perfused with 2

ml of 0.9% sodium chloride followed by ~50mls of 4% paraformaldehyde (PFA) dissolved in 0.1M sodium phosphate buffer pH 7.2 for 15 minutes. Eyes were then removed from each mouse and left in the same fixative for an additional 15 minutes at room temperature. Whole retinas were subsequently dissected from eyes and processed for wholemount preparations or cut into 150 $\mu$ m sections on a Vibratome. Particular care was taken to prevent damage to the inner surface of the retina during dissection.

### **Immunostaining**

Dissected wholemount retinas or sections were incubated in 5% normal donkey serum in phosphate-buffered saline (PBS) with 1% Triton-X for three hours. They were then rinsed in PBS and incubated in primary antibodies diluted in PBS with 1% Triton-X for 72 hrs. All primary antibodies used in this study are listed in Table 4. Occasionally, Hoechst (Invitrogen, Eugene, OR; 1:1000) was added with the primary antibodies to label cell nuclei. In addition, NeuroTrace 530/615 (ThermoFisher Scientific, Waltham, MA; #N21482, 1:500) was used to label Nissl somata and PNA lectin conjugated to Alexa Fluor 647 (ThermoFisher Scientific, Waltham, MA; #L32460, 1:500) was used to label blood vessels, cone inner segments, and cone pedicles. Retinas were subsequently rinsed in PBS and incubated overnight in the secondary antibodies. All secondary antibodies were raised in donkey and conjugated to AlexaFluor dyes (Jackson ImmunoResearch Laboratories, West Grove, PA; 1:200). All steps were conducted under agitation at 4°C.

### **Image Acquisition and Quantification**

Adult wholemount retinal images were assembled from ~250 40 $\times$  maximum projection fields stitched together using Imago 1.5 (Mayachitra Inc., Santa Barbara, CA) to create a single high-resolution image of the entire retina. Postnatal retinal images were comprised of

Antibody	Abbreviation	Target	Supplier	Catalog Number	Dilution
Mouse $\alpha$ Glial Acidic Fibrillary Protein *	GFAP	Astrocytes	Sigma-Aldrich (St. Louis, MO)	C9205	1:400
Rabbit $\alpha$ Paired box protein 2	Pax2	Immature astrocytes	Biolegend (San Diego, CA)	901001	1:200
Rabbit $\alpha$ Collagen IV	-	Blood vessels	BioRad ABD Serotec (Hercules, CA)	2150-1470	1:1,000
Goat $\alpha$ Choline Acetyltransferase	ChAT	Cholinergic amacrine cells	Millipore (Temecula, CA)	AB144P	1:50
Rabbit $\alpha$ Sex determining region Y-box 2	Sox2	Astrocytes and cholinergic amacrine cells	Abcam (Cambridge, MA)	AB97959	1:200
Goat $\alpha$ Sex determining region Y-box 9	Sox9	Astrocytes	R&D Systems (Minneapolis, MN)	AF3075	1:2,000
Mouse $\alpha$ C-terminal binding protein 2	CtBP2	Ribbon synapses	BD Transduction Laboratories (San Jose, CA)	612044	1:500
Sheep $\alpha$ Tyrosine Hydroxylase	TH	Dopaminergic amacrine cells	Millipore (Temecula, CA)	AB152	1:10,000
Mouse $\alpha$ Protein Kinase-A Regulatory Subunit Ib	PKARIIB	Type 3b bipolar cells	BD Transduction Laboratories (San Jose, CA)	610625	1:1,000
Rabbit $\alpha$ Neurofilament M 145kD	-	Retinal ganglion cells and horizontal cell axons	Millipore (Temecula, CA)	AB1987	1:1,000
Rabbit $\alpha$ Allograft inflammatory factor 1	Iba1	Microglia	Wako Laboratory Chemicals (Cape Charles, VA)	019-19741	1:1,000
Mouse $\alpha$ Protein Kinase C	PKC	Rod bipolar cells	Millipore (Temecula, CA)	05-983	1:500
Rabbit $\alpha$ Mouse Cone Arrestin	mCAR	Cone photoreceptors	Millipore (Temecula, CA)	AB15282	1:5,000
Mouse $\alpha$ Neurofilament H non-phosphorylated	SMI32	Retinal ganglion cells and horizontal cells	Biolegend (San Diego, CA)	SMI32R	1:200
Rabbit $\alpha$ Calbindin	-	Horizontal cells	Millipore (Temecula, CA)	PC253L	1:10,000
Mouse $\alpha$ Synaptotagmin2	Syt2	Type 2 cone bipolar cells	Santa Cruz Biotechnologies (Santa Cruz, CA)	SC6026	1:250
Goat $\alpha$ Vesicular glutamate transporter type 3	VGLUT3	VGLUT3 amacrine cells	Santa Cruz Biotechnologies (Santa Cruz, CA)	SC26031	1:500

\* conjugated to Cy3

**Table 4.** Primary antibodies used in Chapter 3.

~18 10× maximum projection fields similarly stitched together. Each projection was taken from ~40 optical sections at 1 μm intervals through the z-axis. For the analysis of astrocytic sprouting, large fields (0.81 mm<sup>2</sup>) were made by stitching 16 individual 40× z-stacks at 4 different locations on the retina, one per quadrant. All images were acquired on an Olympus FV1000 scanning laser confocal microscope.

Retinal ganglion cells were counted from 8 peripheral and 4 central fields (0.09 mm<sup>2</sup>) per animal (CTL: n = 6; CKO: n = 5). Cells were identified as Brn3b-positive profiles within each field using Fiji software (<https://fiji.sc/>). Microglia were similarly counted from 20× fields in the ganglion cell layer (GCL) and inner nuclear layer (Schafer et al.) (CTL: n = 4; CKO: n = 5) using BioQuant Nova Software (BIOQUANT Image Analysis).

Z-stack projection images extended into the inner retina to include all GFAP-positive staining, excluding labeling in the nerve fiber layer. Images were contrast-enhanced in Adobe Photoshop (San Jose, CA) and then Fiji software was used to automatically threshold every labeled profile in the inner retina; values represent the number of pixels that are GFAP-positive across each entire 0.81 mm<sup>2</sup> fields. Counts were averaged to yield values per retina and expressed as mean ± s.e.m. Orthogonal reconstructions were made from 60× z-stacks extending 120 μm into the retina.

Measurements of the extension of the collagen-positive vascular network toward the retinal periphery were made from 4 locations across the developing retina, one in each quadrant. The distance of Collagen-IV-immunopositive profiles was calculated as a percentage of the distance from the optic nerve head to the retinal edge at each location, and subsequently averaged across the quadrants for each retina. Extreme outliers (Q3 + 3\*IQR, Q1 – 3\*IQR) were removed.



Vascular branch points were counted manually from 8 peripheral and 4 central fields (0.09 mm<sup>2</sup>) per animal using Fiji software. A branch point was defined as any intersection of two blood vessels, excluding small capillaries. Total vessel length was also measured from the same fields. Each of these two analyses was conducted without knowledge of genotype, the retinas being coded and randomly intermingled beforehand. The 12 measurements were averaged to yield values for each retina.

### **Statistics**

To ascertain significant differences between CTL and CKO astrocytic sprouting, a two-tailed Mann-Whitney U test was used to test for differences between the groups ( $U = 12$ ,  $n_1 = 8$ ,  $n_2 = 9$ ). Differences in collagen extension at each time point were assessed using a two-tailed Mann-Whitney U test (P5:  $U = 2$ ,  $n_1 = 4$ ,  $n_2 = 5$ ; P10:  $U = 0$ ,  $n_1 = 5$ ,  $n_2 = 5$ ; Adult:  $U = 3$ ,  $n_1 = 5$ ,  $n_2 = 5$ ). Statistics were run on the raw data but are represented as fold changes for visualization purposes. Vascular branch point measurements between CTL and CKO fields were tested for differences using a two-tailed Student's t-test. All statistical analyses were performed using SPSS Statistics (IBM, Armonk, NY) and used a significance threshold of  $p \leq 0.05$ .

## ***D. Results***

### **1. Characterization of the CKO retina**

The conditional deletion of *Sox2* from retinal astrocytes was confirmed in the mature retina by the absence of Sox2 immunoreactivity from all retinal astrocytes. GFAP-positive astrocytes remain present (yellow arrowheads in Figure 21a,e), but they have now lost their Sox2-immunoreactivity in the CKO retina, while those in littermate control retinas remain

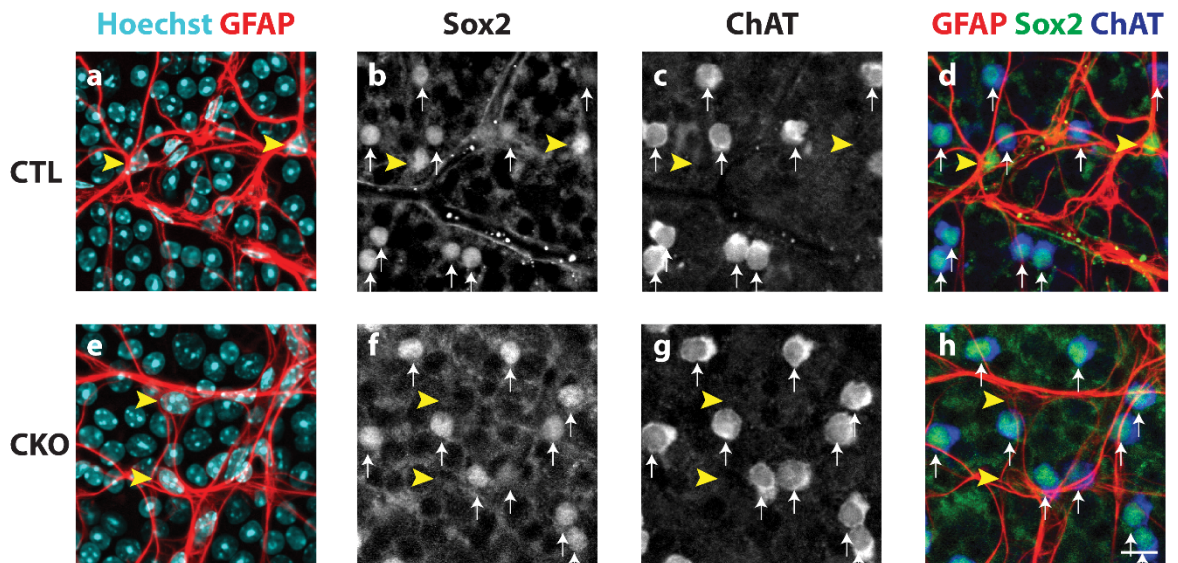


**Figure 21: Characterization of Sox2 conditional knockout mice.** In control animals (CTL), astrocytes are visualized by co-localization of Hoescht and GFAP antibodies (yellow arrowheads, a). These cells are distinct from cholinergic amacrine cells that are both ChAT and Sox2-positive (white arrows, b-d). In the Sox2 conditional knockout retinas (CKO), astrocytes are Sox2-deficient as evidenced by the lack of Sox2 staining in astrocyte cell bodies (yellow arrowheads, e-f, h). However, Sox2 remains in cholinergic amacrine cells (white arrows, f-h), showing that Sox2 is removed from the population of retinal astrocytes. Hoescht = nuclear stain; GFAP = glial fibrillary acidic protein; ChAT = choline acetyltransferase; Sox2 = sex determining region-box 2. Scale bar = 25  $\mu$ m.

Sox2-positive (compare yellow arrowheads in Figure 21b,f). Sox2-immunopositive cells remain in the CKO retinas (white arrows in Figure 21f), however, each one of these cells was confirmed to be a cholinergic amacrine cell, also observed in control retinas (white arrows in Figure 21c,g). These results confirm the loss of Sox2 from the population of astrocytes in CKO retinas. All other features of the mature retinal architecture appear unaltered, evidenced by immunolabeling retinal sections with antibodies to reveal the cellular and synaptic lamination (Figure 22).

## **2. Maturation of Sox2-Deficient Astrocytes**

We first investigated whether the loss of *Sox2* in astrocytes causes a disruption to their development. Immature astrocytes expressing Sox2 migrate into the retina from the optic nerve head around the day of birth, by responding to environmental cues such as platelet-derived growth factor A-chain (PDGF-A) (Fruttiger et al., 1996) and laminins  $\beta 2$  and  $\gamma 3$  (Gnanaguru et al., 2013). These immature astrocytes, visualized by expression of Pax2, migrate radially across the retinal surface, reaching the peripheral edge of the retina by postnatal (P) day 5 (Chu, Hughes, & Chan-Ling, 2001; Ling, Mitrofanis, & Stone, 1989; Sandercoe, Madigan, Billson, Penfold, & Provis, 1999; Stone & Dreher, 1987; Watanabe & Raff, 1988). We observed that at P1, migrating astrocytes are found in both CTL and CKO retinas with no apparent differences in their spatial distribution nor in their morphologies (Figure 23a-d). These cells are found in comparable densities, extending from the optic nerve head (ONH) roughly halfway towards the peripheral edge, coursing across the retinal nerve fiber layer (NFL) (compare Figure 23b with 23d). In the CTL retina, these migrating astrocytes are Sox2-immunopositive (Figure 23e), yet in the CKO retina this Sox2-positive population is no longer detected (Figure 23g). Note that a few cells remain Sox2-

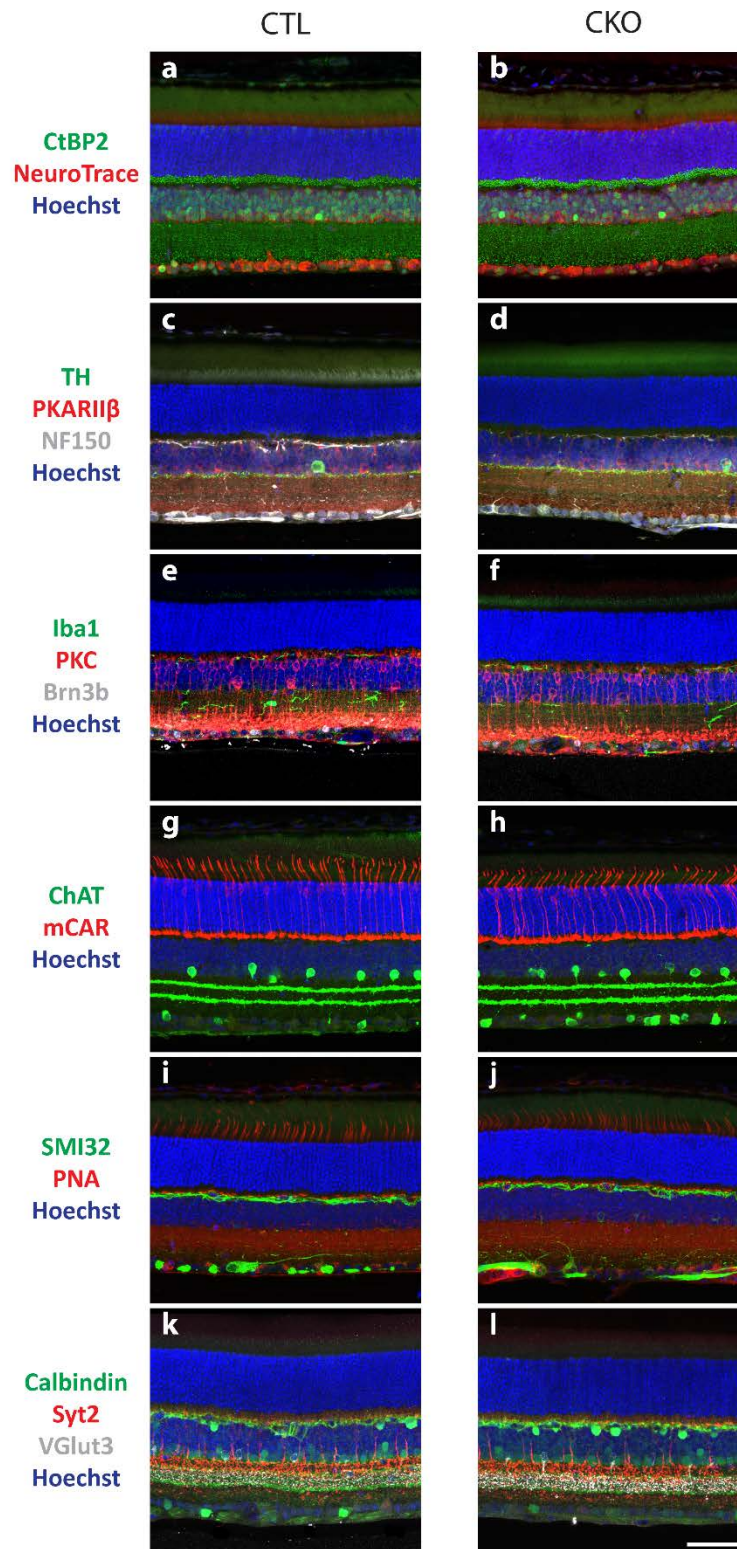


**Figure 22: Retinal histology is unaltered in CKO animals.** The following were used to reveal various cell types and morphological features in retinal sections:  $\alpha$ CtBP2 and NeuroTrace (a,b);  $\alpha$ TH,  $\alpha$ PKAR11 $\beta$ , and  $\alpha$ NF150 (c,d);  $\alpha$ Iba1,  $\alpha$ PKC, and  $\alpha$ Brn3b (e,f);  $\alpha$ ChAT and  $\alpha$ mCAR (g,h); SMI32 and PNA (i,j);  $\alpha$ Calbindin,  $\alpha$ Syt2, and  $\alpha$ VGlut3 (k,l). All sections are co-labeled with Hoechst to show the architecture of the three cellular layers. All sections were taken at a distance of  $\sim$  1 mm from the optic nerve head. Scale bar = 50  $\mu$ m.

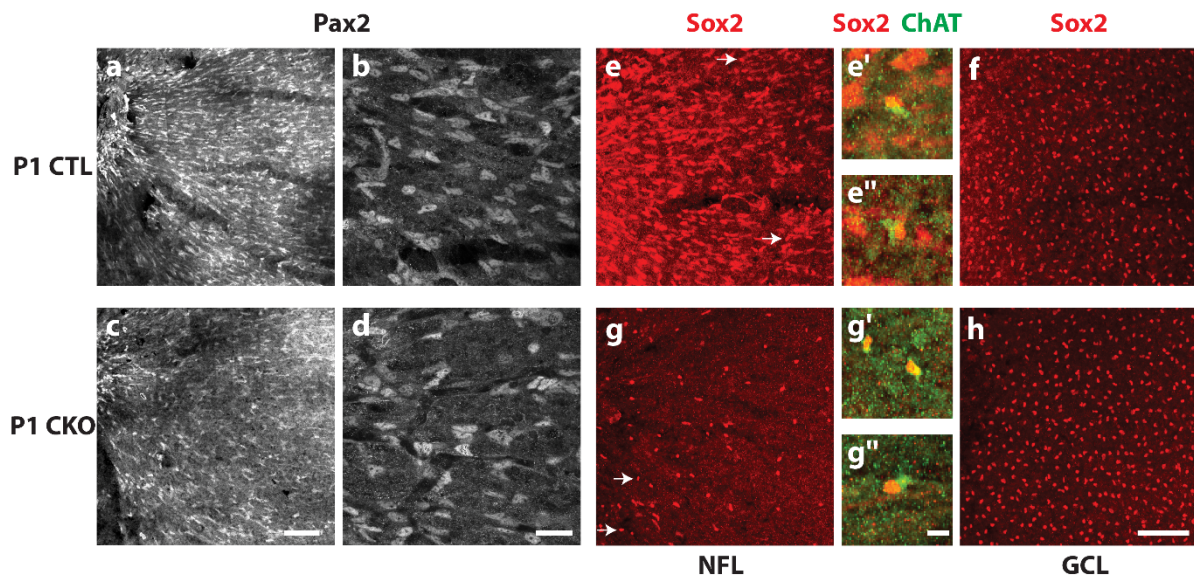


**Figure 23: Pax2-positive astrocytes at P1 migrate normally in CKO retinas.** At low magnification, Pax2-positive astrocytes are seen migrating from the optic nerve head in the central retina (left) towards the periphery in CTLs (a). At higher magnification, an elongated morphology typical of these cells is present (b). CKO Pax2-positive cells appear in comparable density and morphology to CTL retinas (c-d). Almost all Sox2-immunopositive cells in the NFL appear to be astrocytes, with the exception of a few ChAT-positive cells that are occasionally found in the NFL (arrows in e,e',e''), yet are spatially displaced from the population of Sox2-positive cholinergic amacrine cells in the GCL (f). In CKO retinas, by contrast, very few Sox2-positive cells are found in the NFL (g) and are displaced ChAT-positive cells (g' and g''). The population of cholinergic amacrine cells in the GCL appears indistinguishable from CTL retinas (h). All panels are oriented with the optic nerve head to the left. NFL = nerve fiber layer; GCL = ganglion cell layer; Scale bar a,c,e-h = 100  $\mu$ m; b,d = 25  $\mu$ m; e',e'',g',g'' = 10  $\mu$ m.

immunoreactive in the CKO retina (white arrows in Figure 23g); these cells have a smaller and rounder profile, not unlike those that are distributed in the GCL, being the cholinergic amacrine cells (Figure 23f,h). These are also present in the control retina at P1 (white arrows in Figure 23e), but are generally obscured by the more conspicuous Sox2-positive population of astrocytes therein. That these few Sox2-positive cells in the CKO retinas are in fact cholinergic amacrine cells displaced closer to the NFL is evidenced by the presence of weak ChAT-immunoreactivity in their cytoplasm (Figure 23e',e'',g',g''). The Pax2-positive cells continue their migration toward the periphery by P5, in both CKO and CTL retinas (to the right in Figures 24a,d). These data confirm the loss of Sox2 from the population of astrocytes during their period of migration across the developing retina, yet demonstrate no obvious disruption in their migratory progress to the retinal periphery.

Astrocytes express GFAP at low levels during the perinatal period as they invade the retina (West, Richardson, & Fruttiger, 2005), but gradually increase expression throughout postnatal development until expression plateaus around P10 (Sarchy, Fu, & Huang, 1991; Tao & Zhang, 2014), when Pax2 protein levels gradually subsides. Coincident with this transition, the spatial distribution of the astrocytes changes by P5, in association with the emerging vasculature. At this age, these Pax2-positive cells closest to the ONH form ring-like patterns associated with the emerging vasculature and exhibit heavy GFAP expression, diminishing toward peripheral regions already colonized by less mature astrocytes (Figure 24a-c). In comparison, CKO retinas show marginal expression of GFAP, despite the widespread distribution of astrocytes evidenced by their Pax2 immunoreactivity (Figure 24d-f). These Pax2-positive astrocytes in the more central regions of the CKO retina also lack the ring-like formations seen in CTL retinas.

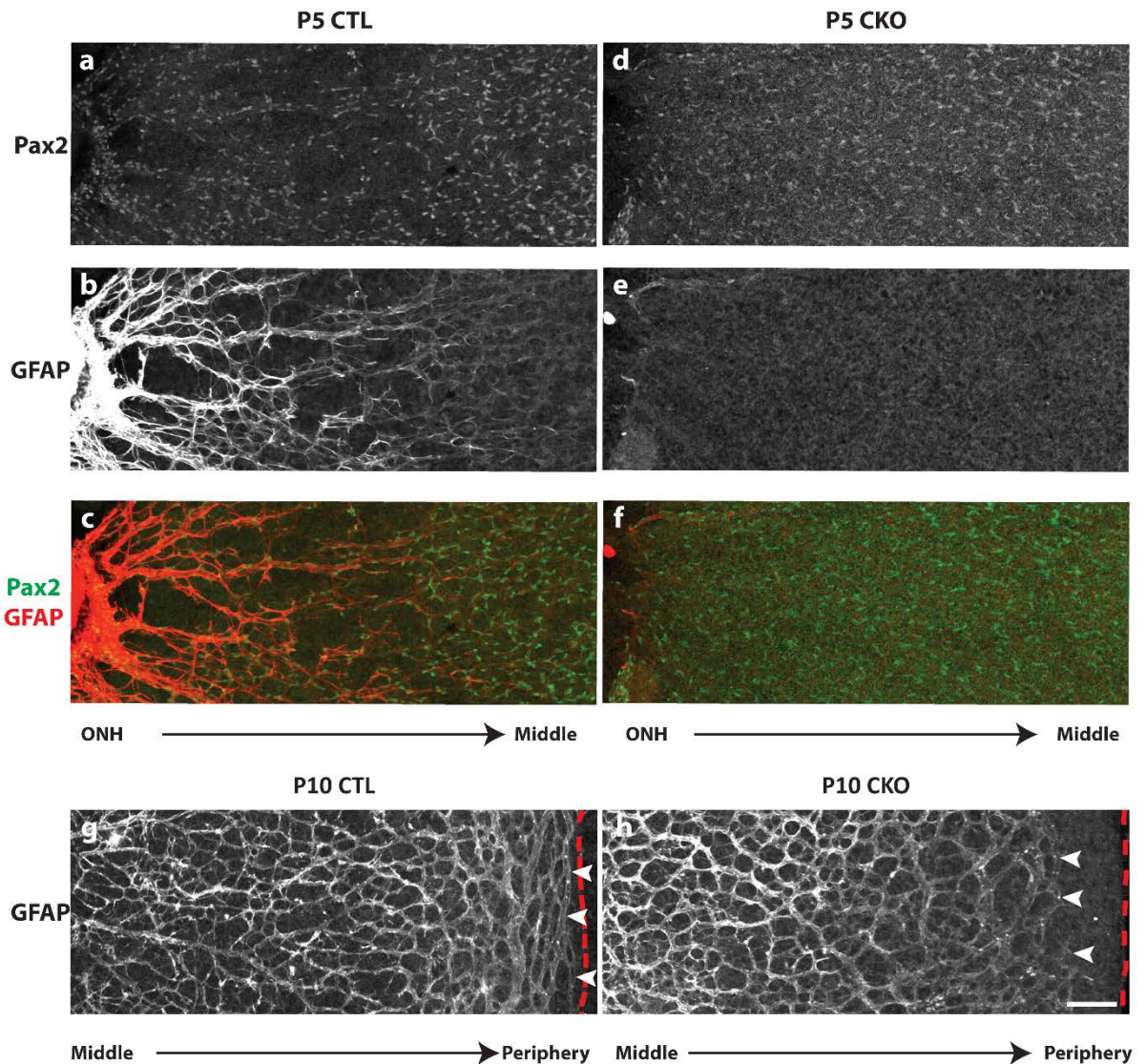


**Figure 24: CKO retinas exhibit a delayed maturation at P5 and P10.** CTL Pax2-positive astrocytes at P5 are arranged in a ring-like pattern (a) and upregulate GFAP robustly near the ONH (b). In this region, the distribution of Pax2-positive cells coincides with the GFAP network (c). Conversely, CKO astrocyte cell bodies do not rearrange themselves as they do in CTLs, evidenced by their more uniform distribution (d,f). CKO astrocytes also fail to upregulate GFAP (e,f). At P10, GFAP-positive astrocyte processes (g, arrowheads) nearly reach the far peripheral edge of the retina (g, dashed line). Processes closer to the central retina become thinner and begin forming the web-like morphology characteristic of GFAP-positive processes seen in mature retinas, while less mature processes at the far periphery show a conspicuously circumferential patterning (g). In P10 CKO retinas however, the extension of GFAP-positive processes (h, arrowheads) is delayed and fails to reach the retinal edge (h, dashed line). In addition, GFAP-positive processes at more central locations show a delay in their acquisition of the more mature patterning exhibited in CTL retinas (h). ONH = optic nerve head; GFAP = glial fibrillary acidic protein; Scale bar = 100  $\mu$ m.

By postnatal day 10, when Pax2 is no longer detected in retinal astrocytes, both CTL and CKO astrocytes robustly express GFAP (Figure 24g,h), yet there remains a delay in GFAP upregulation at the peripheral edge, not quite reaching the retinal margin (compare white arrowheads with red dashed line indicating the retinal margin in Figure 24g,h). There, P10 CTL astrocytes form a web running circumferentially along the retinal margin that is not seen in the CKO retinas. This too is a transitory feature in the CTL retina, ultimately giving way to the characteristic pattern of astrocytes blanketing the mature retina (see below). Note as well that the transition to the web-like patterning seen in maturity is already beginning to materialize more centrally in the CTL retinas (Figure 24g), while this is notably delayed in the CKO retinas (Figure 24h). Taken together, the data from these developmental time-points indicate that Sox2 plays a key role in the maturation of astrocytes in the developing retina.

### **3. GFAP Depletion in Peripheral Retina**

To assess whether these developmental abnormalities might translate into lasting changes within the population of mature astrocytes, we examined retinas from adult animals for perturbations to the mature astrocytic network. Control retinas exhibit a uniform GFAP staining pattern across all retinal eccentricities (Figure 25a). High magnification images reveal the typical web-like network of thin stellate processes that appear evenly distributed (Figure 25a'). Conversely, CKO retinas show a profound if sporadic loss of GFAP staining specifically in peripheral regions, appearing unaffected at central locations (Figure 25b,b'). The severity of this phenotype varies amongst CKO animals, ranging from a single peripheral patch to almost the entirety of the peripheral retina. In those peripheral regions with such atypical GFAP immunolabeling, remaining astrocytic processes show a loss of the



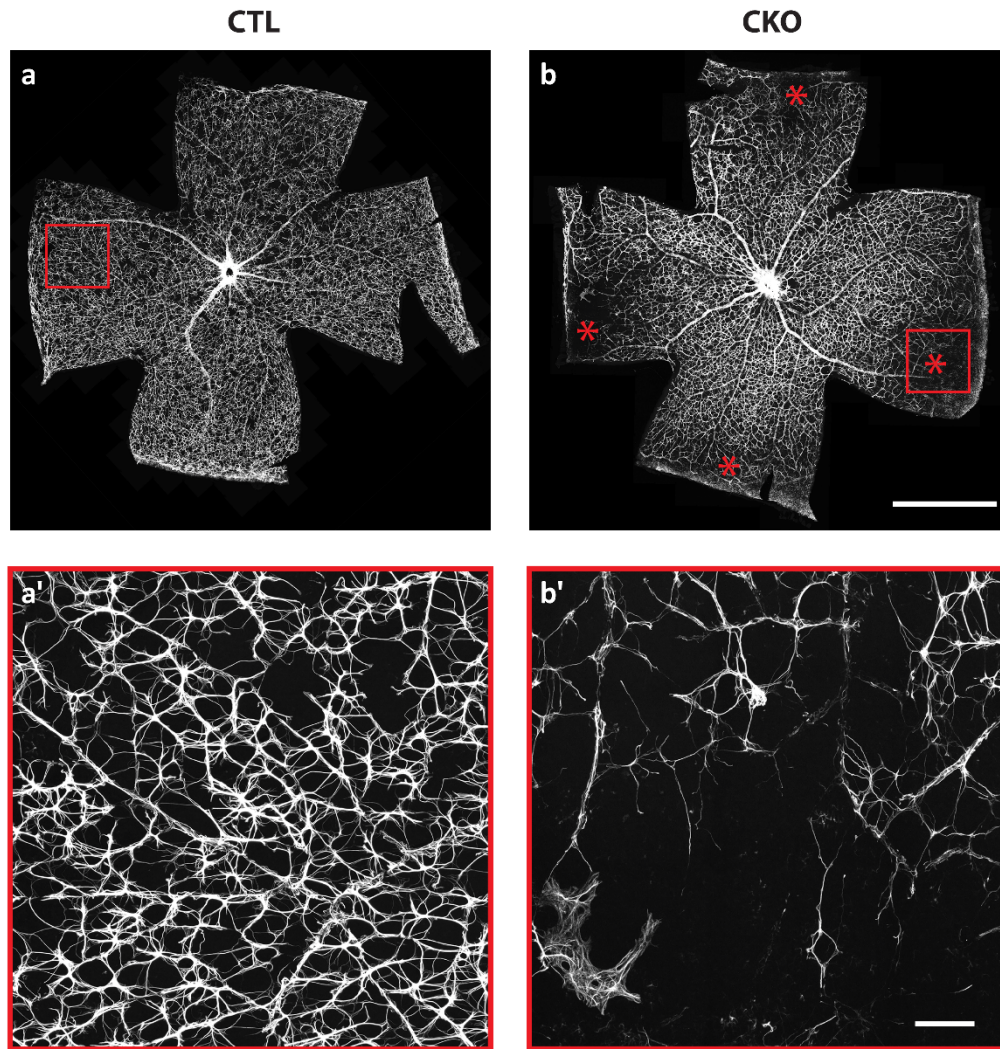


**Figure 25: Peripheral astrocytic abnormalities in CKO retinas.** CTL astrocytes exhibit a uniform GFAP staining pattern across the surface of the retina (a). 40× magnification of the area within the red box in a demonstrates the characteristic web of GFAP-positive processes (a'). CKO retinas show a profound if sporadic loss of GFAP staining in peripheral regions (b). 40× magnification of red box in b (b'). \* = Quadrants with loss of GFAP immunoreactivity. GFAP = glial fibrillary acidic protein; Scale bar a-b = 1 mm; a'-b' = 100 μm.

characteristic web-like distribution of processes when compared to CTL astrocytes (Figure 25a',b').

This depletion in the pattern of GFAP labeling was observed in 23/28 quadrants when sampling across seven CKO retinas, never having been observed in CTL retinas (Figure 26). However, some quadrants remain unaltered, indicating that astrocytes are capable of migrating to the retinal edge in CKO animals. That they had done so, earlier in development in these affected quadrants, is supported by the observation that the retinal vasculature is present in these depleted regions (Figure 26d,d'). These results suggest that the depleted territory reflects a regressive event, for instance, that astrocytes have undergone apoptosis in these regions.

#### **4. Sprouting in CKO Retina**

The processes of wildtype astrocytes, labeled with GFAP, are normally restricted to the retinal NFL, with little to no labeling extending into the inner retina (Figure 27a-d). In injury conditions however, like that of retinal detachment, mouse astrocytes have been shown to extend processes into the inner retina (Luna et al., 2016). In regions of the CKO retina removed from the astrocytic deficit, we observed aberrant astrocytic sprouting into the inner plexiform layer (IPL), well beyond the normal stratified distribution within the NFL (Figure 27e-h). These retinas exhibit, on average, an eight-fold increase in the density of processes extending into the IPL compared to controls, albeit CKO samples showed conspicuous variability (Figure 27i,  $p = 0.012$ ). These sprouted processes in CKO retinas can extend over a hundred microns into the retina and appear to stratify at particular depths as seen in high magnification z-stack reconstructions from 120  $\mu\text{m}$  thick stacks from CTL and CKO retinas (Figure 27j,k).

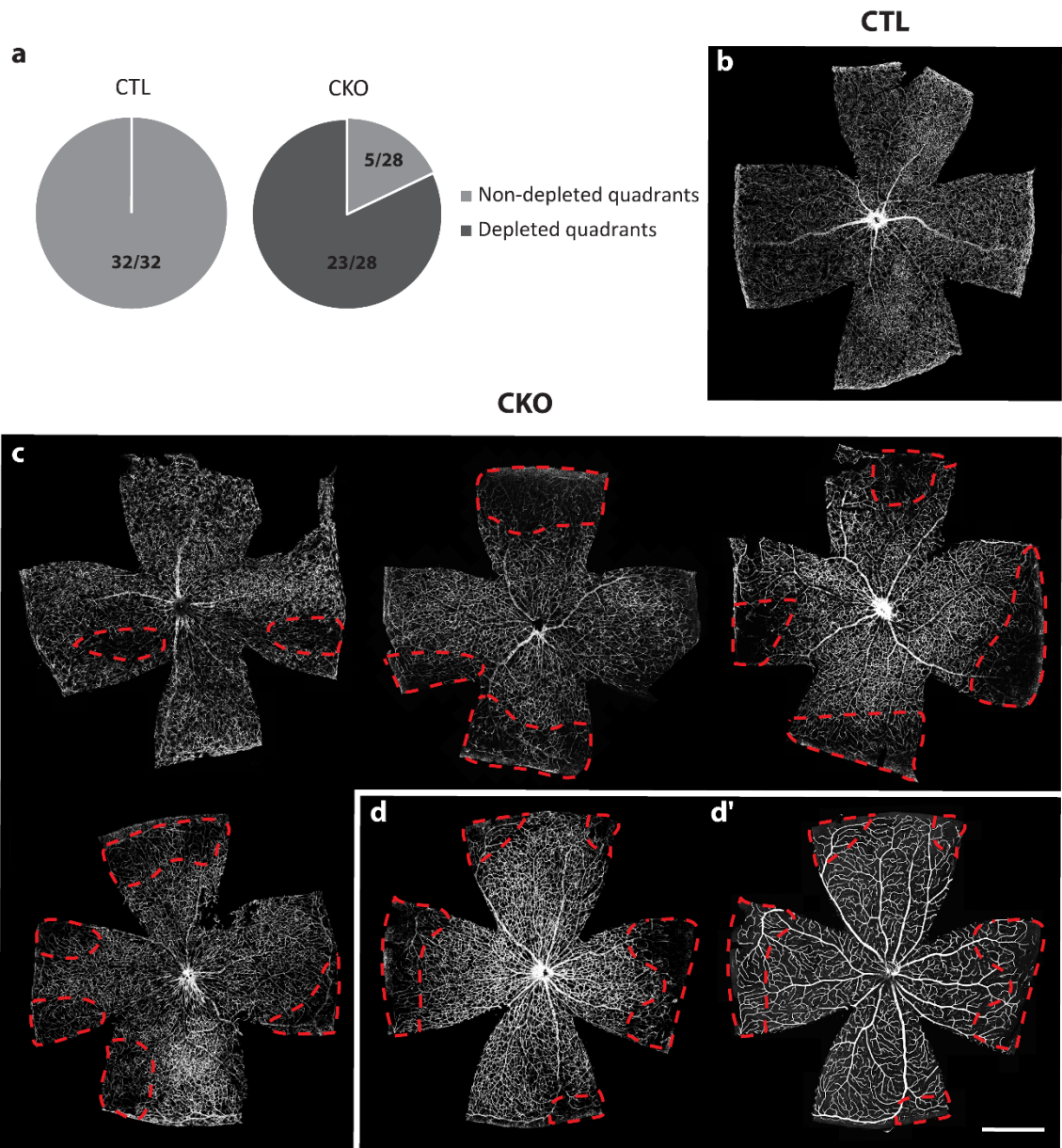


**Figure 26: GFAP depletion is pervasive in peripheral regions of CKO retinas.** Quantification of depleted quadrants between CTL (n = 8) and CKO retinas (n = 7) (a). CTL retina immunostained to label GFAP shows even staining across all eccentricities (b). CKO retinas exhibit a loss of GFAP immunoreactivity in peripheral regions, indicated with dashed red lines surrounding depleted regions from five exemplary retinas (c,d). Vasculature extends into depleted regions, indicated by Collagen IV-positive signal (d' compared with d). n = number of sampled retinas. Scale bar = 1 mm.

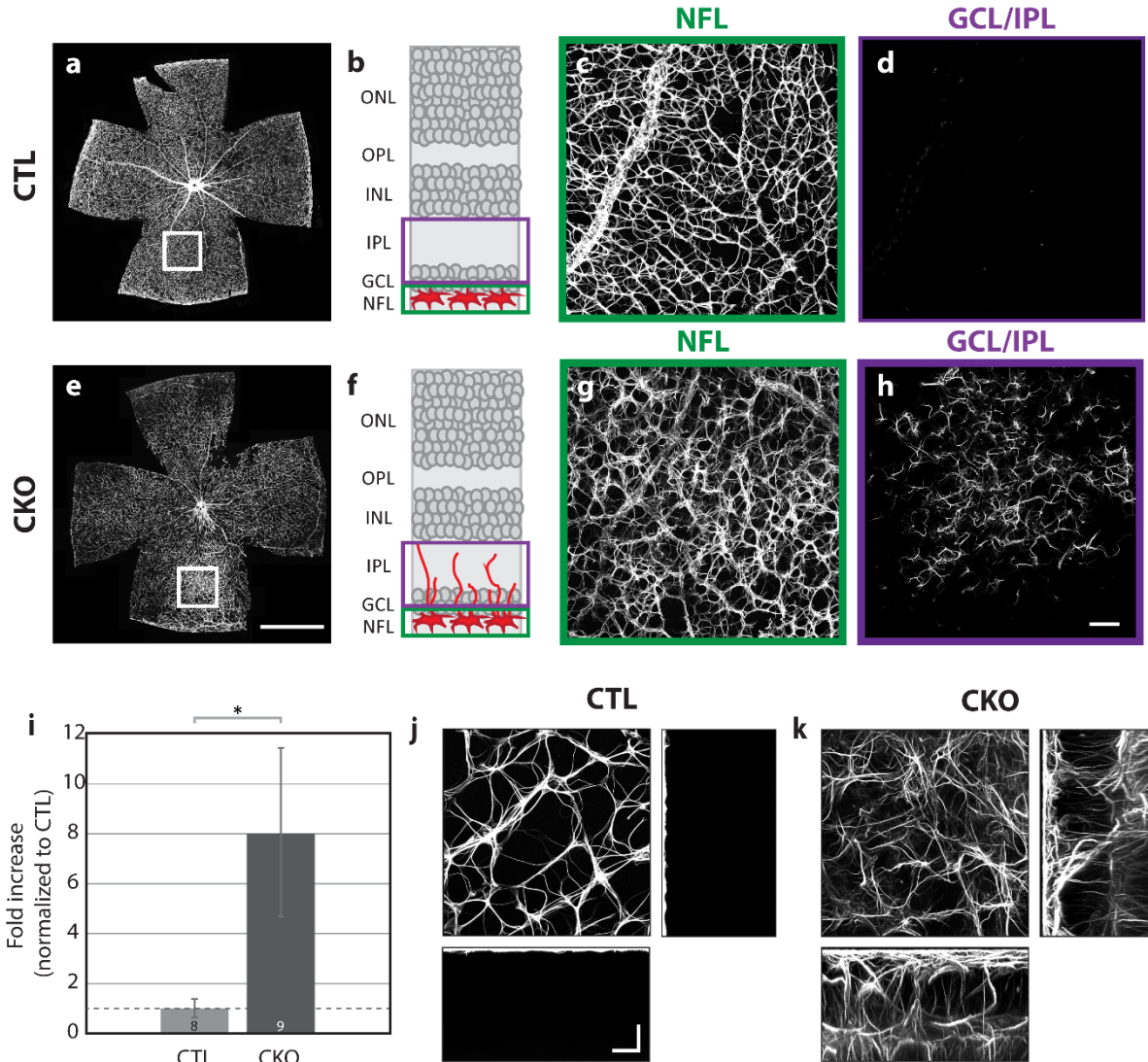


**Figure 27: GFAP processes sprout into the inner retina in CKO animals.** Whole CTL retina immunostained with GFAP (a). Schematic of retinal section showing that GFAP-positive astrocytic processes are almost exclusively confined to the NFL (green box, b). GFAP staining is uniform across the NFL when viewing a field en face (c, magnified from white box in a). The GCL and IPL are largely devoid of GFAP labeling in CTL retinas (d). Whole CKO retina stained with GFAP (e). Schematic of retinal section depicts GFAP-positive processes extending into the retina past the GCL (purple box, f). GFAP staining is uniform across the NFL in this example, as in CTL retinas (g), yet CKO retinas display sprouting of processes well beyond the level of their normal positioning (h, magnified from white box in e). Sprouting is extensive in the CKO retinas relative to CTL retinas (i, dashed line represents CTL retinas normalized to 1). High magnification z-stack reconstruction from CTL retina showing no astrocytic labeling extending into the inner retina (j). High magnification z-stack reconstruction from CKO retina showing aberrant sprouting into the inner retina extending at least 120  $\mu\text{m}$  deep (k). GCL = ganglion cell layer; GFAP = glial fibrillary acidic protein; INL = inner nuclear layer; IPL = inner plexiform layer; NFL = nerve fiber layer; ONL = outer nuclear layer; OPL = outer plexiform layer; Scale bar a,e = 1 mm; c,d,g,h = 100  $\mu\text{m}$ , j,k = 25  $\mu\text{m}$ . n = number of sampled retinas. \* =  $p \leq .05$ .

Despite the sporadic absence of peripheral GFAP and this aberrant sprouting of processes into the inner retina elsewhere, other assessments of retinal histology (e.g. Figure 22), including retinal area (Figure 28a), appear unchanged between CTL and CKO retinas. However, in a few rare cases, we observed large regions lacking GFAP labeling (Figure 28e, compare with 28c) and a reduction in the density of retinal ganglion cells and their axons labeled with antibodies to neurofilaments, the severity of which never mapped precisely upon the changes in the astrocytic array (Figure 28f, compare with 28d). When analyzing mature retinas without biasing our sampling protocol to depleted regions, CKO retinas exhibited a slight if non-significant reduction in the density of Brn3b-positive retinal ganglion cells compared to CTLs (Figure 28b). Because of such rare extreme examples showing depleted neurofilament-positive retinal ganglion cells (e.g. Figure 28f), the Brn3b+ cell counts are likely indicative of a slight reduction in ganglion cell density.

Counts of microglia, at P17, sampled without biasing to astrocyte-depleted regions, show a similar slight, if non-significant, increase in their frequency, restricted to the GCL (Figure 29a-c), which may be indicative of an apoptotic loss of these RGCs, or possibly the astrocytic changes noted above. That the astrocytes have died in those regions depleted of GFAP labeling is supported by the observation that another marker for mature astrocytes, Sox9, is similarly missing from those depleted regions (Figure 30a-i). Nevertheless, these results would suggest that, despite the complete loss of Sox2 from the entire astrocytic population, these retinas rarely show conspicuous changes or other histological signs of severe degeneration. Rather, the pattern of mature astrocytes shows only a regional loss as well as aberrant sprouting, suggesting a modest level of cellular stress that, in more extreme cases, impacts the population of neurons most intimately associated with the astrocytes.

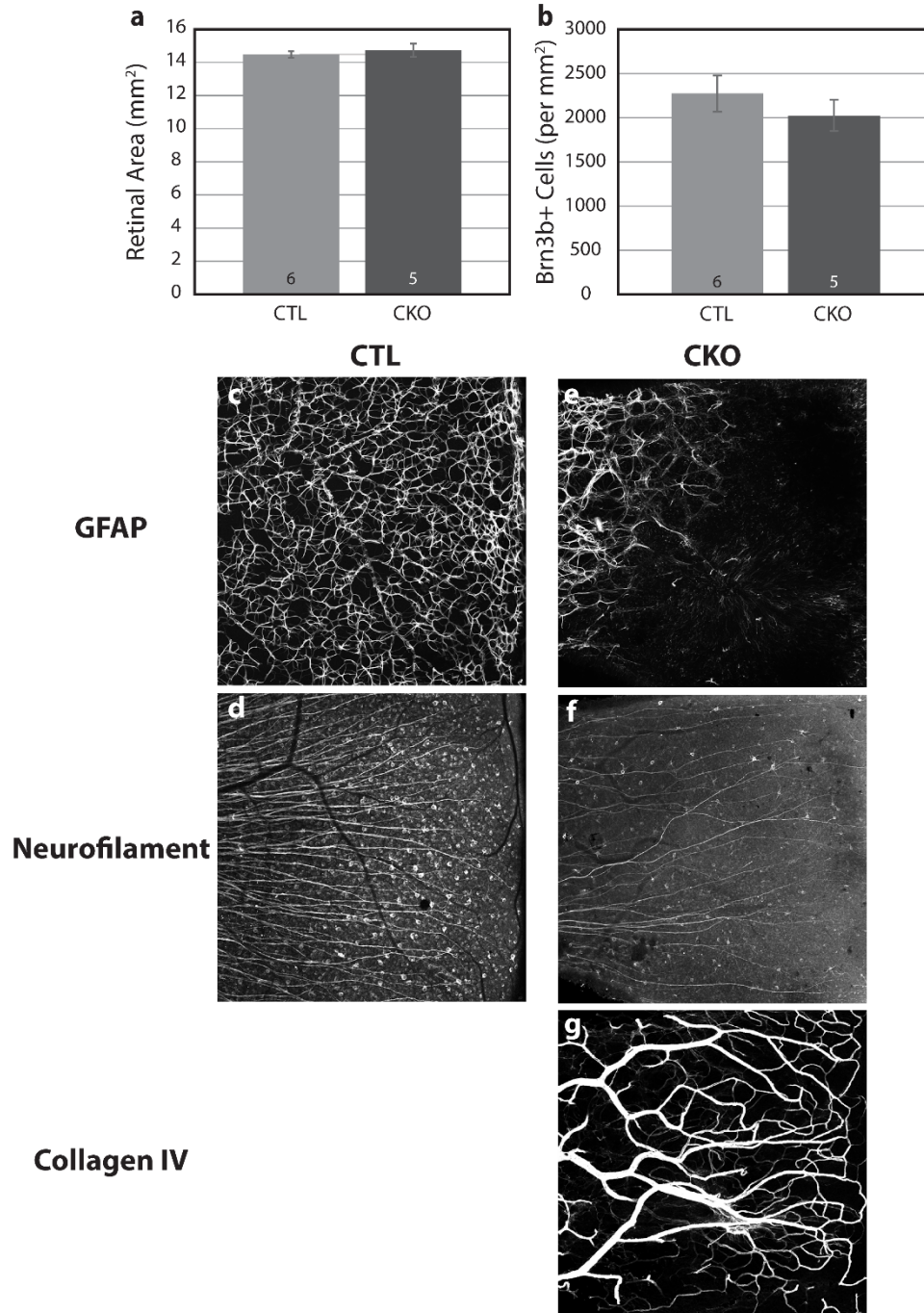


**Figure 28: CKO retinas can exhibit extreme abnormalities.** Retinal area is unchanged between CTL and CKO retinas (a). CKO retinas show a non-significant decrease in the density of Brn3b-positive retinal ganglion cells compared to CTL retinas (b). n = number of sampled retinas. CTL retinas show even GFAP staining across the surface (c). CKO retinas can exhibit quadrants with an almost complete loss of GFAP (e). Neurofilament staining, labeling retinal ganglion cell axons and some retinal ganglion cells, shows an even radiating distribution of axons across the central to peripheral axis (left to right, d). In extreme cases, CKO retinas show a dramatic loss of neurofilament staining evidenced by both a loss of axons and cell bodies (f). In this same severely depleted region, retinal vasculature appeared abnormal in GCL, although some inner retinal vasculature is included in projection image due to a decrease in retinal thickness (g). Collagen IV immunostaining was not captured for CTL retina. Vertical panels in each column are from the same retinal quadrant. n = number of sampled retinas. Scale bar = 250  $\mu$ m.

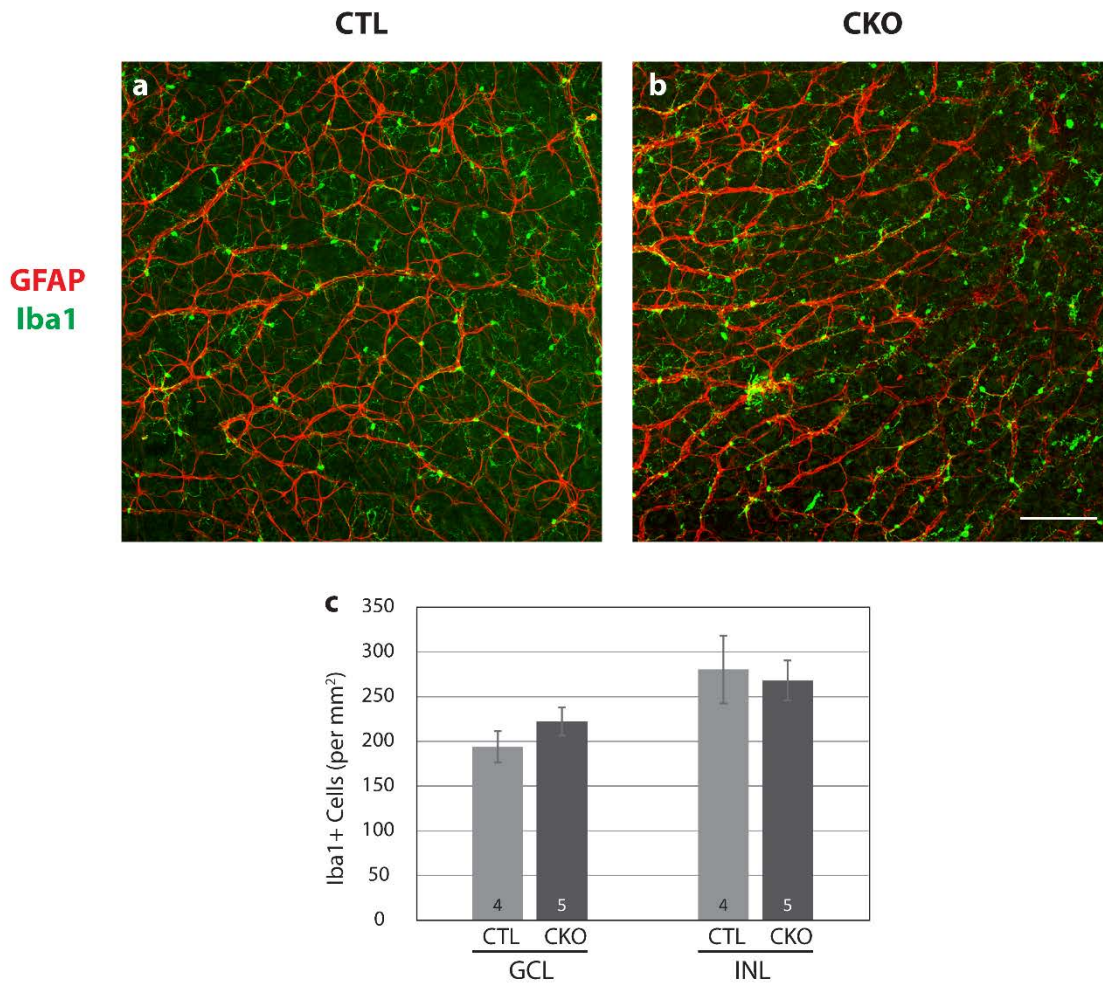


**Figure 29. CKO microglia density is not significantly increased in GCL.** Representative images from CTL (a) and CKO (b) retinal wholemounts showing astrocytes in red and microglia in green within the GCL. Quantification shows a slight yet non-significant increase in microglial cell density in the GCL but not in the INL (c). GCL = ganglion cell layer; INL = inner nuclear layer. n = number of sampled retinas. Scale bar = 100  $\mu$ m.

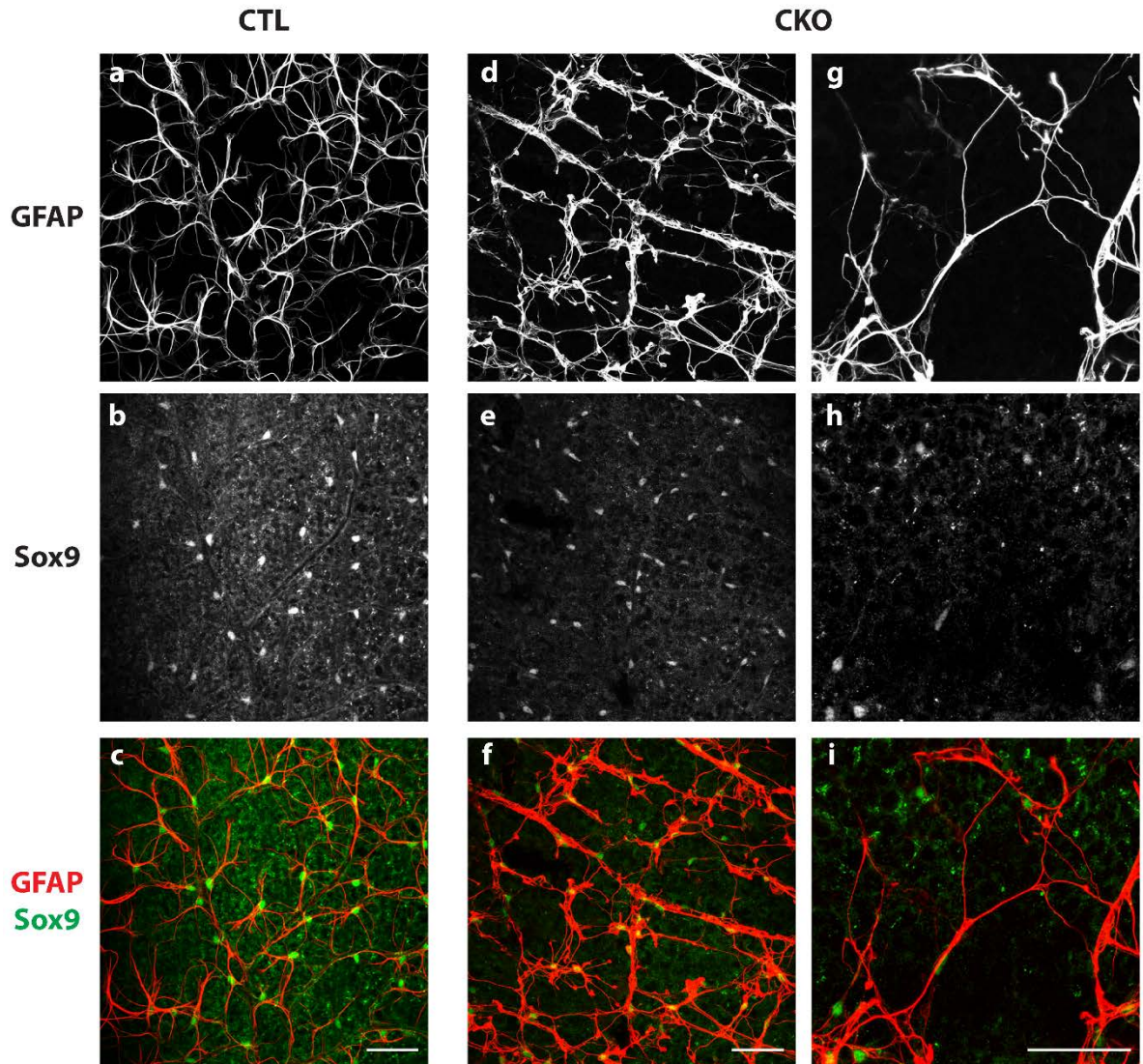


**Figure 30: CKO depleted regions appear Sox9-negative.** Astrocytes cell bodies in CTL retinas appear Sox9-positive (a-c). CKO peripheral retinas likewise show Sox9 immunoreactivity colocalized with GFAP immunostaining, in peripheral regions with varying degrees of GFAP depletion. Sox9 is rarely, if ever, seen in GFAP-negative regions (d-i). Scale bars = 50  $\mu$ m.



## 5. Vascular Abnormalities in CKO retinas

It is known that as astrocytes enter the retina, they secrete many factors, including VEGF, which serve as migratory guides for endothelial tip cells residing on the leading edge of the developing retinal vasculature (Fruttiger, 2002; Jiang, Bezhadian, & Caldwell, 1995; Y. Zhang et al., 2014). The apparent delay in astrocyte maturation suggested a potential effect upon the maturation of the vasculature itself. Indeed, the normal invasion of the vasculature, from the ONH to the retinal periphery, was conspicuously delayed compared to that of controls, as evidenced by the pattern of Collagen IV immunostaining in whole retinas (Figure 31a-g). At P5, the developing retinal vasculature in CTL retinas extends from the ONH to roughly 55% of the distance to the peripheral edge. In the more central regions, this web of maturing vessels contours nicely with the ring-like pattern of astrocytes at this same age (compare with Figure 3c). By contrast, the developing retinal vasculature is delayed in the CKO retinas, having extended only 33% of this centro-peripheral dimension (Figure 31a,d,g,  $p = 0.050$ ). By P10, the CKO vasculature continues to show a delay in advancement towards the retinal edge, extending 92% towards the retinal edge, compared to 99% in CTL retinas (Figure 31b,  $p = 0.009$ ). CKO retinas, interestingly, show a lasting significant if slight reduction in the establishment of the vascular network at the peripheral margin of the retina in adulthood compared to controls (Figure 31c,f,g,  $p = 0.047$ , e.g. compare Figure 31f with 31c). These observations show that delays in vascular invasion mimic those delays seen in astrocytic maturation.

Given the sprouting observed in the population of mature astrocytes in CKO retinas, we examined other features of the mature vascular network in further detail. But with one exception (Figure 28g), the CKO vasculature showed no gross morphological differences

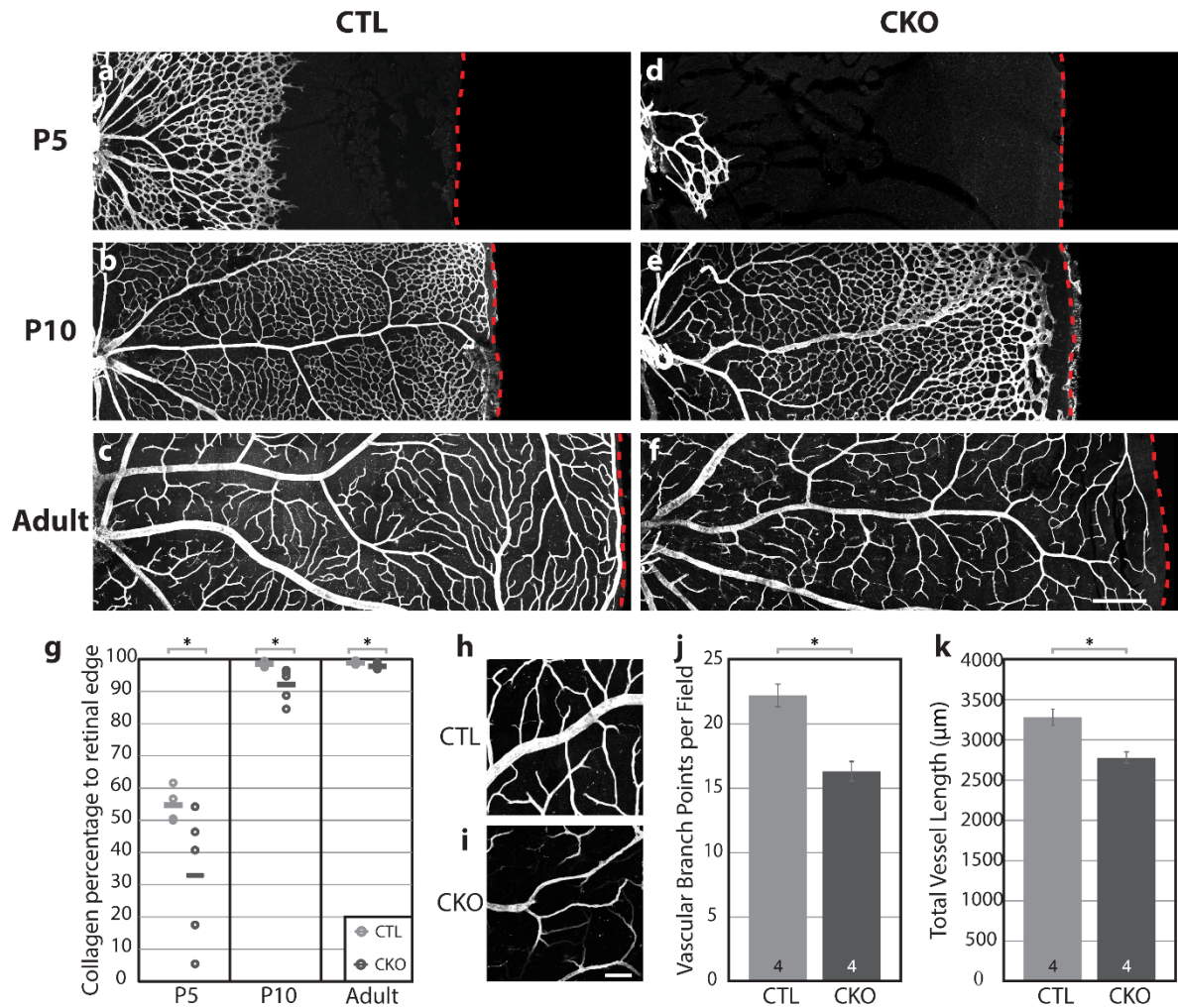


**Figure 31: Retinal vasculature develops abnormally in CKO retinas.** Representative images showing extent of vascular outgrowth in CTL retinas (a-c) and CKO (d-f) at P5, P10, and adult (P22), respectively. At P5, CKO retinas show a significant decrease in the invasion of Collagen IV-positive blood vessels as evidenced by a marked decrease in the percentage of their extension to the retinal edge compared to CTL retinas (g). CKO vascular invasion still shows a delay at P10 and this disparity is sustained into adulthood when CKO retinas show a significant reduction in the extension of the vascular network towards the peripheral margin (g). Representative fields from adult CTL (h) and CKO (i) retinas stained with Collagen IV reveal that CKO retinas have significantly fewer vascular branch points (j) and an overall decrease in total vessel length per field than CTL retinas (k). Dashed red line represents the retinal edge. Panels in a-f are oriented with ONH to left. In panel g, open circles represent individual retinas and horizontal lines are averages. Scale bar a-f = 1 mm; h,i = 100 μm. n = number of sampled retinas. \* =  $p \leq .05$ .

from control animals, aside from the above-mentioned absence at the extreme margin of the retina (Figure 31c,f,g); detailed analysis, however, revealed subtle changes to the vascular architecture, pervasive throughout the retina (Figure 31h,i). CKO retinas have significantly fewer vascular branch points than controls (Figure 31j,  $p = 0.002$ ). Abnormal blood vessel branching is thought to result from a disordered development of the retinal angioarchitecture (DiMaio & Sheibani, 2008), implying that CKO animals have impairments in the formation of their vascular network causing a subsequent decrease in the number of vascular branch points. This was corroborated by the CKO retinas showing a significant decrease in overall vessel length when compared to fields from CTL retinas (Figure 31k,  $p = 0.006$ ). These results suggest that the delayed arrival of the retinal vasculature may impede normal vascular branch formation, resulting in a lasting diminution of the vascular architecture, raising the possibility that the CKO retina might be mildly anoxic during development and in maturity.

### ***E. Discussion***

Here we identify a novel role for the transcription factor Sox2 in the development of retinal astrocytes and vasculature. We show that Sox2 is necessary for the time course of astrocytic maturation in early postnatal development, as well as for the establishment and/or maintenance of astrocytic morphology in adulthood, evidenced by the regional loss of GFAP expression and aberrant sprouting into the inner retina after its removal. Vascular invasion into the retina in these CKO animals is also delayed and defects to the vascular network are present in adulthood.

To our knowledge this is the first evidence that Sox2 plays a role in astrocytic

development and one of the few instances of a role for the gene outside of very early embryonic development. In addition, very few studies have examined the role of Sox2 specifically in retinal tissue. Recently, *Sox2* was shown to be expressed, uniquely amongst retinal neurons, in the cholinergic amacrine cell population, where its conditional deletion affected the positioning of cholinergic somata and the stratification of their dendrites (Whitney et al., 2014). *Sox2* has also been shown to be critical for developing Müller glia, as its conditional deletion from these cells alters their progenitor capacity and cellular morphology (Bachleda, Pevny, & Weiss, 2016; Surzenko et al., 2013). The present study now highlights new roles for this transcription factor in retinal astrocytes, the only other cellular population expressing Sox2 in the mature retina. Taken together these studies show that Sox2 plays a different role postnatally than it does during early embryonic development, notably by influencing cellular maturation and morphology.

*Sox2* is a highly conserved master transcriptional regulator known to play an essential role in all stages of CNS development in mammals (Kiefer, 2007). As astrocyte precursor cells mature, they downregulate genes such as *Pax2* and *Vimentin* while concurrently upregulating *GFAP* and *S100b*, among others (reviewed in Tao & Zhang, 2014). While it is known that Sox2 is present in astrocyte precursor cells and in mature astrocytes, how it interacts with other genes, in cells other than neural stem cells, remains to be determined.

Our data implicate *Sox2* as essential for astrocytic maturation as evidenced by the delayed upregulation of GFAP when *Sox2* is genetically removed from developing astrocytes. In addition, Sox2 likely plays a role in cellular maintenance, given the observed regional loss of astrocytes and their atypical sprouted morphology in the mature retina. Sox2 is traditionally regarded as a transcriptional activator, although more recent studies

have suggested that Sox2 can function as a repressor in neural stems cells (Liu et al., 2014). Indeed, Sox2 has been reported to repress the *GFAP* promoter *in vitro*, although it is known that genes can act as both activators and repressors depending on the tissue and cell type they are expressed in, as well as the availability of cofactors (Liu et al., 2014). Those studies would suggest that *GFAP* may be an activational target of Sox2, either directly, or indirectly. That *GFAP* is eventually upregulated shows that other factors must participate; despite this, the lasting changes make clear the critical role for Sox2 expression at a particular developmental stage for normal astrocytic maturation.

It has been postulated that astrocyte maturation, indexed by GFAP upregulation, could result from the heightened availability of oxygen following angiogenesis (West et al., 2005; Y. Zhang, Porat, Alon, Keshet, & Stone, 1999). In the present study, we observed a delay in vascularization following the removal of Sox2 from astrocytes. Given that vessels spread radially across the retinal surface following factors produced by astrocytes, a likely hypothesis is that Sox2-deficient astrocytes may alter this process leading to abnormal angiogenesis.

Developing astrocytes are known to secrete VEGF (Chan-Ling & Stone, 1991; West et al., 2005) in response to the hypoxic conditions present before tissue vascularization has taken place (Provis et al., 1997; West et al., 2005). Endothelial tip cells, at the leading edge of the developing vascular network, express the VEGF receptor VEGFR2 (Gerhardt et al., 2003). Their activation by VEGF has been shown to promote their extension towards the retinal periphery (Dorrell et al., 2002; Gerhardt et al., 2003; Ruhrberg et al., 2002; Stone et al., 1995; West et al., 2005). This arrival of blood vessels brings oxygen and therefore reduces the anoxic state. As it has been proposed that the availability of oxygen itself may

trigger the maturation of the astrocytes (including by the upregulation of GFAP) (West et al., 2005; Y. Zhang et al., 1999), the present results suggest that the role of Sox2 is a complex and likely indirect one, and implicates VEGF as a potential upstream player. Our data show that CKO astrocytes migrate into the retina normally, evidenced by Pax2-positive profiles being present at early postnatal stages; however, angiogenesis and astrocytic maturation are delayed. Astrocytes deprived of Sox2 may be deficient at initiating angiogenesis in response to the initial hypoxic conditions (due to a deficiency in VEGF signaling), thereby causing the delay in oxygenation of the retina, consequently leading to the delay in GFAP upregulation. Further experiments are needed to determine if Sox2-deficient astrocytes are unable to sense and/or properly respond to a hypoxic environment and therefore alter their secretion of angiogenic-promoting factors like VEGF.

Although unlikely, it is possible that the delayed astrocytic maturation and the delay in angiogenesis that we observe are the result of two separate processes. It has been shown that factors other than VEGF play a role in the interplay between astrocyte and vascular development of the retina. For example, leukemia inducing factor (LIF) expression by endothelial cells is believed to inhibit astrocytic VEGF expression and promote GFAP activation, thereby promoting maturation of astrocytes (Kubota, Hirashima, Kishi, Stewart, & Suda, 2008; Kubota & Suda, 2009; Mi, Haerberle, & Barres, 2001; Nakashima, Yanagisawa, Arakawa, & Taga, 1999). The astrocytic deletion of *Sox2* could cause a delayed maturation by indirectly decreasing LIF production, for example, to further impede astrocytic maturation.

While there is strong evidence for the interaction between astrocytes and blood vessels in development as previously described, less is known about their relationship in mature

animals. In this study we have not only uncovered a role for Sox2 in the developing retina but observe permanent aberrations to the astrocytic and vasculature networks in the mature retina as well. CKO retinas show a regional loss of GFAP immunoreactivity at peripheral locations, yet this has never been observed at central eccentricities near the optic nerve head. Curiously, this regional difference is only observed for this specific phenotype; the astrocytic sprouting, as well as changes to the vasculature, occur at all locations across the retinal surface.

Given our observation that angiogenesis is delayed in CKO animals, this suggests that the peripheral retina may experience a prolonged period of anoxia, in turn further impacting the maturation of the astrocytes, perhaps by the diminished availability of other factors. While speculative, it appears plausible given the sustained interaction, both physical and metabolic, between astrocytes and blood vessels in the mature animal (reviewed in Sofroniew & Vinters, 2010).

We first observe the peripheral loss of GFAP labeling around P15, yet it appears in all CKO animals by P21. The extent of these depleted regions is not age-dependent; older animals do not exhibit more quadrants or larger peripheral patches with GFAP loss. This implies that the diminution of GFAP in the peripheral retina is not a severe degenerative phenotype but instead a consequence of an earlier developmental deficit. Immunostaining for an alternative astrocytic marker, Sox9, yields no evidence for astrocytes remaining within GFAP-deficient peripheral patches (Figure 30). This further supports our speculation that astrocytes have undergone apoptosis in these regions, mentioned above. It is conceivable however that some astrocytes remain in these depleted regions; they could have diminished or retracted processes, or could lose their cellular identity as an astrocyte, and

therefore be unrecognizable by markers such as GFAP and Sox9. This is not so implausible when considering the loss of cellular identity when Sox2 is removed from cholinergic amacrine cells in the retina; while these cells retain their cholinergic status, they lose other features that discriminate between the ON versus OFF populations, including the loss of monostratified dendritic arbors in the ON population, and the loss P2X2 receptor labeling in the OFF population (Whitney et al., 2014).

What remains to be elucidated is how the aberrant astrocytic sprouting relates to our other described adult phenotype, namely that of the peripheral GFAP loss. It has been previously reported that in mouse models of retinal detachment, astrocytes not only sprout into the neural retina but also upregulate GFAP (Luna et al., 2016). In this injury condition, remodeled astrocytic processes follow blood vessels into the inner retina, yet in our CKO retinas we have not observed any obvious correlation. In addition, we do not observe any upregulation of GFAP, rather the opposite, implying that different processes control the two astrocytic phenotypes we describe. Conversely, the loss of Sox2 could create an intrinsic level of cellular stress thereby causing some astrocytes to undergo apoptosis, perhaps in regions providing less trophic support, while causing others to remodel by aberrantly extending their processes.

We observed a less complex superficial blood vessel network in CKO retinas, by measures of branch points and vessel length. We believe this to be a lasting result of the delay in angiogenesis, yet it could be due to a remodeling of the network after reaching the retinal margin. Other groups have argued that if vascular branch points are decreased then overall vessel length should increase conversely (Giocanti-Auregan et al., 2015), yet we observe a significant decrease in both. This indicates an overall underdevelopment of the



vascular network consisting of a less complex branching pattern accompanied by shorter processes. In severely astrocyte-depleted patches we have observed substantial aberrations to blood vessel patterning, i.e. the appearance of tortuous thickened processes lacking finer capillary networks (Figure 28g). Most CKO retinas did not exhibit conspicuous abnormalities such as this, yet all showed an overall diminution of the superficial vascular plexus (Figure 31f,j,k). Taken together these data implicate *Sox2* as an important if indirect player in the development of the vascular network, mediated by the retinal astrocytes.

The functional consequences of an astrocytic loss of *Sox2* remains to be determined. Astrocytes play a fundamental role in responding to CNS injury and disease. A massive increase in the number of astrocytes at the site of an injury is a prominent feature in early stages of many diseases including multiple sclerosis, Alzheimer' disease, and ALS, as well as in brain and spinal cord injuries even before any physical signs of the disease are detectable. Following CNS insult, astrocytes aim to reestablish homeostasis by entering a "reactive" state defined by morphological changes, alterations in protein expression, secretion of growth factors and ECM molecules (Kettenmann, Kettenmann, & Ransom, 2013), and formation of a glial scar around the injury site (Sofroniew, 2009; Sun & Jakobs, 2012). Given that astrocyte morphology and maturation appear abnormal in CKO retinas, it is plausible that astrocytes might have a diminished ability to trigger an injury response. Future studies to test this hypothesis could elucidate the role of *Sox2* by observing the astrocytic response following an inducible retinal injury, such an optic nerve crush or retinal detachment. Elucidating the role of *Sox2* following injury will be critical for a full understanding of how retinal astrocytes mature and function, thereby illuminating the intricacies of central nervous system formation.

## IV. Conclusions

The retina is a complex tissue that contains various specialized populations of cells, each of which develops through a unique set of processes that ultimately determine its function in the mature nervous system tissue. In this dissertation, I have explored the developmental mechanisms that underlie how two distinct retinal populations arise, being the bipolar cells and the astroglia. While these cellular populations are distinct in their development, morphology, molecular identity, and function, they constitute two of the many cell types that are necessary for retinal function. These cells are similar in that they both communicate extensively with retinal ganglion cells during development and in adulthood, albeit in very distinct ways. For this reason, understanding how they develop may ultimately provide insight into the role they play in the modulation of information that will ultimately be relayed to the brain.

Given the complexity of the mammalian retina and the cell types therein, no one approach can be taken to uncover all possible mechanisms of development. This dissertation has therefore utilized both a forward and reverse genetics approach to elucidate how different populations develop (J. S. Takahashi, Pinto, & Vitaterna, 1994). In the first chapter I discovered a role for the genes *Xkr8* and *Ggct* in the modulation of retinal bipolar cell number by using a forward genetic screen as a tool to uncover novel genes from phenotypic changes across mouse strains. The second chapter, conversely, uncovered an undescribed role for the well-studied transcription factor *Sox2* in the maturation and maintenance of astrocytes through a reverse genetics technique; I genetically removed *Sox2* from the developing mouse and examined the consequences upon the retina. Together, these approaches enable the analysis of both novel and previously studied genes that

underlie the complex development of the retina.

As previously discussed, neuronal number is a complex trait, whereby variation occurs due to genomic variants within multiple genes. This is also true of many, if not all, demographic features of the retina, including neuronal patterning and connectivity (Reese & Keeley, 2016). Recombinant inbred strains provide a resource for identifying these genomic locations that contribute to a trait of interest. I utilized a panel of RI strains to locate genomic loci responsible for controlling bipolar cell number in Chapter 2, and screened several genes at these locations via overexpression methods. This approach proved useful, given that I was able to identify two genes at different genomic loci that significantly altered cell number from control conditions, while several other overexpressed genes had no effect. While neither gene is solely responsible for the modulation of bipolar cell number, knowledge about the contribution of each gene helps to better understand the players involved in assembling a functional retina. It is not surprising that we uncovered more than one gene that when overexpressed, yielded comparable phenotypes, given that cell number varies gradually across RI strains (Figures 9 b,c). This graded distribution confirms the presence of more than one variant controlling the cell number trait, whereby a single variant would demonstrate a more step-wise distribution. Future studies can employ this overexpression approach to test the function of the remaining candidate genes at the identified loci discussed in Chapter 2.

Neuronal number can be influenced by several developmental events including fate determination, proliferation and cell death. Neither *Xkr8* nor *Ggct* have a previously described role in the developing retina, however, documented roles for *Xkr8* in the apoptotic pathway (Suzuki et al., 2013; Suzuki et al., 2014) and for *Ggct* in cancer pathogenesis (W.

Zhang et al., 2016), give insight to a potential apoptotic mechanism by which these genes modulate bipolar cell number. Independent overexpression of these genes caused a decrease in the relative number of bipolar cells generated (Figures 14 and 18), potentially due to the increased likelihood of an apoptotic event within progenitors that were transfected with *Xkr8* or *Ggct* overexpression plasmids. This may be a mechanism that all bipolar cells utilize in order to establish the final number of cells that will comprise their mature population, yet this remains to be determined.

In order to identify if specific variants between inbred mouse strains could underlie gene expression changes, I performed luciferase assays as described in Chapter 2. By elucidating the specific sequence variation underlying functional changes to neuronal number, we can better understand if there are common mechanisms that regulate the development of retinal populations via changes to gene expression, and use this knowledge to inform future studies. Small sequence variations, such as SNPs, can cause the creation or disruption of new transcription factor binding sites, for example. By knowing the specific variants that exist between mouse strains with known phenotypic differences in a trait of interest, we can identify these potential transcriptional regulators and test their function in various mouse strains. We can also detect the presence of large sequence variations, like structural variants, that can have greatly affect gene expression and/or function. Chapter 2 describes regulatory variants for both *Xkr8* and *Ggct*, in the forms of SNPs and structural variants respectively, and the means by which I tested the consequence of this variation between mouse strains. Future investigation is needed to elucidate all of the mechanisms involved in the establishment of retinal cell number, as well as the consequences of disruptions to these operations.

In the second experimental chapter, I sought to elucidate a novel developmental role for *Sox2*. This gene has been described for its critical role in the maintenance of stem cell pluripotency (Matsushima et al., 2011; Taranova et al., 2006), yet has not been well studied in the retina and its role in the population of astrocytes had not previously been explored. I document a new role for *Sox2* in the maturation of astrocytes and in the maintenance of their morphology in adulthood. In addition, I discovered that *Sox2* is critical for proper vascularization of the retina, given that alterations to astrocytic development caused abnormalities in the vasculature in the developing and mature retina as well. Both the population of astrocytes as well as the vascular network contribute to overall retinal health in important ways. Astrocytes play key roles in maintaining retinal homeostasis but also aid in repair mechanisms following injury. The network of blood vessels serves to provide oxygen and nutrients to the retina, while concurrently removing carbon dioxide and waste products. It has been proposed that the developing astrocytic network provides a template that guides retinal vascularization, yet the specific mechanisms by how it does so remains unclear. The results in Chapter 3 uncover a role for the gene *Sox2* in this process, whereby its removal from astrocytes caused abnormalities to their development as well as the development of the vascular network.

*Sox2* is a master transcriptional regulator that is involved in many different signaling pathways and can act as both an activator and suppressor of gene transcription. It is an essential factor in the maintenance of stem cell pluripotency and important in early development, yet also has been shown to be involved in cancer pathogenesis (Sarkar & Hochedlinger, 2013; K. Takahashi & Yamanaka, 2006; Weina & Utikal, 2014). The mechanism of action by which *Sox2* is functioning to influence astrocytic development

remains unknown, yet is an important question for future studies. One of the known downstream targets of *Sox2*, like *Hes5*, could play a role in astrocytic maturation whereby a change in expression of that gene disrupts normal astrocyte development (Takanaga et al., 2009). It is also plausible that *Sox2* could directly affect expression of an astrocyte-specific gene such as *Pax2* or *GFAP*, thereby altering the maturation of those cells. Furthermore, it remains unclear if the developmental delay in astrocytic maturation is due to direct changes in the expression of a gene within astrocyte precursors or indirectly through environmental factors, such as a change in a growth factor availability. Future studies are needed to elucidate how *Sox2* functions in astrocytic and vascular development.

The results described in the dissertation provide a deeper understanding of how both neuronal and glial populations develop in the central nervous system. My findings describe new genes involved in the development of the mammalian retina, while also illuminating novel roles for known genes. Understanding the genetic mechanisms required for the development of these single cellular populations provides insight into how they contribute to overall retinal function under basal conditions. This information can inform our therapeutic strategies when targeting an organism or tissue that has undergone an insult. Taken together, the findings in this dissertation provide a framework for dissecting mechanisms of cellular development in order to parse apart the complexities of nervous system development.

## References

1. Allen, N. J., Bennett, M. L., Foo, L. C., Wang, G. X., Chakraborty, C., Smith, S. J., & Barres, B. A. (2012). Astrocyte glypicans 4 and 6 promote formation of excitatory synapses via GluA1 AMPA receptors. *Nature*, *486*(7403), 410-414.  
doi:10.1038/nature11059
2. Azevedo, F. A., Carvalho, L. R., Grinberg, L. T., Farfel, J. M., Ferretti, R. E., Leite, R. E., . . . Herculano-Houzel, S. (2009). Equal numbers of neuronal and nonneuronal cells make the human brain an isometrically scaled-up primate brain. *J Comp Neurol*, *513*(5), 532-541. doi:10.1002/cne.21974
3. Bachleda, A. R., Pevny, L. H., & Weiss, E. R. (2016). Sox2-Deficient Muller Glia Disrupt the Structural and Functional Maturation of the Mammalian Retina. *Invest Ophthalmol Vis Sci*, *57*(3), 1488-1499. doi:10.1167/iovs.15-17994
4. Barker, A. J., & Ullian, E. M. (2008). New roles for astrocytes in developing synaptic circuits. *Commun Integr Biol*, *1*(2), 207-211.
5. Barres, B. A. (2008). The mystery and magic of glia: a perspective on their roles in health and disease. *Neuron*, *60*(3), 430-440. doi:10.1016/j.neuron.2008.10.013
6. Bassett, E. A., & Wallace, V. A. (2012). Cell fate determination in the vertebrate retina. *Trends Neurosci*, *35*(9), 565-573. doi:10.1016/j.tins.2012.05.004
7. Bialas, A. R., & Stevens, B. (2013). TGF-beta signaling regulates neuronal C1q expression and developmental synaptic refinement. *Nat Neurosci*, *16*(12), 1773-1782. doi:10.1038/nn.3560

8. Blackshaw, S., Croix, B. S., Polyak, K., Kim, J. B., & Cai, L. (2007). Serial analysis of gene expression (SAGE): experimental method and data analysis. *Curr Protoc Mol Biol, Chapter 25*, Unit 25B 26. doi:10.1002/0471142727.mb25b06s80
9. Bramblett, D. E., Pennesi, M. E., Wu, S. M., & Tsai, M. J. (2004). The transcription factor Bhlhb4 is required for rod bipolar cell maturation. *Neuron, 43*(6), 779-793. doi:10.1016/j.neuron.2004.08.032
10. Brzezinski, J. A. t., Lamba, D. A., & Reh, T. A. (2010). Blimp1 controls photoreceptor versus bipolar cell fate choice during retinal development. *Development, 137*(4), 619-629. doi:10.1242/dev.043968
11. Brzezinski, J. A. t., Uoon Park, K., & Reh, T. A. (2013). Blimp1 (Prdm1) prevents re-specification of photoreceptors into retinal bipolar cells by restricting competence. *Dev Biol, 384*(2), 194-204. doi:10.1016/j.ydbio.2013.10.006
12. Burmeister, M., Novak, J., Liang, M. Y., Basu, S., Ploder, L., Hawes, N. L., . . . McInnes, R. R. (1996). Ocular retardation mouse caused by Chx10 homeobox null allele: impaired retinal progenitor proliferation and bipolar cell differentiation. *Nat Genet, 12*(4), 376-384. doi:10.1038/ng0496-376
13. Bushong, E. A., Martone, M. E., Jones, Y. Z., & Ellisman, M. H. (2002). Protoplasmic astrocytes in CA1 stratum radiatum occupy separate anatomical domains. *J Neurosci, 22*(1), 183-192.
14. Cahoy, J. D., Emery, B., Kaushal, A., Foo, L. C., Zamanian, J. L., Christopherson, K. S., . . . Barres, B. A. (2008). A transcriptome database for astrocytes, neurons, and oligodendrocytes: a new resource for understanding brain development and function. *J Neurosci, 28*(1), 264-278. doi:10.1523/JNEUROSCI.4178-07.2008



15. Calenda, G., Peng, J., Redman, C. M., Sha, Q., Wu, X., & Lee, S. (2006). Identification of two new members, XPLAC and XTES, of the XK family. *Gene*, 370, 6-16. doi:10.1016/j.gene.2005.10.037
16. Cepko, C. (2014). Intrinsically different retinal progenitor cells produce specific types of progeny. *Nat Rev Neurosci*, 15(9), 615-627. doi:10.1038/nrn3767
17. Cepko, C. L., Austin, C. P., Yang, X., Alexiades, M., & Ezzeddine, D. (1996). Cell fate determination in the vertebrate retina. *Proc Natl Acad Sci U S A*, 93(2), 589-595.
18. Chan-Ling, T., & Stone, J. (1991). Factors determining the morphology and distribution of astrocytes in the cat retina: a 'contact-spacing' model of astrocyte interaction. *J Comp Neurol*, 303(3), 387-399. doi:10.1002/cne.903030305
19. Chen, L., Yang, P., & Kijlstra, A. (2002). Distribution, markers, and functions of retinal microglia. *Ocul Immunol Inflamm*, 10(1), 27-39.
20. Christopherson, K. S., Ullian, E. M., Stokes, C. C., Mullowney, C. E., Hell, J. W., Agah, A., . . . Barres, B. A. (2005). Thrombospondins are astrocyte-secreted proteins that promote CNS synaptogenesis. *Cell*, 120(3), 421-433. doi:10.1016/j.cell.2004.12.020
21. Chu, Y., Hughes, S., & Chan-Ling, T. (2001). Differentiation and migration of astrocyte precursor cells and astrocytes in human fetal retina: relevance to optic nerve coloboma. *FASEB J*, 15(11), 2013-2015. doi:10.1096/fj.00-0868fje
22. Chung, W. S., Welsh, C. A., Barres, B. A., & Stevens, B. (2015). Do glia drive synaptic and cognitive impairment in disease? *Nat Neurosci*, 18(11), 1539-1545. doi:10.1038/nn.4142

23. Cookson, M. R. (2010). The role of leucine-rich repeat kinase 2 (LRRK2) in Parkinson's disease. *Nat Rev Neurosci*, *11*(12), 791-797. doi:10.1038/nrn2935
24. DiMaio, T. A., & Sheibani, N. (2008). PECAM-1 isoform-specific functions in PECAM-1-deficient brain microvascular endothelial cells. *Microvasc Res*, *75*(2), 188-201. doi:10.1016/j.mvr.2007.10.001
25. Dong, J., Zhou, Y., Liao, Z., Huang, Q., Feng, S., & Li, Y. (2016). Role of gamma-glutamyl cyclotransferase as a therapeutic target for colorectal cancer based on the lentivirus-mediated system. *Anticancer Drugs*, *27*(10), 1011-1020. doi:10.1097/CAD.0000000000000407
26. Dorrell, M. I., Aguilar, E., & Friedlander, M. (2002). Retinal vascular development is mediated by endothelial filopodia, a preexisting astrocytic template and specific R-cadherin adhesion. *Invest Ophthalmol Vis Sci*, *43*(11), 3500-3510.
27. Euler, T., Haverkamp, S., Schubert, T., & Baden, T. (2014). Retinal bipolar cells: elementary building blocks of vision. *Nat Rev Neurosci*, *15*(8), 507-519.
28. Ezzeddine, Z. D., Yang, X., DeChiara, T., Yancopoulos, G., & Cepko, C. L. (1997). Postmitotic cells fated to become rod photoreceptors can be respecified by CNTF treatment of the retina. *Development*, *124*(5), 1055-1067.
29. Fantes, J., Ragge, N. K., Lynch, S. A., McGill, N. I., Collin, J. R., Howard-Peebles, P. N., . . . FitzPatrick, D. R. (2003). Mutations in SOX2 cause anophthalmia. *Nat Genet*, *33*(4), 461-463. doi:10.1038/ng1120
30. Feng, L., Xie, X., Joshi, P. S., Yang, Z., Shibasaki, K., Chow, R. L., & Gan, L. (2006). Requirement for Bhlhb5 in the specification of amacrine and cone bipolar subtypes in mouse retina. *Development*, *133*(24), 4815-4825. doi:10.1242/dev.02664

31. Fischer, A. J., Zelinka, C., & Scott, M. A. (2010). Heterogeneity of glia in the retina and optic nerve of birds and mammals. *PLoS One*, *5*(6), e10774.  
doi:10.1371/journal.pone.0010774
32. Fogel, B. L., Wexler, E., Wahnich, A., Friedrich, T., Vijayendran, C., Gao, F., . . . Geschwind, D. H. (2012). RBFOX1 regulates both splicing and transcriptional networks in human neuronal development. *Hum Mol Genet*, *21*(19), 4171-4186.  
doi:10.1093/hmg/dds240
33. Fruttiger, M. (2002). Development of the mouse retinal vasculature: angiogenesis versus vasculogenesis. *Invest Ophthalmol Vis Sci*, *43*(2), 522-527.
34. Fruttiger, M., Calver, A. R., Kruger, W. H., Mudhar, H. S., Michalovich, D., Takakura, N., . . . Richardson, W. D. (1996). PDGF mediates a neuron-astrocyte interaction in the developing retina. *Neuron*, *17*(6), 1117-1131.
35. Gerhardt, H., Golding, M., Fruttiger, M., Ruhrberg, C., Lundkvist, A., Abramsson, A., . . . Betsholtz, C. (2003). VEGF guides angiogenic sprouting utilizing endothelial tip cell filopodia. *J Cell Biol*, *161*(6), 1163-1177. doi:10.1083/jcb.200302047
36. Giocanti-Auregan, A., Tadayoni, R., Fajnkuchen, F., Dourmad, P., Magazzeni, S., & Cohen, S. Y. (2015). Predictive Value of Outer Retina En Face OCT Imaging for Geographic Atrophy Progression. *Invest Ophthalmol Vis Sci*, *56*(13), 8325-8330.  
doi:10.1167/iovs.14-15480
37. Gnanaguru, G., Bachay, G., Biswas, S., Pinzon-Duarte, G., Hunter, D. D., & Brunken, W. J. (2013). Laminins containing the beta2 and gamma3 chains regulate astrocyte migration and angiogenesis in the retina. *Development*, *140*(9), 2050-2060.  
doi:10.1242/dev.087817

38. Godinho, L., & Link, B. (2006). Cell migration. *Retinal Development*, 59-74.  
doi:Doi 10.1017/Cbo9780511541629.006
39. Godinho, L., Mumm, J. S., Williams, P. R., Schroeter, E. H., Koerber, A., Park, S. W., . . . Wong, R. O. (2005). Targeting of amacrine cell neurites to appropriate synaptic laminae in the developing zebrafish retina. *Development*, 132(22), 5069-5079. doi:10.1242/dev.02075
40. Goldstein, S., Fordis, C. M., & Howard, B. H. (1989). Enhanced transfection efficiency and improved cell survival after electroporation of G2/M-synchronized cells and treatment with sodium butyrate. *Nucleic Acids Res*, 17(10), 3959-3971.
41. Harry, G. J. (2013). Microglia during development and aging. *Pharmacol Ther*, 139(3), 313-326. doi:10.1016/j.pharmthera.2013.04.013
42. Hatakeyama, J., Tomita, K., Inoue, T., & Kageyama, R. (2001). Roles of homeobox and bHLH genes in specification of a retinal cell type. *Development*, 128(8), 1313-1322.
43. Herculano-Houzel, S., Mota, B., & Lent, R. (2006). Cellular scaling rules for rodent brains. *Proc Natl Acad Sci U S A*, 103(32), 12138-12143.  
doi:10.1073/pnas.0604911103
44. Hock, R., Furusawa, T., Ueda, T., & Bustin, M. (2007). HMG chromosomal proteins in development and disease. *Trends Cell Biol*, 17(2), 72-79.  
doi:10.1016/j.tcb.2006.12.001
45. Hollander, H., Makarov, F., Dreher, Z., van Driel, D., Chan-Ling, T. L., & Stone, J. (1991). Structure of the macroglia of the retina: sharing and division of labour

- between astrocytes and Muller cells. *J Comp Neurol*, 313(4), 587-603.  
doi:10.1002/cne.903130405
46. Jeon, C. J., Strettoi, E., & Masland, R. H. (1998). The major cell populations of the mouse retina. *J Neurosci*, 18(21), 8936-8946.
47. Jiang, B., Bezhadian, M. A., & Caldwell, R. B. (1995). Astrocytes modulate retinal vasculogenesis: effects on endothelial cell differentiation. *Glia*, 15(1), 1-10.  
doi:10.1002/glia.440150102
48. Joshi, P. S., Molyneaux, B. J., Feng, L., Xie, X., Macklis, J. D., & Gan, L. (2008). Bhlhb5 regulates the postmitotic acquisition of area identities in layers II-V of the developing neocortex. *Neuron*, 60(2), 258-272. doi:10.1016/j.neuron.2008.08.006
49. Katoh, K., Omori, Y., Onishi, A., Sato, S., Kondo, M., & Furukawa, T. (2010). Blimp1 suppresses Chx10 expression in differentiating retinal photoreceptor precursors to ensure proper photoreceptor development. *J Neurosci*, 30(19), 6515-6526. doi:10.1523/JNEUROSCI.0771-10.2010
50. Kay, J. N., Chu, M. W., & Sanes, J. R. (2012). MEGF10 and MEGF11 mediate homotypic interactions required for mosaic spacing of retinal neurons. *Nature*, 483(7390), 465-469. doi:10.1038/nature10877
51. Keane, T. M., Goodstadt, L., Danecek, P., White, M. A., Wong, K., Yalcin, B., . . . Adams, D. J. (2011). Mouse genomic variation and its effect on phenotypes and gene regulation. *Nature*, 477(7364), 289-294. doi:10.1038/nature10413
52. Keane, T. M., Wong, K., Adams, D. J., Flint, J., Reymond, A., & Yalcin, B. (2014). Identification of structural variation in mouse genomes. *Front Genet*, 5, 192.  
doi:10.3389/fgene.2014.00192

53. Keeley, P. W., Madsen, N. R., St John, A. J., & Reese, B. E. (2014). Programmed cell death of retinal cone bipolar cells is independent of afferent or target control. *Dev Biol*, 394(2), 191-196. doi:10.1016/j.ydbio.2014.08.018
54. Keeley, P. W., Whitney, I. E., Madsen, N. R., St John, A. J., Borhanian, S., Leong, S. A., . . . Reese, B. E. (2014). Independent genomic control of neuronal number across retinal cell types. *Dev Cell*, 30(1), 103-109. doi:10.1016/j.devcel.2014.05.003
55. Kettenmann, H., Kettenmann, H., & Ransom, B. R. (2013). *Neuroglia* (3rd ed. ed.). New York ; Oxford: Oxford University Press.
56. Kiefer, J. C. (2007). Back to basics: Sox genes. *Dev Dyn*, 236(8), 2356-2366. doi:10.1002/dvdy.21218
57. Kimani, S. G., Geng, K., Kasikara, C., Kumar, S., Sriram, G., Wu, Y., & Birge, R. B. (2014). Contribution of Defective PS Recognition and Efferocytosis to Chronic Inflammation and Autoimmunity. *Front Immunol*, 5, 566. doi:10.3389/fimmu.2014.00566
58. Koike, T., Wakabayashi, T., Mori, T., Hirahara, Y., & Yamada, H. (2015). Sox2 promotes survival of satellite glial cells in vitro. *Biochem Biophys Res Commun*, 464(1), 269-274. doi:10.1016/j.bbrc.2015.06.141
59. Kubota, Y., Hirashima, M., Kishi, K., Stewart, C. L., & Suda, T. (2008). Leukemia inhibitory factor regulates microvessel density by modulating oxygen-dependent VEGF expression in mice. *J Clin Invest*, 118(7), 2393-2403. doi:10.1172/JCI34882
60. Kubota, Y., & Suda, T. (2009). Feedback mechanism between blood vessels and astrocytes in retinal vascular development. *Trends Cardiovasc Med*, 19(2), 38-43. doi:10.1016/j.tcm.2009.04.004

61. Kulkeaw, K., Inoue, T., Mizuochi, C., Horio, Y., Ishihama, Y., & Sugiyama, D. (2012). Ectopic expression of Hmgn2 antagonizes mouse erythroid differentiation in vitro. *Cell Biol Int*, 36(2), 195-202. doi:10.1042/CBI20110169
62. Liesi, P., & Silver, J. (1988). Is astrocyte laminin involved in axon guidance in the mammalian CNS? *Dev Biol*, 130(2), 774-785.
63. Lin, Y. P., Ouchi, Y., Satoh, S., & Watanabe, S. (2009). Sox2 plays a role in the induction of amacrine and Muller glial cells in mouse retinal progenitor cells. *Invest Ophthalmol Vis Sci*, 50(1), 68-74. doi:10.1167/iovs.07-1619
64. Linden, R. (2000). The anti-death league: associative control of apoptosis in developing retinal tissue. *Brain Res Brain Res Rev*, 32(1), 146-158.
65. Linden, R., Martins, R. A., & Silveira, M. S. (2005). Control of programmed cell death by neurotransmitters and neuropeptides in the developing mammalian retina. *Prog Retin Eye Res*, 24(4), 457-491. doi:10.1016/j.preteyeres.2004.10.001
66. Ling, T. L., Mitrofanis, J., & Stone, J. (1989). Origin of retinal astrocytes in the rat: evidence of migration from the optic nerve. *J Comp Neurol*, 286(3), 345-352. doi:10.1002/cne.902860305
67. Liu, Y. R., Laghari, Z. A., Novoa, C. A., Hughes, J., Webster, J. R., Goodwin, P. E., . . . Scotting, P. J. (2014). Sox2 acts as a transcriptional repressor in neural stem cells. *BMC Neurosci*, 15, 95. doi:10.1186/1471-2202-15-95
68. Lucey, M. M., Wang, Y., Bustin, M., & Duncan, M. K. (2008). Differential expression of the HMGN family of chromatin proteins during ocular development. *Gene Expr Patterns*, 8(6), 433-437. doi:10.1016/j.gep.2008.04.002

69. Luna, G., Keeley, P. W., Reese, B. E., Linberg, K. A., Lewis, G. P., & Fisher, S. K. (2016). Astrocyte structural reactivity and plasticity in models of retinal detachment. *Exp Eye Res*, *150*, 4-21. doi:10.1016/j.exer.2016.03.027
70. Macosko, E. Z., Basu, A., Satija, R., Nemesh, J., Shekhar, K., Goldman, M., . . . McCarroll, S. A. (2015). Highly Parallel Genome-wide Expression Profiling of Individual Cells Using Nanoliter Droplets. *Cell*, *161*(5), 1202-1214. doi:10.1016/j.cell.2015.05.002
71. Marquardt, T., & Gruss, P. (2002). Generating neuronal diversity in the retina: one for nearly all. *Trends Neurosci*, *25*(1), 32-38.
72. Mathers, P. H., Grinberg, A., Mahon, K. A., & Jamrich, M. (1997). The Rx homeobox gene is essential for vertebrate eye development. *Nature*, *387*(6633), 603-607. doi:10.1038/42475
73. Matsuda, T., & Cepko, C. L. (2004). Electroporation and RNA interference in the rodent retina in vivo and in vitro. *Proceedings of the National Academy of Sciences of the United States of America*, *101*(1), 16-22. doi:10.1073/pnas.2235688100
74. Matsushima, D., Heavner, W., & Pevny, L. H. (2011). Combinatorial regulation of optic cup progenitor cell fate by SOX2 and PAX6. *Development*, *138*(3), 443-454. doi:10.1242/dev.055178
75. Mears, A. J., Kondo, M., Swain, P. K., Takada, Y., Bush, R. A., Saunders, T. L., . . . Swaroop, A. (2001). Nrl is required for rod photoreceptor development. *Nat Genet*, *29*(4), 447-452. doi:10.1038/ng774
76. Mi, H., Haerberle, H., & Barres, B. A. (2001). Induction of astrocyte differentiation by endothelial cells. *J Neurosci*, *21*(5), 1538-1547.



77. Molofsky, A. V., Krencik, R., Ullian, E. M., Tsai, H. H., Deneen, B., Richardson, W. D., . . . Rowitch, D. H. (2012). Astrocytes and disease: a neurodevelopmental perspective. *Genes Dev*, *26*(9), 891-907. doi:10.1101/gad.188326.112
78. Morrow, E. M., Chen, C. M., & Cepko, C. L. (2008). Temporal order of bipolar cell genesis in the neural retina. *Neural Dev*, *3*, 2. doi:10.1186/1749-8104-3-2
79. Mumm, J. S., & Lohmann, C. (2006). Dendritic growth. *E. Sernagor, S. Eglen, B. Harris, R. Wong. Retinal development* (pp. 242-264): Cambridge University Press.
80. Murali, D., Kawaguchi-Niida, M., Deng, C. X., & Furuta, Y. (2011). Smad4 is required predominantly in the developmental processes dependent on the BMP branch of the TGF-beta signaling system in the embryonic mouse retina. *Invest Ophthalmol Vis Sci*, *52*(6), 2930-2937. doi:10.1167/iovs.10-5940
81. Nakashima, K., Yanagisawa, M., Arakawa, H., & Taga, T. (1999). Astrocyte differentiation mediated by LIF in cooperation with BMP2. *FEBS Lett*, *457*(1), 43-46.
82. Newman, E. A. (1986). High potassium conductance in astrocyte endfeet. *Science*, *233*(4762), 453-454.
83. Ng, P. C., & Henikoff, S. (2003). SIFT: predicting amino acid changes that affect protein function. *Nucleic Acids Research*, *31*(13), 3812-3814.  
doi:10.1093/nar/gkg509
84. Oakley, A. J., Yamada, T., Liu, D., Coggan, M., Clark, A. G., & Board, P. G. (2008). The identification and structural characterization of C7orf24 as gamma-glutamyl cyclotransferase. An essential enzyme in the gamma-glutamyl cycle. *J Biol Chem*, *283*(32), 22031-22042. doi:10.1074/jbc.M803623200

85. Paolicelli, R. C., Bolasco, G., Pagani, F., Maggi, L., Scianni, M., Panzanelli, P., . . . Gross, C. T. (2011). Synaptic pruning by microglia is necessary for normal brain development. *Science*, *333*(6048), 1456-1458. doi:10.1126/science.1202529
86. Pequignot, M. O., Provost, A. C., Salle, S., Taupin, P., Sainton, K. M., Marchant, D., . . . Abitbol, M. (2003). Major role of BAX in apoptosis during retinal development and in establishment of a functional postnatal retina. *Dev Dyn*, *228*(2), 231-238. doi:10.1002/dvdy.10376
87. Pow, D. V., & Robinson, S. R. (1994). Glutamate in some retinal neurons is derived solely from glia. *Neuroscience*, *60*(2), 355-366.
88. Provis, J. M., Leech, J., Diaz, C. M., Penfold, P. L., Stone, J., & Keshet, E. (1997). Development of the human retinal vasculature: cellular relations and VEGF expression. *Exp Eye Res*, *65*(4), 555-568. doi:10.1006/exer.1997.0365
89. Ramirez, J. M., Trivino, A., Ramirez, A. I., Salazar, J. J., & Garcia-Sanchez, J. (1996). Structural specializations of human retinal glial cells. *Vision Res*, *36*(14), 2029-2036.
90. Rapaport, D. H. (2006). Retinal Neurogenesis *E. Sernagor, S. Eglén, B. Harris, R. Wong. Retinal Development* (pp. 30-58). Cambridge University Press: Cambridge University Press.
91. Reese, B. E. (2011). Development of the retina and optic pathway. *Vision Res*, *51*(7), 613-632. doi:10.1016/j.visres.2010.07.010
92. Reese, B. E., & Keeley, P. W. (2015). Design principles and developmental mechanisms underlying retinal mosaics. *Biol Rev Camb Philos Soc*, *90*(3), 854-876. doi:10.1111/brv.12139

93. Reese, B. E., & Keeley, P. W. (2016). Genomic control of neuronal demographics in the retina. *Prog Retin Eye Res*, 55, 246-259. doi:10.1016/j.preteyeres.2016.07.003
94. Rhee, K. D., & Yang, X. J. (2010). Function and mechanism of CNTF/LIF signaling in retinogenesis. *Adv Exp Med Biol*, 664, 647-654. doi:10.1007/978-1-4419-1399-9\_74
95. Rochman, M., Taher, L., Kurahashi, T., Cherukuri, S., Uversky, V. N., Landsman, D., . . . Bustin, M. (2011). Effects of HMGN variants on the cellular transcription profile. *Nucleic Acids Research*, 39(10), 4076-4087. doi:10.1093/nar/gkq1343
96. Ruhrberg, C., Gerhardt, H., Golding, M., Watson, R., Ioannidou, S., Fujisawa, H., . . . Shima, D. T. (2002). Spatially restricted patterning cues provided by heparin-binding VEGF-A control blood vessel branching morphogenesis. *Genes Dev*, 16(20), 2684-2698. doi:10.1101/gad.242002
97. Ryan, S. J. (1989). *Retina*. St. Louis: Mosby.
98. Saito, T. (2006). In vivo electroporation in the embryonic mouse central nervous system. *Nat Protoc*, 1(3), 1552-1558. doi:10.1038/nprot.2006.276
99. Sandercoe, T. M., Madigan, M. C., Billson, F. A., Penfold, P. L., & Provis, J. M. (1999). Astrocyte proliferation during development of the human retinal vasculature. *Exp Eye Res*, 69(5), 511-523. doi:10.1006/exer.1999.0730
100. Sanes, J. R., & Masland, R. H. (2015). The types of retinal ganglion cells: current status and implications for neuronal classification. *Annu Rev Neurosci*, 38, 221-246. doi:10.1146/annurev-neuro-071714-034120

101. Sarkar, A., & Hochedlinger, K. (2013). The sox family of transcription factors: versatile regulators of stem and progenitor cell fate. *Cell Stem Cell*, *12*(1), 15-30. doi:10.1016/j.stem.2012.12.007
102. Sarthy, P. V., Fu, M., & Huang, J. (1991). Developmental expression of the glial fibrillary acidic protein (GFAP) gene in the mouse retina. *Cell Mol Neurobiol*, *11*(6), 623-637.
103. Schafer, D. P., Lehrman, E. K., Kautzman, A. G., Koyama, R., Mardinly, A. R., Yamasaki, R., . . . Stevens, B. (2012). Microglia sculpt postnatal neural circuits in an activity and complement-dependent manner. *Neuron*, *74*(4), 691-705. doi:10.1016/j.neuron.2012.03.026
104. Schneider, A., Bardakjian, T., Reis, L. M., Tyler, R. C., & Semina, E. V. (2009). Novel SOX2 mutations and genotype-phenotype correlation in anophthalmia and microphthalmia. *Am J Med Genet A*, *149A*(12), 2706-2715. doi:10.1002/ajmg.a.33098
105. Segawa, K., Kurata, S., Yanagihashi, Y., Brummelkamp, T. R., Matsuda, F., & Nagata, S. (2014). Caspase-mediated cleavage of phospholipid flippase for apoptotic phosphatidylserine exposure. *Science*, *344*(6188), 1164-1168. doi:10.1126/science.1252809
106. Siegert, S., Cabuy, E., Scherf, B. G., Kohler, H., Panda, S., Le, Y. Z., . . . Roska, B. (2012). Transcriptional code and disease map for adult retinal cell types. *Nat Neurosci*, *15*(3), 487-495, S481-482. doi:10.1038/nn.3032
107. Sofroniew, M. V. (2009). Molecular dissection of reactive astrogliosis and glial scar formation. *Trends Neurosci*, *32*(12), 638-647. doi:10.1016/j.tins.2009.08.002

108. Sofroniew, M. V., & Vinters, H. V. (2010). Astrocytes: biology and pathology. *Acta Neuropathol*, *119*(1), 7-35. doi:10.1007/s00401-009-0619-8
109. Stevens, B., Allen, N. J., Vazquez, L. E., Howell, G. R., Christopherson, K. S., Nouri, N., . . . Barres, B. A. (2007). The classical complement cascade mediates CNS synapse elimination. *Cell*, *131*(6), 1164-1178. doi:10.1016/j.cell.2007.10.036
110. Stone, J., & Dreher, Z. (1987). Relationship between astrocytes, ganglion cells and vasculature of the retina. *J Comp Neurol*, *255*(1), 35-49. doi:10.1002/cne.902550104
111. Stone, J., Itin, A., Alon, T., Pe'er, J., Gnessin, H., Chan-Ling, T., & Keshet, E. (1995). Development of retinal vasculature is mediated by hypoxia-induced vascular endothelial growth factor (VEGF) expression by neuroglia. *J Neurosci*, *15*(7 Pt 1), 4738-4747.
112. Strettoi, E., & Volpini, M. (2002). Retinal organization in the bcl-2-overexpressing transgenic mouse. *J Comp Neurol*, *446*(1), 1-10.
113. Sun, D., & Jakobs, T. C. (2012). Structural remodeling of astrocytes in the injured CNS. *Neuroscientist*, *18*(6), 567-588. doi:10.1177/1073858411423441
114. Surzenko, N., Crowl, T., Bachleda, A., Langer, L., & Pevny, L. (2013). SOX2 maintains the quiescent progenitor cell state of postnatal retinal Muller glia. *Development*, *140*(7), 1445-1456. doi:10.1242/dev.071878
115. Suzuki, J., Denning, D. P., Imanishi, E., Horvitz, H. R., & Nagata, S. (2013). Xk-related protein 8 and CED-8 promote phosphatidylserine exposure in apoptotic cells. *Science*, *341*(6144), 403-406. doi:10.1126/science.1236758

116. Suzuki, J., Imanishi, E., & Nagata, S. (2014). Exposure of phosphatidylserine by Xk-related protein family members during apoptosis. *J Biol Chem*, 289(44), 30257-30267. doi:10.1074/jbc.M114.583419
117. Takahashi, J. S., Pinto, L. H., & Vitaterna, M. H. (1994). Forward and reverse genetic approaches to behavior in the mouse. *Science*, 264(5166), 1724-1733.
118. Takahashi, K., & Yamanaka, S. (2006). Induction of pluripotent stem cells from mouse embryonic and adult fibroblast cultures by defined factors. *Cell*, 126(4), 663-676. doi:10.1016/j.cell.2006.07.024
119. Takanaga, H., Tsuchida-Straeten, N., Nishide, K., Watanabe, A., Aburatani, H., & Kondo, T. (2009). Gli2 is a novel regulator of sox2 expression in telencephalic neuroepithelial cells. *Stem Cells*, 27(1), 165-174. doi:10.1634/stemcells.2008-0580
120. Tao, C., & Zhang, X. (2014). Development of astrocytes in the vertebrate eye. *Dev Dyn*, 243(12), 1501-1510. doi:10.1002/dvdy.24190
121. Taranova, O. V., Magness, S. T., Fagan, B. M., Wu, Y., Surzenko, N., Hutton, S. R., & Pevny, L. H. (2006). SOX2 is a dose-dependent regulator of retinal neural progenitor competence. *Genes Dev*, 20(9), 1187-1202. doi:10.1101/gad.1407906
122. Tomita, K., Moriyoshi, K., Nakanishi, S., Guillemot, F., & Kageyama, R. (2000). Mammalian achaete-scute and atonal homologs regulate neuronal versus glial fate determination in the central nervous system. *EMBO J*, 19(20), 5460-5472. doi:10.1093/emboj/19.20.5460
123. Tomita, K., Nakanishi, S., Guillemot, F., & Kageyama, R. (1996). Mash1 promotes neuronal differentiation in the retina. *Genes Cells*, 1(8), 765-774.

124. Tremblay, M. E., Lowery, R. L., & Majewska, A. K. (2010). Microglial interactions with synapses are modulated by visual experience. *PLoS Biol*, *8*(11), e1000527. doi:10.1371/journal.pbio.1000527
125. Ullian, E. M., Sapperstein, S. K., Christopherson, K. S., & Barres, B. A. (2001). Control of synapse number by glia. *Science*, *291*(5504), 657-661. doi:10.1126/science.291.5504.657
126. Wang, S., Sengel, C., Emerson, M. M., & Cepko, C. L. (2014). A gene regulatory network controls the binary fate decision of rod and bipolar cells in the vertebrate retina. *Dev Cell*, *30*(5), 513-527. doi:10.1016/j.devcel.2014.07.018
127. Watanabe, T., & Raff, M. C. (1988). Retinal astrocytes are immigrants from the optic nerve. *Nature*, *332*(6167), 834-837. doi:10.1038/332834a0
128. Weina, K., & Utikal, J. (2014). SOX2 and cancer: current research and its implications in the clinic. *Clin Transl Med*, *3*, 19. doi:10.1186/2001-1326-3-19
129. Weischenfeldt, J., Symmons, O., Spitz, F., & Korbel, J. O. (2013). Phenotypic impact of genomic structural variation: insights from and for human disease. *Nat Rev Genet*, *14*(2), 125-138. doi:10.1038/nrg3373
130. West, H., Richardson, W. D., & Fruttiger, M. (2005). Stabilization of the retinal vascular network by reciprocal feedback between blood vessels and astrocytes. *Development*, *132*(8), 1855-1862. doi:10.1242/dev.01732
131. Whitney, I. E., Keeley, P. W., St John, A. J., Kautzman, A. G., Kay, J. N., & Reese, B. E. (2014). Sox2 regulates cholinergic amacrine cell positioning and dendritic stratification in the retina. *J Neurosci*, *34*(30), 10109-10121. doi:10.1523/JNEUROSCI.0415-14.2014

132. Whitney, I. E., Raven, M. A., Ciobanu, D. C., Williams, R. W., & Reese, B. E. (2009). Multiple genes on chromosome 7 regulate dopaminergic amacrine cell number in the mouse retina. *Invest Ophthalmol Vis Sci*, 50(5), 1996-2003. doi:10.1167/iovs.08-2556
133. Williams, R. W., Gu, J., Qi, S., & Lu, L. (2001). The genetic structure of recombinant inbred mice: high-resolution consensus maps for complex trait analysis. *Genome Biol*, 2(11), RESEARCH0046.
134. Yalcin, B., Wong, K., Agam, A., Goodson, M., Keane, T. M., Gan, X., . . . Flint, J. (2011). Sequence-based characterization of structural variation in the mouse genome. *Nature*, 477(7364), 326-329. doi:10.1038/nature10432
135. Young, R. W. (1984). Cell death during differentiation of the retina in the mouse. *J Comp Neurol*, 229(3), 362-373. doi:10.1002/cne.902290307
136. Young, R. W. (1985). Cell differentiation in the retina of the mouse. *Anat Rec*, 212(2), 199-205. doi:10.1002/ar.1092120215
137. Zhang, W., Chen, L., Xiang, H., Hu, C., Shi, W., Dong, P., & Lv, W. (2016). Knockdown of GGCT inhibits cell proliferation and induces late apoptosis in human gastric cancer. *BMC Biochem*, 17(1), 19. doi:10.1186/s12858-016-0075-8
138. Zhang, X., Serb, J. M., & Greenlee, M. H. (2011). Mouse retinal development: a dark horse model for systems biology research. *Bioinform Biol Insights*, 5, 99-113. doi:10.4137/BBLIS6930
139. Zhang, Y., Chen, K., Sloan, S. A., Bennett, M. L., Scholze, A. R., O'Keefe, S., . . . Wu, J. Q. (2014). An RNA-sequencing transcriptome and splicing database of glia,



neurons, and vascular cells of the cerebral cortex. *J Neurosci*, 34(36), 11929-11947.  
doi:10.1523/JNEUROSCI.1860-14.2014

140. Zhang, Y., Porat, R. M., Alon, T., Keshet, E., & Stone, J. (1999). Tissue oxygen levels control astrocyte movement and differentiation in developing retina. *Brain Res Dev Brain Res*, 118(1-2), 135-145.

## Appendix

**Appendix A:** Coding sequences for gene fragments amplified via PCR and cloned into destination vector for *in vivo* electroporation experiments. All sequences are listed 5' to 3'.

### Dhdds

ATGTCATGGATCAAAGAAGGAGAGCTGTCACTGTGGGAACGGTTCTGTGCTAACATCATAAAGGCTG  
GCCCAGTACCCAAACATATCGCGTTCATAATGGACGGCAACCGTCGCTATGCCAAGAAGTGTGAGGT  
GGAGCGCCAGGAGGGCCACACACAGGGCTTCAATAAGCTTGCTGAGACTCTCCGCTGGTGTGTTGAAC  
CTGGGCATCCTAGAAGTGACTGTCTACGCATTGAGAACTTCAAACGTTCCAAGAGTGAGG  
TTGACGGACTCCTGGATCTAGCCAGACAGAAGTTGAGCTGCTTGATGGAAGAACAGGAGAAGTTGCA  
GAAGCACGGGGTGTGCATCCGCGTCTGGGTGATCTGCATCTGCTGCCCTTGGACCTCCAGGAGAAG  
ATTGCGCATGCCATCCAGGCTACTAAGAACTACAATAAGTGTTCCTCAATGTCTGCTTTGCATACA  
CATCACGTCATGAGATTGCCAATGCTGTGAGAGAGATGGCCTGGGGCGTGAACAAGGTCTGCTGGA  
ACCCAGTGATGTCTCCGAGTCTCTGCTCGATAAGTGCCTCTATAGCAACCCTCTCCTCATCCCAGC  
ATCCTGATCCGGACTTCTGGGGAGGTGCGGCTGAGTGACTTCTTGCTCTGGCAGACGTCCTCCTCCT  
GCCTCGTGTTCAGCCTGTCTGTGGCCAGAATACACATTTTGAACCTGTGTGAGGCAATTCTGCA  
GTTTTAGAGGAACCATGGTGCACCTCAGAAGGCCCGAGACATGTACGCTGAGGAGCGGAAGAGGCGC  
CAGCTGGAGAGGGACCAGGCCGAGTGACAGAGCAGCTGCTTCGAGAGGGGCTCCAGGCCAGTGGGG  
ATGCCAACTCCGACGGACACGCTTGACAAACTCTCCACCAAACGGGAAGAGCGAGTCCAAGGCTT  
CCTGAAGGCCTTGGAACCTAAACGGGCCAACTGGCTGGCACCTTTGGGGCACTGCATCTGCCTAAGTG  
GAGCTGGCTACCAGCCACTTTGCCCT

### Egfr

ATGCGACCCTCAGGGACCGCGAGAACCACACTGCTGGTGTGCTGACCGCGCTCTGCGCCGCAGGTG  
GGGCGTTGGAGGAAAAGAAAGTCTGCCAAGGCACAAGTAACAGGCTCACCCAACTGGGCAC'TTTTGA  
AGACCACTTTCTGAGCCTGCAGAGGATGTACAACAACCTGTGAAGTGGTCC'TTGGGAACCTTGGAAATT  
ACCTATGTGCAAAGGAATTACGACCTTTCCTTCTTAAAGACCATCCAGGAGGTGGCCGGCTATGTCC  
TCATTGCCCTCAACACCGTGGAGAGAATCCCTTTGGAGAACCTGCAGATCATCAGGGGAAATGCTCT  
TTATGAAAACACCTATGCCTTAGCCATCCTGTCCAACCTATGGGACAAACAGAACTGGGCTTAGGGAA  
CTGCCCATGCGGAACCTTACAGGAAATCCTGATTGGTGTGCTGTGCGATTGAGCAACAACCCATCCTCT  
GCAATATGGATACTATCCAGTGGAGGGACATCGTCCAAAACGCTCTTTATGAGCAACATGTCAATGGA  
CTTACAGAGCCATCCGAGCAGTTGCCCAAATGTGATCCAAGCTGTCCAATGGAAGCTGCTGGGGA  
GGAGGAGAGGAGAAGTCCAGAAATTGACCAAATCATCTGTGCCAGCAATGTTCCATCGCTGTC  
GTGGCAGGTCCCCAGTGACTGCTGCCACAACCAATGTGCTGCGGGGTGTACAGGGCCCCGAGAGAG  
TGACTGTCTGGTCTGCCAAAAGTTCCAAGATGAGGCCACATGCAAAGACACCTGCCACCCTCATG  
CTGTACAACCCACCACCTATCAGATGGATGTCAACCCTGAAGGGAAGTACAGCTTTGGTGCCACCT  
GTGTGAAGAAGTGCCCCGAAACTACGTGGTGACAGATCATGGCTCATGTGTCCGAGCCTGTGGGCC  
TGACTACTACGAAGTGGAGAAGATGGCATCCGCAAGTGTAATAAATGTGATGGGCCCTGTGCGAAA  
GTTTGTAAATGGCATAGGCATTGGTGAATTTAAAGACACACTCTCCATAAATGCTACAAACATCAAAC  
ACTTCAAATACTGCACTGCCATCAGCGGGGACCTTCACATCCTGCCAGTGGCCTTTAAGGGGGATTCT  
TTTACGCGCACTCCTCCTCTAGACCCACGAGAAGTAGAAATTTCTAAAACCGTAAAGGAAATAACA  
GGCTTTTTTGCTGATTGAGCTTGGCCTGATAACTGGACTGACCTCCATGCTTTGAGAACCTAGAAA  
TAATACGTGGCAGAACAAGCAACATGGTCAGTTTTCTTTGGCGGTGCTTGGCCTGAACATCACATC  
ACTGGGGCTGCGTTCCCTCAAGGAGATCAGTGATGGGGATGTGATCATTTCTGGAAACCGAAATTTG  
TGCTACGCAAACACAATAAATCTGGAAAAACTCTTCGGGACACCCAATCAGAAAACCAAAATCATGA  
ACAACAGAGCTGAGAAAGACTGCAAGGCCGTGAACCACGCTGCAATCCTTTATGCTCCTCGGAAGG  
CTGCTGGGGCCCTGAGCCCAGGGACTGTGTCTCCTGCCAGAATGTGAGCAGAGGCAGGGAGTGCGTG  
GAGAAATGCAACATCCTGGAGGGGGAAACCAAGGGAGTTTGTGGAAAATTTGAATGCATCCAGTGCC  
ATCCAGAATGTCTGCCCCAGGCCATGAACATCACCTGTACAGGCAGGGGACCAGACAACCTGCATCCA  
GTGTGCCCACTACATTGATGGCCCACTGTGTCAAGACCTGCCAGCTGGCATCATGGGAGAGAAC

AACACTCTGGTCTGGAAGTATGCAGATGCCAATAATGTCTGCCACCTATGCCACGCCAACTGTACCT  
ATGGATGTGCTGGGCCAGGTCTTCAAGGATGTGAAGTGTGGCCATCTGGGTACGTTCAATGGCAGTG  
GATCTTAAAGACCTTTTGGATCTAAGACCAGAAGCCATCTCTGACTCCC

*Urgcp*

ATGGAAGGAGATGACTGCGGGTTCCATTATGGAGATGGTACAAACGAGGCTCAGGACAATGACTTCC  
CCACAGTGGAGAGAAGCAGGCTTCAGGAGATGCTGTCCCTGTTGGGACTGGAGACATAACCAGGCACA  
GAAGCTCACCCCTCCAGGACTCCCTGCAGATCAGTTTTGACAGCATGAAGAACTGGGCTCCTCAGGTT  
CCCAAGGACCTTCCCTGGCATTTCCTCAGGAAGCTGCAGGCACTCAACGCCGAAGCCAGGAACACCA  
CCATGGTGTGGACGTGCCCTCAGAGGCTGGCCTGCAGAGAAGGAGAGCCAGGCAGAGGAGGAGAT  
GATGTACTGGGACCCAGCGGAGGACGTGCTGCTGACATCTACTCTTCTCAGAGCTGCCCATGCCT  
GATACGCTGTGAACCCCTGGATCTTCTCTGCGCCCTCCTGCTGTCTTCAGACACCTTCTGTCAGC  
AGGAAGTCTGTGAAGATGTCCCTCTGTCAGTTTGCCTCCACTTGTGTTGCCCGATTCTGAAAA  
CCACTACCACACCTTCTGCTCTGGGCCCTGCGGGGTGTTGTGCGGACGTGGTGGTTCCAGCCCCTC  
CGGAGCCTGGGGAGTTTCCGAGAAGACAGTGTGGTCTCAGGGTGCCACGTTTTGCCTTCGTGC  
GCATGGATGTCAGCAGCAACTCCAAGTCCAGCTGCTCAATGCCGTCTCAGCCCAGCCGCGCCGCA  
GTGGGACTGCTTCTGGCATCGGGACCTCAATTTAGGCACTAATCCTCGCGAGATCTCGGATGGGTTA  
GTAGAGATCTCCTGGTTTTTCCCCAGTGGTAAGGAGGACCTGGATGTTTTCCCGGAGCCCATGGCCT  
TTCTGAACTTGAGAGGTGACATTGGGTCTCACTGGCTGCAGTTCAAGCTCTTGACAGAAGTCTCCTC  
TGCTGTGTTTATTTTTGACTGACAACATCAGCAAGAAGGAATACAACTGCTGTACTCCATGAAGGAG  
TCAACCACAAAGTACTACTTTCATCCTGAGTCCCTACCGAGGGAAACGGAACACGAACCTGCGCTTCC  
TCAACAGGCTGATCCAGTGTGGAAGATAGACCACTCTCACGTCTGGTGAAGGTGAGCAGCAGGA  
CAGCGAGGGCTTCGTGAGGCGCATCCGAGCCATCATGTGCAGTGTGGCTCGCTCTCCCTGCAGGAGG  
GTGTCTGTGGAGGACATGGCACACGCGGCACGTAAGCTCGGCCTCAGAGTTGATGAGGACTTTGAGG  
AGTGTGAGAAGGCAAAGGACCGGATGGAGAAAATCCTCAGGAAGATCAAGGATGTGGACGCCTACAA  
GAGAGACGAGCTGCGGCTGCAGGGCGAGCTGCGAGGAGGGCCGCCCCAAGCTGAAAGAGAGTTCTGC  
CAGCTCCAGTGGGTCCCGGAGCCCCAGAGAAGCACCGGGCCGAGCTGAGACGGCGCGTCTTGGAGC  
TCCGGGTGCAGCAGAATGGCCAGGAGCCCACCTCAGGGGTCCAGGAGTTCATCCTGGGAATAAGCAG  
CCCCTCCCTGTAG

*Dtx4*

CCGGAGGAAGCGCAGAAGGCCGGGCCCGGGAGGTGGGCAGCACCGCGCCGCAACCCCGGGCTCGCCA  
TGCTCCTGGCCTCGGCAGTGGTGGTGTGGGAATGGCTGAACGAACACGGCCGCTGGCGTCCCTACAG  
CCCAGCCGTGAGTACCACATCGAGGCGGTGGTGCAGCTGGTCCCCGCGCCGGGGGCGAGCGTGGTG  
TTGGGCCAGGTGGACAGCCGGCTCGCGCCCTACATCATCGACCTGCAGTCCATGAACCAGTTCGGCC  
AAGACACGGGGACCCCTCCGCCAGTTCGACGAACTACTATGACCCATCCTCAGCCCCTGGTAAGGG  
AGTCGTGTGGGAATGGGAGAATGACAATGGTTCCTGGACTCCCTATGACATGGAAGTCGGCATCACC  
ATCCAGTATGCCATATGAGAAGCAGCACCCATGGATCGACCTCACCTCCATTGGCTTCCAGTACATAA  
TAGACTTCAGCACCATGGGCCAGATCAACAGGCAGACCCAAACGCCAGCGCCGTGTGAGACGACGACT  
AGACCTCATCTACCCCATGGTACAGGGCACTATGCCAAAGACTCAGTCCCTGGCCAGTCAGTCCCTGGA  
CCGGCGACGTCCCTCCCTGCACCACCTTGCTCCTGTCCACAGTGTGTTTTGGTGTGAGCGTCAAGG  
CTGCTGTGGTCCATGGGGGCACTGGGCCTCAGCAGTACGAAAGAACATGGCCCTCTCTGGAGTGGG  
CAAGCTGCCCCAGCCACCTGGCCCTGGAGCAAAGCCACTAGACACCACTGGCACCATTGAGGCCCCA  
GGGAAGACAGCCCCATCGCAGGTTATCAGAAGACAAGTCTCTAATGCACCAGCTGGGGCGACTGTAG  
GCTCCCCTGCCAGCCCACAAGGAAGCAACAGGAAGACTGGAAGGGTGGCACTGGCCACTTTGAATCG  
GTCCAATCTGCAGCGACTGGCCATTGCCAGTCCCGGGTGTGATTGCCTCCGGGGTTCCTACTGTG  
CCTGTGAAAACTTGAATGGGTCCAGCCCTGTTAATCCTGCCTTGGCAGGAATCACCGGATACTCA  
TGAGTGCAGCGGATGCTGTGTGCCTCACTCGCCACCAAAGCTGGTCCCTCCACCCGCCCCCTGT  
CAGCAAGAGTGTGATAAAGTCCATCCAGGGGTCTCGAACACGAGCCGCAAGACCACCAAAAAGCAA  
GCCAAGAAAGGTAAAACCCAGAGGAAGTGCTAAAGAAGTACCTGCAGAAGGTCCGGCACCCACCAG  
AAGAGGATTGTACCATCTGTATGGAGCGTCTCACAGCCCCCTCTGGCTACAAAGGCCACAGCCTAC

AGTCAAGCCTGACCTGGTGGGAAAGCTGTCCAGGTGTGGCCACATCTACCACATCTACTGCCTGGTG  
GCTATGTACAACAATGGGAACAAGGATGGGAGTTTACAGTGCCCAACATGTAAGACCATTTATGGCG  
TCAAGACAGGCACCCAGCCTCCAGGGAAGATGGAATACCACCTCATCCCCACTCCTTGCCTGGCCA  
TCCGGACTGCAAGACCATCCGGATCATCTACAGTATCCCCCTGGCATTTCAGGGACCAGAGCATCCG  
AATCCTGGGAAGAGCTTCAGTGCCCGTGGCTTCCCACGACATTGTTACCTTCCAGACAGCGAGAAGG  
GGAGAAAAGTTCTGAAGCTGCTTCTAGTGGCCTGGGACC GCCGTCTCATCTTTGCCATTGGAACCTC  
CAGCACCACGGGCGAGTCCGATACTGTCATCTGGAATGAGGTTTACCACAAAACAGAATTTGGCTCT  
AATCTCACTGGCCATGGCTACCCAGATGCCAATTACCTGGATAACGTGCTGGCTGAACTGGCTGCC  
AGGGTATCTCTGAAGACAGCACTTCCCATGAAAAGGACTGAGGAGGGAGGGTACTGGGGACCACAGG  
GCAGAAAATGGAGAGAGTCAAGGTTGATGCCATGCCTCCTGACTCCCTCATGTCCC

**Ccm2**

ATGGAGGAGGAGGGCAAGAAGGGCAAGAAGCCTGGAATTGTGTGCCATTTAAACGAGTATTCCTAA  
AAGGTGAAAAGAGTAGAGATAAGAAAGCCCATGAGAAGGTGACAGAGAGGGCGCCCTCTGCACACTGT  
GGTGCTGGCGTTACCTGAGCGCGTTCGAGCCAGACAGACTGCTGAGCGACTATATTGAGAAGGAGGTG  
AAGTATTTAGGTTCAGTTAACATCCATTCCCGGCTACCTGAACCCTTCCAGTAGGACGGAAATCCTGC  
ATTTTCATAGACAAGGCAAGCGGTCCCACCAGCTTCTGGGCACCTGACTCAGGAGCACGATGCTGT  
GCTCAGTCTGTCTGCCTACAATGTCAAGTTGGCCTGGAGGGACGGGGAGGACATTATCCTCAGGGTG  
CCCATCCATGATATCGCTGCTGTCTCCTATGTCCGAGATGATGCTGCACACCTGGTGGTCTGAAGA  
CAGCCCAGGACCCAGGCATCTCTCCAGCCAGAGTCTGTGTGCAGAAAGTTCTAGAGGCCTCAGCGC  
AGGTTCCCTTGTGCAGAAAGTGCAGTGGGGCCAGTAGAGGCATGTTGCCTGGTTCATCATGGCCACAGAG  
AGCAAGGTGCGCGCTGAAGAGTTGTGCTCCCTGCTCAGCCAGGTCTTCCAGATTGTTTACACGGAGT  
CCACCATCGACTTTCTGGACCGAGCAATATTTGATGGGGCTTCCACACCTACCCACCACCTGTGCT  
GCACAGTACTGACTCTTCCACGAAAGTGGACATGAAGGACAGTTACGATGCTGACGCCAGCACCTTC  
TGCTTCCCGACTCTGGGGATGTGGGAGGCCTGCCGCCCTTACCCTTCTGCATGCAGACATCACCCC  
ATAGCAAGACTGTTCAGTGAGAGCGAGCTGAGCACCAGCGCCACGAACTGCTGCAGGACTACATGCT  
CACGTTACGTACGAAGCTGTCATCACAGGAGATCCAGCAGTTCGCAGCTCTGCTACATGAGTACCGC  
AATGGGGCCTCTATCCATGAGTTTTGCATCAGCCTGCCGAGCTCTATGGGGACAGCCGCAAGTTCC  
TGCTACTTGGTCTCAGACCCTTCATACCTGAGAAGGACAGTCAGCACTTGA AAACTTCTGGAGAC  
CATTGGCGTGAAAGACGGCCGTGGCATCATCACTGACAGCTTTGGTAGGCATCGTCGTGCCCTGAGT  
ACCACCTCCACATCCACCATCAATGGGAACAGGACCACAGGCAGCCCTGATGACCGCTCTGCGCCCT  
CAGAGGGGGATGAGTGGGACCGCATGATTTTCAGACATCAGTAGTGATATTGAAGCGCTAGGCTGCAG  
CATGGACCAGGACTCAGCGTGA

**Zmiz2**

ATGAACCCCATGAACCCCATGAACCCCGCCCTGCCCCCTGCACCACACGGTGATGGTTCATTTGCAT  
ATGAGTCTGTGCCCTTGGCAACAAAGTGCCACTCAGCCAGCTGGGTCACTGTCTGTGGTCACTACTGT  
GTGGGGAGTTGGCAACGCAACCCAGAGCCAGTGCCTGGGACAGCAGGCGTTTGTGAAGGAGGTGCT  
AGCAAGAGCTACGTACAGCAAGGCGTGTATGGCCGAGGGAGCTACCCTGGGGGATCCAGCTTCACTA  
CTGGGTATGCAGGAGGCCCTGCAGGCCTGGGGCTCCCCACACATGCAGCACGGCCCTCAACTGACTT  
CACACAAGCAGCAGCTGCAGCTGCCATGGCTGCTGCTGCAGCCACCGCGACAGCCACAGCCACAGCC  
ACGGTGGCTGCCCTGCAGGAGAAGCAGAGCCAGGAGCTAAGTCAGTATGGAGCGATGGGGACTGGGC  
AGTCTTTTAAACAGCCAGTTTCTGCAGCATGGAGGTCTCTGAGGACCCAGTGTGCCCCCTGGCATGAA  
CCCTTTCAGGCATGGGAGGAATGATGGGCCCTTCTGGCCTTTCTTCAATGGCCATGACTCCTACCCGG  
GCAGCAGGCATGACACCCTTATATGCAGGACAGCGACTGCCTCAGCATGGGTACCCTGGGCCTCCGC  
AGGGGCAGCCACTGCCTCGACAGGGGATCAAGAGAGCCTACTCAGAGGTGTATCCTGGGCAGCAGTA  
TCTGCAAGGAGGCCAGTATGCAGCCAACACTGCCCAGTATGCTCCTGGCCCTGGGCAGCCCCCTGGC  
CCTGCCTCCTCCTATGCAGGACACAGACTACCCCTGCAGCAGGGAATGGCCAGTCCCTGTCTGCGC  
CTGGCCCCACGGGACTGCATTACAAGCCACAGAGCAGTTCAACGGGCAGGGCGCCAGCTTCAACGG  
GGGCAGCATCAGCTACAGCCAGCCTGGCTTGAGTGGGCCTTCCCGCTCCATCCCTGGTTACCCACAGC  
TCCCCACTGCCGGGAATCCCACACCACCCATGACGCCTAGCAGCAATGTTCCCTACATGTCCCCAA

GCCAGGAAGTCAAGTCTCCTTTCCCTGCCTGACCTCAAGCCAGGCCTCAGCTCCTTGCACCCGTCACC  
CTCCGCAAGTGTCCATTGTGATGAGCTGCGCCTGACCTTCCCAGTTCGAGATGGGGTGGTCCCTGGAG  
CCCTTCCGCTGCAGCACAACCTGGCTGTGAGCAACCATGTCTTCCAGCTCCGAGATTCTGTCTATA  
AGACCCTGATGCTGAGGCCTGACCTGGAGCTGCAGTTTAAGTGCTATCACCATGAGGACCGGCAGAT  
GAACACCAACTGGCCAGCATCTGTGCAGGTGAGCGTCAATGCCACACCCCTCAGCATTGAGCGTGGA  
GACAACAAGACCTCGCACAAGCCCCTCTACCTGAAGCATGTGTGCCAGCCAGGTGCGAACACCATCC  
AGATCACTGTCACCGCTGCTGCTGTTCCACCTCTTCGTGCTGCAGCTGGTGCACCGTCCGTCTGT  
CCGTTCCGTGCTGCAGGGCCTCCTCAAGAAGCGCCTATTGCCAGCTGAACACTGCATCACCAAGATA  
AAGCGGAACTTCAGTAGCGGCACCATCCCTGGCACCCCTGGGCCAATGGAGAGGATGGGGTGGAGC  
AGACGGCTATCAAGGTGTCCCTGAAGTGCCCATCACCTTCCGCAGGATCCAGCTCCAGCCCGTGG  
TCACGACTGTGCACATATACAGTGCTTTGACCTGGAGTCATACTTACAGCTCAACTGTGAGCGGGGG  
ACCTGGAGGTGTCCGGTATGCAACAAGACGGCATTGCTGGAGGGCCTGGAGGTGGATCAGTATATGC  
TGGGCATCCTGATTTATATTCAGAACTCAGACTACGAGGAGATCACCATTGACCCACGTGCAGCTG  
GAAGCCAGTGCCTGTGAAGCCTGACCTACACATCAAGGAGGAGCCGGATGGGCCAGTGTGAAGCGC  
TGCCGCACTGTGAGCCCTGCCATGTGCTCATGCCAGTGTGATGGAGATGATTGCAGCCCTGGGCC  
CTGGCGCTGCCCCTTTTGGCCATTGCAGCCCCCTTCGGCCCCAACCCCAAGCGACTATCCCAGCCA  
GGGTTCCAACCTCATGGGGCCTGGAACCTTCCCAGAATCCTTCCCATCTGCTACACCCACCACCCCA  
AACCTTGCTGAGTTCACCCAGGGGCCACCCCAATCTCCTACCAGTCTGACATTCACAGCAGCCTCC  
TGACTCCAGACAAGTCTACTCCTTGCCCTCCAGGCCAGATGGCACACAGCAGGCCACCTGGACCCAGC  
CCATAATCCTGGACCACCAGGACTGCACACTCCCAACCTCGGGCCACCCCAAGGCACTCAGCTACAC  
CATCCAAACCCCTTCCCTGCATCCCGGCAGCCCTGGGCCAACCAAAACACAGGACCCATCAGCGAAC  
TGGCTTTCAATCCTGCCTCAGGCATGATGGGGCCTCCAGCATGACTGGGGCAGGGGAGGCCTCAGA  
ACCAGCTTTGGACCTGCTCCAGAAGTACCAATCCTGATGAACTGCTCTCCTACCTGGGCCACCT  
GACCTCCCCACAAACAGCAGTATGATCTGCTCTCACTCTTCGAGAACAACCTGA

**Xkr8**

TTGCTTGGAGAGGATCATGCCTCTGTCCGTGCACCACCATGTGGCCTTAGACGTGGTCTGAGGCCTG  
GTGAGTATCTTGTCTTTCCCTGCTGGATCTGGTGCCTGACCTGTGGGCCGTTGTCCAGTACGTGCTCC  
TTGGCCGTTATCTGTGGGCCGCGCTGGTACTGGTCTGCTGGGCCAAGCTTCGGTGTGCTGCAGCT  
CTTACAGCTGGCTCTGGCTGACAGCTGATCCACCGAGCTGCACCATTTCGAGCTCTCGCGTCTTTTC  
CTGGCTCTGCTGCACCTGCTGCAGCTCGGCTACCTGTATAGGTGTTTGCACGGAATGCATCAAGGGC  
TGTCATATGCTACCAGGAGATGCCATCCGAGTGTGACCTGGCCTACGCAGACTTTCTCTCCCTGGA  
CATCAGCATGCTGAAGCTTTTCGAGAGCTTCCCTGGAGGCGACGCCACAGCTCACACTGGTGTGGCA  
ATTGTATTGCAGAATGGCCAGGCGGAATACTACCAGTGGTTTGGCATCAGCTCATCCTTTCTTGGCA  
TCTCGTGGGCACCTGCTGGATTACCATCGGTCTCTGCGTACCTGTCTTCCCTCCAAGCCACGCCTGGG  
CCGGAGTTCTCTGCTATCTACTTCTGTGGAACCTGCTGCTGCTGGGGCCAGAATCTGTGCCATC  
GCCTTGTCTCAGCTGTCTTCCCCTACTATGTGGCCCTGCATTTCTTACAGCTGTGGCTGGTACTTT  
TGTTCTGGATCTGGCTTCAAGGCACAAATTTTATGCCTGACTCCAAAGGTGAGTGGCTGTACCGGGT  
GACAATGGCCCTCATCCTCTATTTCTCTGTTCAACGTGTCTGGGGGCCGCACTCGAGGCCGGGCC  
GTCATCCACCTGATCTTCATCTTCAAGTACAGTGTCTGCTGGTACCACCTCCTGGGTGACACACG  
GCACCTGGCTGCCCAGTGGGATCTCATTGCTGATGTGGGTGACAATAGGAGGAGCCTGCTTCTTCT  
GGGACTGGCTTTGCGTGTGATCTACTACCTCTGGCTGCACCCTAGCTGCAGCTGGGACCCTGACCTC  
GTGGATGGGACCCTAGGACTCCTTTCTCCCATCGTCTCCTAAGCTGATTTATAACAGGCGTGCCA  
CCCTGTTAGCAGAGAACTTCTTCGCCAAGGCCAAAGCTCGGGCTGTCTGACAGAGGAGGTGCAGCT  
GAATGGAGTCTCTGAGGCAGGGTCTGATTACGCCAGTGAAGATAATGCGAGTGGGGCCTTGCA  
AGGGACAAGGCGGGCCAGTCAATGTGCAAGCCATTTTTTTTTCTTCTGAAGCCGATGGAACCTGTGCA  
GCAAACACTCGGTTGTTGTTGTTCTCACCTCTCAGGTGATTGGTGGCGTCTGGCTCCTGGTTCCC  
TAGCCCCTCTAGATGACACAAGATTCTGGGAGAACTCTTCCCTACCCATCCCATCCATTCACTTC  
AACCAACAAATGCTAAAGGCACTTTATGTTCTGGGAACACCATCCTGGCTTCTGAACTGCCTGCCAC  
TCTAGCTTCTTTCCCTGCCACCTGGACAGATCCTGGGTAGACTCCTAAACAGTGAAGCCAGGTATG  
TCCCTCCAGTGTCTGATGCTCAGGCCACCTTTATAACCAAGTGCCTTATGGACCTGTGGTCTAGGCC

ATGTGATGCCAGTAAGTATTTTCATTCTCCTACCTCAGTCTATGTGGAAGAACATATATGCATGTG  
TTTAACAGTATTTAAAGCCTCATGAGATTCTCCAGACCAGTATGTACCACTAAGTGTAGTCTATCACC  
CTTTACAGACACGTAGAAGGCGCCTGGAACCCCTTAAAACTGACACAGACCCCTGGCATACAAATGT  
GGGCATAGGTTTACTTAATTTTGCTTCCCAAGACGCAGGGGCTAGTGAGCCCGAGCCGGTTGATCA  
TTCGGCTAGCAGAACTCATGGGCAGATGCTAGTGTATTCTTTTAGCAGCTCCGTAAGTACTGAGCCTAAAG  
AGGACTTGAGGATGGGGATGGCAGGTTTGAGGGGCTGGATGGAAGGTAAAGGATTGGGGTTCTTTT  
TGGGTGAGAGGTGCAGTGGCTTCTGGGATGTGGTCAATAGCTCCGTGGAGGTGGCGTGTCTGCTCT  
CGGAGGTTTGTGGTCTTGTGGGAAAAGGGAACAGGAGAGAGGCTCCAGGGGCAGAAGAAAAGGTTT  
CAGGTCCCAGTGTGGGACCCAGATAGTTCTAGCAGTCAATTCATTTATTTGTGTGGACGTGAAATAA  
CCTGTGACCCAAACAAGCACCAAGTACTGAAAGAAAACCAGATGGAGAGGTGAGAGGGAGGATGTAT  
GTTGTGGGTGGAAGTTGCAGCTTTATAAAAAACCATTGGGGAGGACCCCTCTGAGAACTGAGGCAT  
AGACTGTAAGCTACTTCAGCAGTACTGCAGCATGGAGTCTGCGTGGTTTGTGGAGAAGGAATCTG  
CGAATGCTGTTCCCTGTGGCACAGCAACCCACTGTAAGAGGACTGTGGGGTGCAGGTTGGCTCACAG  
CCAAGGAGGCTGCAGAGATGCAGGTGGGGGCTGGAAGAGGCTCTGGGAGAAGGTAATTTACTTATACT  
AAAAGGTACAGGCTGACTATGGACAGAAAGGACCTAATTTCCAGACCTGAATTTTACAGACCAGGAA  
AAGGAGCCAAAGTGGTTGTGATGTTAAAAGGGTCTGAAAAACAGTACCACCTCCGTGTTCACTCT  
CATGGAAAAACGGATGTAATCACACCAGAAGGTGTATCCTCTAAACAGATGCCCCACAGGTACAC  
ACCTGAAATCACTGTTACTCTCATTATGAAAATGGTAAGATAGGGATGAGCCAGTGTGACACACCT  
ACCAGTCTGGGCAAGGACATCAGGAGTTCAGACTCCTCAGTACAATGTCAGAGGCCAGCTTGGGCT  
ACATGAGACCCTGTCTCCAACAAAATGAAATTAATTTATTTATTTATTTATTTATTTGGCTTTTTGAGACG  
GGTTTTCTCTGTGTAGCCCTGGCTGTCTGGAACACTACTCTGTAGACCAGGCTATCCTCAAACCTCAG  
AAATCTGCCTGCCTCTGCCTCCCAAGTGTGGGATTAAGGCATGCGCCACCACGCCTGGCACATTT  
TTTTTTTTAAATTAAGAAAAGAAAGACGTTACTACCCTGCTCTTGTTTTGTGACACACAATCTGGTCT  
GAGAGGACCCTGAGCACATCTTCCCTTCCCTCAACACTACCGTGTAAAGTTCTTAAATCTGGGACTT  
AAAACCAGGTTAGTGACATTACCCGTAGTTAGGATGTTTGGTTTGTGGGGATTGGTTCTAATGCTC  
TGTCTTAATTCGGCTCCAGAAATCACACGGGAATCTGCTCTGCTAAAGGAAGCCTGTCACTAGTTGG  
CTGTGATTGGGAATAAAGTTGCCAGGGCTGGCTGGGCAGGAAAGAGGCGGGACTTTTAGGTTGTG  
AGGGCAAGGAACCCCGGGGAGTTGGAAGCAGAGGGATTTACTGCGCAGTTGGGTCTGGGGCAGCAG  
AGATGAAATGATGACTTAGCAAGTCTGACTCAGGGAGGTTAGGGGGGTAGAATGTATGCTAGTCGCAC  
GGAGGGTTAGACACGTCCAGCCACTGAGCTAGTCAGAGCATATCAAAGTTAGATGGTGTGTCTCT  
CATTACAAAATCCCGGGAACACTTGGCCAGCCGGGAGTCAAGGCTTAAAGCACTACAGGGTTTGGAA  
ACCAGCCAACACTAGAATCTGCACTTGTGACTGAGCAGGGGTACGGACAACAGCTAACAGTCTACTT  
GAGCTGCACTGCGGCTCAGAAGATCACTTCCCGGAGAAAATTCACCTTGGAGTCCGACATATCTCAC  
CTTTGGAAGCTAGAAAACAACCTTCTAATTTCCCTTCACTGGAACAATGGGTAAAAGCCCTCTTGTAA  
CTAGTGGGGGCCAATCAGACCAAATGTGGCAGAATGTAGAACACCTGGTTGGTGGGACGGGAAGTCA  
GGATTTATTTGGTTGCGGCTTAATTAATGCTCAGCACAGACTGACTCCTCCTTGGTAACGTTTCAGCA  
CACTCGACAGCTCTGAAATCCATTCCATTTCTATACCTTAAAAAGCAGTGTATTTTAGAAACAATTC  
AAATAAACATTTCTCTCGCAAAAAAAAAAAAAAAAAA

**Ggct**

ATGGCGAGCTCCGACTGTGAGGGCCATGCGGGCCAGGAGGGGAGACATTCCTGTACTTCGCCTACG  
GCAGCAATCTCCTGACCGAGAGGATCCACCTGCGAAACCCCTCGGCCGTGTTCTGCTGCGTGGCGTG  
CCTGCAGGACTTTAAGCTCGACTTCGGCAATTTCCAAGGCAAATGAGTGAGAGGTGGCACGGAGGT  
ATAGCTACCATTTTTCAAAGTCCCTGGCGACGAAGTGTGGGGAGTGGTATGGAGAATGAACAAAAGCA  
ATATAAGTTCCCTGGATGAGCAAGAAGGAGTTAAAAGTGGAGTCTATGTTGTAATAGAAATTAAGT  
TTCAACTCGAGAAGGGAAGGAATAACCTGCCGAAGTTACCTGATGACGAACACTACGAGAGCGCGCCC  
CCATCACACAGTATAAGAAGGTTATCTGCATGGGTGCGAAAGAAAACGTTTTGCCACAGGAATATC  
AAGAGAAATTAAGCAATAGAACCAAATGAGTATAAAGGAAAGATCTCCGACGAAATGGAAGACAT  
CATCAAAAAGGGAGAGTCAAACTGTCAATAACAGACTCTGAAGCTATGTGTGCTAGTATGAAGTGT  
TTTAACGTTTGCGAACAGGAGTCTGGACCTTCTTGG



**Appendix B: Candidate gene analysis for QTL on Chromosome 4.** Listed for each of the 55 genes are the number of: coding variants (STOP gained/lost, frameshift, inframe insertions/deletions, initiator codon, splice acceptor/donor/region, and missense); regulatory variants (within 1 kb putative promoter, 3' untranslated region, 5' untranslated region, upstream, downstream, and introns); likelihood of missense mutation being damaging to function if present; presence of significant *cis*-eQTL when mapping variation in gene expression across RI strains; and known expression within A/J and B6/J mice from the AXB/BXA dataset in GeneNetwork. Hyphens denote unavailable information. Boxes highlighted in green indicate information of interest, and the corresponding gene to be investigated.

Chromosome 4 QTL															
Gene	Genetic Variants													Expression	
	Coding						Regulatory						Damaging Missense	<i>cis</i> -eQTL	Adult Expression (GeneNetwork)
	Stop G/L	Frameshift	Inframe I/D	Initiator	Splice A/D/R	Missense	Promoter (1 kb)	3' UTR	5' UTR	Upstream	Downstream	Intron			
<i>Epb4.1</i>	0	0	0	0	0	0	0	0	0	0	1	1	-	No	-
<i>Snhg12</i>	0	0	0	0	0	0	0	0	0	0	0	0	-	No	-
<i>Oprd1</i>	0	0	0	0	0	0	0	0	0	0	0	1	-	No	-
<i>Ythdf2</i>	0	0	0	0	0	0	0	0	0	1	0	1	-	No	Yes
<i>Gmeb1</i>	0	0	0	0	0	0	0	0	0	0	1	0	-	No	No?
<i>Taf12</i>	0	0	0	0	0	0	0	0	0	0	1	0	-	No	Yes
<i>Rab42</i>	0	0	0	0	0	0	0	0	0	1	0	0	-	No	-
<i>Trspap1</i>	0	0	0	0	0	0	0	0	0	0	0	0	-	No	-
<i>Rcc1</i>	0	0	0	0	0	0	0	0	0	2	0	0	-	No	-
<i>Phactr4</i>	0	0	0	0	0	0	0	1	0	1	1	0	-	No	Yes
<i>4930451E06Rik</i>	0	0	0	0	0	0	-	0	0	0	0	0	-	No	-
<i>Med18</i>	0	0	0	0	0	0	1	2	0	5	5	0	-	No	Yes?
<i>Sesn2</i>	0	0	0	0	0	0	0	0	0	1	3	0	-	No	No?
<i>Alpl1</i>	0	0	0	0	0	0	1	0	0	2	8	2	-	No	Yes
<i>Dnajc8</i>	0	0	0	0	0	0	1	1	0	7	12	12	-	No	Yes?
<i>Ptafr</i>	0	0	0	0	0	1	0	14	0	5	31	30	No	No	Yes
<i>Eya3</i>	0	0	0	0	0	0	11	1	2	112	52	194	-	No	Yes
<i>5830409B07Rik</i>	0	0	0	0	0	0	-	0	0	0	0	0	-	No	-
<i>Xkr8</i>	0	0	0	0	0	0	1	8	0	7	2	14	-	Yes	Yes
<i>Smpd13b</i>	0	0	0	0	0	1	0	0	0	0	8	58	No	No	Yes
<i>Rpa2</i>	0	0	0	0	0	0	1	0	0	2	0	1	-	No	Yes
<i>BC013712</i>	0	0	0	0	0	0	0	0	0	0	0	0	-	No	-
<i>Ppp1r8</i>	0	0	0	0	0	0	1	2	0	14	35	16	-	No	Yes
<i>Six12</i>	0	0	0	0	0	0	9	2	1	32	21	89	-	No	Yes
<i>C530007A02Rik</i>	0	0	0	0	0	0	-	0	0	0	0	0	-	No	-
<i>Fam76a</i>	0	0	0	0	0	0	1	10	0	24	41	130	-	No	Yes
<i>Fgr</i>	0	0	0	0	0	0	0	0	1	45	1	23	-	No	No
<i>Ahd1</i>	0	0	1	0	0	1	1	10	2	25	124	143	No	No	Yes
<i>Wasf2</i>	0	0	0	0	0	0	6	21	2	122	180	836	-	No	Yes
<i>Gpr3</i>	0	0	0	0	0	0	6	6	6	40	87	8	-	No	Yes?
<i>Cd16412</i>	0	0	0	0	1	0	3	2	2	74	54	77	-	No	No
<i>Map3k6</i>	0	0	0	0	4	6	24	1	4	173	105	99	No	Yes	Yes
<i>Syn1</i>	0	0	1	0	2	6	6	1	0	30	0	131	No	No	Yes
<i>Tmem222</i>	0	0	0	0	0	0	11	1	1	107	68	102	-	No	Yes
<i>Wdpc1</i>	0	0	0	0	3	0	2	16	2	174	212	732	-	No	No
<i>NHE1 (Slc9a1)</i>	0	0	0	0	0	0	2	16	0	0	0	214	-	No	Yes
<i>1700091J24Rik</i>	0	0	0	0	0	0	-	0	0	0	0	0	-	No	-
<i>Fam46b</i>	0	0	0	0	1	3	5	5	0	37	38	35	Yes	No	-
<i>Trnp1</i>	0	0	0	0	0	0	16	8	1	53	9	47	-	No	Yes
<i>Kdfl</i>	0	0	0	0	0	1	30	2	2	137	71	156	No	No	Yes
<i>Nudc</i>	0	0	0	0	0	0	19	2	0	163	14	192	-	No	Yes
<i>Nr0b2</i>	0	0	0	0	0	0	10	0	0	88	54	8	-	No	No
<i>Gpatch3</i>	0	0	1	0	2	5	13	5	0	112	65	133	-	No	No
<i>Gpn2</i>	0	0	0	0	1	0	14	8	2	73	147	81	Yes	No	-
<i>Sfn</i>	0	0	0	0	0	0	3	3	0	22	22	0	-	No	No?
<i>Zdhhc18</i>	0	0	0	0	0	0	11	22	0	167	200	568	-	No	Yes?
<i>4930429E23Rik</i>	0	0	0	0	0	0	-	0	0	0	0	0	-	No	-
<i>Pigv</i>	0	0	0	0	0	0	14	13	0	22	78	95	-	No	No
<i>1700041L08Rik</i>	0	0	0	0	0	0	-	0	0	0	0	0	-	No	-
<i>Arid1a</i>	0	0	2	0	1	0	6	0	5	87	57	368	-	No	No?
<i>Aim11</i>	0	0	0	0	0	0	7	0	0	0	0	0	-	No	-
<i>Rps6ka1</i>	0	0	0	0	2	0	7	10	7	146	200	360	-	No	Yes
<i>Hmgcn2</i>	0	0	0	0	1	0	8	3	4	43	70	19	-	Yes	Yes
<i>Dhdds</i>	0	0	0	0	1	0	16	7	3	157	109	284	-	Yes	Yes
<i>Lin28a</i>	0	0	0	0	0	0	5	14	2	90	95	145	-	No	No



**Appendix C: Candidate gene analysis for QTL on Chromosome 6.** Listed for each of the 70 genes are the number of: coding variants (STOP gained/lost, frameshift, inframe insertions/deletions, initiator codon, splice acceptor/donor/region, and missense); regulatory variants (within 1 kb putative promoter, 3' untranslated region, 5' untranslated region, upstream, downstream, and introns); likelihood of missense mutation being damaging to function if present; presence of significant *cis*-eQTL when mapping variation in gene expression across RI strains; and known expression within A/J and B6/J mice from the AXB/BXA dataset in GeneNetwork. Hyphens denote unavailable information. Boxes highlighted in green indicate information of interest, and the corresponding gene to be investigated.

Chromosome 6 QTL															
Gene	Genetic Variants													Expression	
	Coding						Regulatory						Damaging Missense	<i>cis</i> -eQTL	Adult Expression (GeneNetwork)
	Stop G/L	Frameshift	Inframe I/D	Initiator	Splice A/D/R	Missense	Promoter (1 kb)	3' UTR	5' UTR	Upstream	Downstream	Intron			
<i>Hoxa1</i>	0	0	1	0	0	0	0	0	0	2	3	0	-	No	-
<i>Hoxa2</i>	0	0	0	0	0	0	2	1	0	0	2	0	-	No	No
<i>Hoxas2</i>	0	0	0	0	0	0	2	0	0	0	0	0	-	No	No
<i>Hoxa3</i>	0	0	0	0	0	0	0	1	0	12	4	5	-	No	-
5730596B20Rik	0	0	0	0	0	0	1	0	0	5	8	0	-	No	No
<i>Hoxa4</i>	0	0	0	0	0	1	3	1	7	5	8	0	Yes	No	No
<i>Hoxas3</i>	0	0	0	0	0	0	1	0	0	0	0	0	-	No	No
<i>Hoxa5</i>	0	0	0	0	0	0	0	0	0	1	1	0	-	No	-
<i>Hoxa6</i>	0	0	0	0	0	0	0	0	0	0	2	0	-	No	No
<i>Hoxa7</i>	0	0	0	0	0	0	0	0	0	0	0	0	-	No	-
<i>Hoxa9</i>	0	0	0	0	0	0	0	0	0	1	0	2	-	No	-
9930038K12Rik	0	0	0	0	0	0	-	0	0	3	0	0	-	No	No
<i>Hoxa10</i>	0	0	0	0	0	0	0	0	0	2	2	3	-	No	-
<i>Hoxa11</i>	0	0	0	0	0	0	1	0	0	0	2	0	-	No	No
<i>Hoxa11os</i>	0	0	0	0	0	0	1	0	0	0	0	0	-	No	No
9530018H14Rik	0	0	0	0	0	0	-	0	0	0	0	0	-	No	-
<i>Hoxa13</i>	0	2	0	0	2	2	0	0	4	1	0	5	No	No	-
<i>Evx1os</i>	0	0	0	0	0	0	0	0	1	0	0	0	-	No	No?
<i>Evx1</i>	0	0	0	0	0	0	0	0	0	0	1	0	-	No	-
1700094M24Rik	0	0	0	0	0	0	0	0	0	0	0	0	-	No	Yes
<i>Hibadh</i>	0	0	0	0	0	0	0	0	0	0	1	18	-	No	-
<i>Tax1bp1</i>	0	0	0	0	0	0	0	0	0	4	8	15	-	No	Yes
<i>Jazf1</i>	0	0	0	0	0	0	0	0	0	1	0	48	-	No	Yes
<i>Gm4872</i>	0	0	0	0	0	0	2	0	0	0	0	0	-	No	Yes?
<i>Creb5</i>	0	0	0	0	0	1	2	4	0	18	6	451	No	Yes	-
<i>Tril</i>	0	0	0	0	0	0	0	1	0	1	2	0	-	No	Yes?
<i>Gm16499</i>	0	0	0	0	0	0	0	0	0	2	1	0	-	No	Yes
<i>Cpvl</i>	0	0	0	0	0	0	0	0	0	42	1	47	-	No	-
4921529L05Rik	0	0	0	0	0	0	2	0	0	0	0	0	-	No	No
4930590G02Rik	0	0	0	0	0	0	-	0	0	0	0	0	-	No	-
9530036M11Rik	0	0	0	0	0	0	7	0	0	30	18	0	-	No	-
<i>Chn2</i>	0	0	0	0	0	2	0	3	0	82	95	940	No	No	-
9030405F24Rik	0	0	0	0	0	0	-	0	0	0	0	0	-	No	No
<i>Prr15</i>	0	0	0	0	0	0	11	0	6	72	59	0	-	No	-
9130019P16Rik	0	0	0	0	1	0	0	0	0	3	15	840	-	No	Yes
<i>Wipf3</i>	0	0	0	0	0	0	0	0	1	2	2	17	-	No	No
<i>Scrn1</i>	0	0	0	0	0	0	1	1	2	76	69	268	-	No	Yes
<i>Fkbp14</i>	0	0	0	0	0	0	0	0	0	14	1	4	-	No	Yes
<i>Plekha8</i>	0	0	0	0	0	0	0	0	1	0	4	19	-	No	Yes
<i>Mtorn</i>	0	0	0	0	0	0	8	8	0	0	0	56	-	No	Yes
2610209C05Rik	0	0	0	0	0	0	-	0	0	0	0	0	-	No	Yes
<i>Zmf2</i>	0	0	0	0	0	0	0	1	0	1	0	9	-	No	-
<i>Nod1</i>	0	0	0	0	0	0	10	0	1	20	2	69	-	No	Yes
<i>Ggct</i>	0	0	0	0	0	1	5	52	0	17	26	16	Yes	Yes	Yes
<i>Gars</i>	0	0	0	0	0	1	0	0	0	4	9	120	No	No	Yes
<i>Ctshr2</i>	0	0	0	0	0	1	0	3	8	16	25	34	No	No	Yes
<i>Inmt</i>	0	0	0	0	0	0	24	1	0	75	60	53	-	Yes	Yes?
<i>Fam188b</i>	0	0	0	0	0	1	3	1	1	22	3	387	Yes	No	Yes
<i>Aqp1</i>	0	0	0	0	0	0	0	1	0	2	5	3	-	No	No
<i>Ghrhr</i>	0	0	0	0	1	0	7	0	0	29	10	55	-	No	Yes
6430584L05	0	0	0	0	0	0	2	0	0	0	0	0	-	No	No
<i>Adcyap1r1</i>	0	0	0	0	0	0	6	11	2	42	51	101	-	No	-
<i>Neurod6</i>	0	0	0	0	0	0	0	0	0	0	0	0	-	No	No
<i>Ccdc129</i>	0	0	0	0	0	0	0	0	0	1	0	3	-	No	-
<i>Gsbs</i>	0	0	0	0	0	0	0	0	0	0	0	0	-	No	Yes
<i>Pde1c</i>	0	0	0	0	0	0	0	0	0	1	1	11	-	No	-
<i>Lsm5</i>	0	0	0	0	0	0	0	0	0	0	0	0	-	No	Yes?
4933427C19Rik	0	0	0	0	0	0	-	0	0	0	0	0	-	No	-
<i>Avl9</i>	0	0	0	0	0	0	0	0	0	0	0	0	-	No	-

Chromosome 6 QTL continued

Gene	Genetic Variants												Expression		
	Coding						Regulatory						Damaging Missense	cis-eQTL	Adult Expression (GeneNetwork)
	Stop G/L	Frameshift	Inframe I/D	Initiator	Splice A/D/R	Missense	Promoter (1 kb)	3' UTR	5' UTR	Upstream	Downstream	Intron			
<i>3110035G12Rik</i>	0	0	0	0	0	0	-	0	0	0	0	0	-	No	-
<i>Kbtbd2</i>	0	0	0	0	0	0	0	0	0	0	0	0	-	No	-
<i>Fkbp9</i>	0	0	0	0	0	0	0	0	0	0	0	0	-	No	-
<i>Ni5c3</i>	0	0	0	0	0	0	0	0	0	0	0	0	-	No	-
<i>Vmn1r4</i>	0	0	0	0	0	0	0	0	0	0	0	3	-	No	-
<i>Vmn1r5</i>	0	0	0	0	0	0	0	0	0	0	0	0	-	No	-
<i>Vmn1r6</i>	0	0	0	0	0	0	0	0	0	0	0	0	-	No	-
<i>Vmn1r8</i>	0	0	0	0	0	0	0	0	0	0	0	0	-	No	-
<i>Vmn1r9</i>	0	0	0	0	0	0	0	0	0	0	0	0	-	No	-
<i>Vmn1r10</i>	0	0	0	0	0	0	0	0	0	1	0	0	-	No	-
<i>Vmn1r11</i>	0	0	0	0	0	0	0	0	0	0	0	0	-	No	No

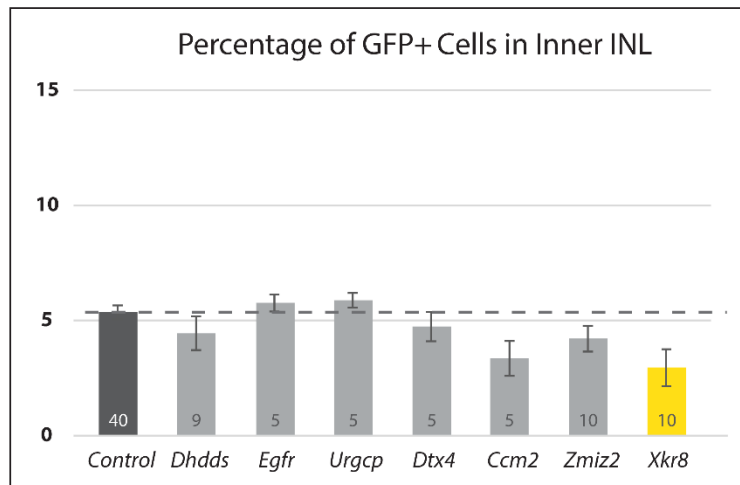
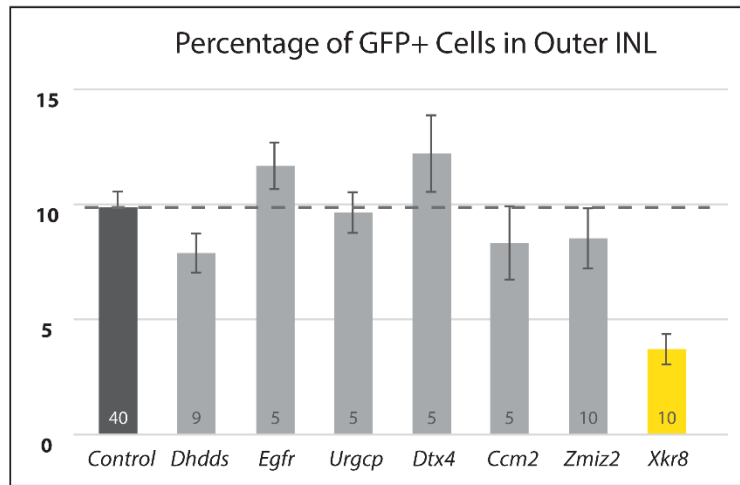
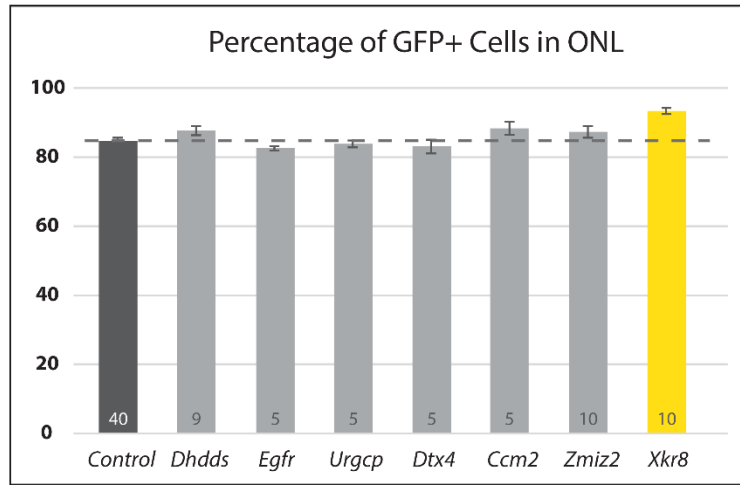
**Appendix D: Candidate gene analysis for QTL on Chromosome 8.** Listed for each of the 96 genes are the number of: coding variants (STOP gained/lost, frameshift, inframe insertions/deletions, initiator codon, splice acceptor/donor/region, and missense); regulatory variants (within 1 kb putative promoter, 3' untranslated region, 5' untranslated region, upstream, downstream, and introns); likelihood of missense mutation being damaging to function if present; presence of significant *cis*-eQTL when mapping variation in gene expression across RI strains; and known expression within A/J and B6/J mice from the AXB/BXA dataset in GeneNetwork. Hyphens denote unavailable information. Boxes highlighted in green indicate information of interest, and the corresponding gene to be investigated.

Chromosome 8 QTL															
Gene	Genetic Variants													Expression	
	Coding						Regulatory						Damaging Missense	<i>cis</i> -eQTL	Adult Expression (GeneNetwork)
	Stop G/L	Frameshift	Inframe I/D	Initiator	Splice A/D/R	Missense	Promoter (1 kb)	3' UTR	5' UTR	Upstream	Downstream	Intron			
<i>Gm2716</i>	0	0	0	0	0	0	12	0	0	0	0	0	-	No	-
<i>Tmem188</i>	0	0	0	0	2	0	12	19	0	55	37	145	-	No	Yes?
<i>Heatr</i>	0	0	0	0	0	1	9	15	4	158	93	269	No	No	-
<i>9430002A10Rik</i>	0	1	0	0	0	3	-	0	0	46	116	0	No	No	No
<i>Adcy7</i>	0	0	0	0	2	0	16	0	5	254	0	290	-	No	No?
<i>Brd7</i>	0	0	0	0	0	0	0	0	0	0	0	0	-	No	Yes
<i>Nkd1</i>	0	0	0	0	0	0	0	0	0	0	0	1	-	No	Yes
<i>Papd5</i>	0	0	0	0	0	0	11	3	2	102	86	481	-	No	No
<i>Snx20</i>	0	0	0	0	0	0	0	0	0	0	0	0	-	No	No
<i>Nod2</i>	0	0	0	0	0	0	0	0	0	0	1	1	-	No	No
<i>Cyld</i>	0	0	0	0	0	0	0	0	0	0	0	0	-	No	Yes?
<i>Sall1</i>	0	0	0	0	0	0	0	0	0	0	0	0	-	No	Yes
<i>Rps6-ps2</i>	0	0	0	0	0	0	0	0	0	0	0	0	-	No	-
<i>Tox3</i>	0	0	0	0	0	0	1	0	0	0	0	1	-	No	Yes
<i>4930405E02Rik</i>	0	0	0	0	0	0	-	0	0	0	0	0	-	No	-
<i>Chd9</i>	0	0	0	0	0	0	0	0	0	0	0	13	-	No	Yes
<i>EG626231</i>	0	0	0	0	0	0	-	0	0	0	0	0	-	No	-
<i>Rbl2</i>	0	0	0	0	0	0	0	0	0	0	0	0	-	No	No
<i>Aktip</i>	0	0	0	0	0	0	0	0	0	0	1	1	-	No	Yes
<i>Rpgrip11</i>	0	0	0	0	0	0	0	0	0	0	0	1	-	No	-
<i>Fto</i>	0	0	0	0	0	1	0	0	0	0	5	11	No	No	Yes?
<i>B130011D17Rik</i>	0	0	0	0	0	0	-	0	0	0	0	0	-	No	-
<i>4831440D22Rik</i>	0	0	0	0	0	0	0	0	0	0	0	0	-	No	-
<i>Irx3</i>	0	0	0	0	0	0	0	0	0	0	4	0	-	No	Yes
<i>Irx3os</i>	0	0	0	0	0	0	0	0	0	0	0	0	-	No	No
<i>Crnde</i>	0	0	0	0	0	0	0	0	0	0	3	2	-	No	Yes
<i>Irx5</i>	0	0	0	0	0	0	0	0	0	0	0	0	-	No	Yes
<i>Irx6</i>	0	0	0	0	0	0	0	0	0	0	0	0	-	No	Yes
<i>Mmp2</i>	0	0	0	0	4	0	7	3	1	24	33	315	-	No	Yes
<i>Lpcat2</i>	0	0	0	0	1	5	7	13	0	82	160	978	Yes	Yes	Yes
<i>Capns2</i>	0	0	0	0	0	1	0	0	2	82	42	4	Yes	No	Yes
<i>Slc6a2</i>	0	0	0	0	2	0	7	44	3	66	58	492	-	No	No
<i>Ces1a</i>	0	0	0	0	3	6	3	3	0	72	70	411	No	No	-
<i>Ces1b</i>	0	1	0	0	8	11	29	0	2	29	23	426	-	No	-
<i>Ces1c</i>	0	0	0	0	1	13	19	6	0	192	166	484	-	No	-
<i>Ces1d</i>	0	0	0	0	0	0	0	0	0	0	0	1	-	No	-
<i>Ces1e</i>	0	0	0	0	0	0	0	0	0	0	0	0	-	No	-
<i>Ces1f</i>	0	0	0	0	0	0	0	0	0	1	0	1	-	No	-
<i>Ces1g</i>	0	0	0	0	0	0	0	0	0	0	0	1	-	No	-
<i>Ces3a</i>	0	0	0	0	0	0	0	0	0	0	0	2	-	No	-
<i>Gnao1</i>	0	0	0	0	0	0	0	1	0	0	0	7	-	No	Yes?
<i>4930488L21Rik</i>	0	0	0	0	0	0	0	0	0	0	0	0	-	No	-
<i>Amfr</i>	0	0	0	0	0	0	0	0	0	0	1	0	-	No	Yes?
<i>Nudt21</i>	0	0	0	0	0	0	0	0	0	0	0	0	-	No	Yes
<i>Ogfd1</i>	0	0	0	0	0	0	0	0	0	0	0	1	-	No	Yes
<i>Bbs2</i>	0	0	0	0	0	0	0	0	0	0	1	0	-	No	Yes
<i>Mt4</i>	0	0	0	0	0	0	0	0	0	0	0	0	-	No	Yes
<i>Mt3</i>	0	0	0	0	0	0	0	0	0	0	0	0	-	No	Yes
<i>Mt2</i>	0	0	0	0	0	0	0	0	0	0	0	0	-	No	Yes
<i>Nup93</i>	0	0	0	0	0	0	0	0	0	0	0	1	-	No	Yes?
<i>Slc12a3</i>	0	0	0	0	0	0	0	0	0	0	1	1	-	Yes	Yes?
<i>Herpud1</i>	0	0	0	0	0	0	0	0	0	9	21	17	-	No	Yes
<i>9330175E14Rik</i>	0	0	0	0	0	0	1	0	0	0	0	0	-	No	No
<i>Nrlc5</i>	0	0	0	0	2	10	1	3	0	10	0	181	Yes	No	-
<i>Tmem28</i>	0	0	0	0	0	0	2	0	0	0	0	0	-	No	No
<i>Cpne2</i>	0	0	0	0	0	0	1	0	0	1	11	28	-	No	Yes
<i>Fam192a</i>	0	0	0	0	0	0	0	0	1	1		7	-	No	-
<i>Rspry1</i>	0	0	0	0	0	0	3	0	0	4	4	13	-	No	Yes
<i>Arl2bp</i>	0	0	0	0	0	0	0	0	0	3	0	1	-	Yes	Yes

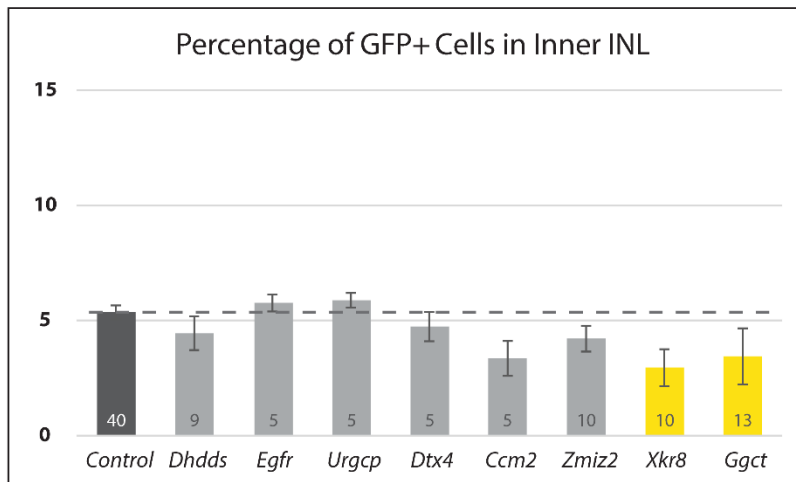
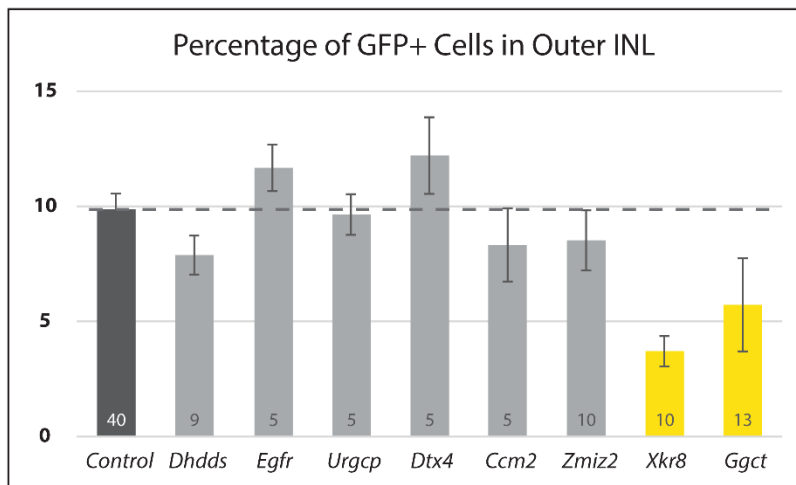
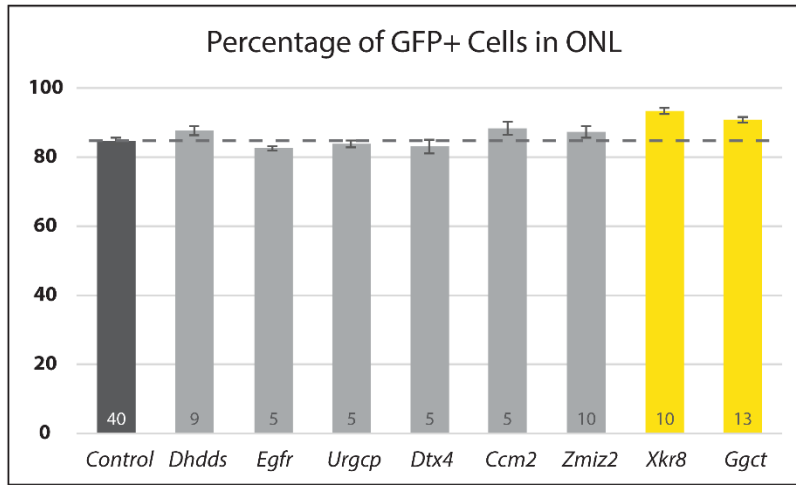
Chromosome 8 QTL continued

Gene	Genetic Variants													Expression	
	Coding						Regulatory						Damaging Missense	<i>cis</i> -eQTL	Adult Expression (GeneNetwork)
	Stop G/L	Frameshift	Inframe I/D	Initiator	Splice A/D/R	Missense	Promoter (1 kb)	3' UTR	5' UTR	Upstream	Down- stream	Intron			
<i>Pllp</i>	0	0	0	0	0	0	0	0	0	0	0	3	-	No	Yes
<i>Ccl22</i>	0	0	0	0	0	0	0	0	0	1	1	0	-	No	No?
<i>Cx3cl1</i>	0	0	0	0	0	0	0	2	0	8	28	12	-	No	Yes?
<i>1700121C10Rik</i>	0	0	0	0	0	0	-	0	0	0	0	0	-	No	-
<i>Ccl17</i>	0	0	0	0	0	0	2	1	0	17	9	2	-	No	Yes
<i>Ciapin1</i>	0	0	0	0	2	0	16	14	8	209	87	139	-	No	Yes
<i>Coq9</i>	0	0	0	0	2	0	13	8	0	162	157	246	-	No	Yes
<i>Polr2c</i>	0	0	0	0	0	0	5	0	0	34	6	0	-	No	No
<i>Dok4</i>	0	0	0	0	0	0	3	1	1	22	6	18	-	No	Yes
<i>Ccdc102a</i>	0	0	0	0	0	0	3	0	0	40	30	26	-	No	Yes?
<i>Gpr114</i>	0	0	0	0	0	1	11	10	0	39	48	138	Yes	No	No
<i>NSMUSG0000007</i>	0	0	0	0	0	0	-	0	0	0	0	0	-	No	-
<i>Gm10286</i>	0	0	0	0	0	0	-	0	0	7	7	0	-	No	-
<i>Gpr56</i>	0	0	0	0	0	2	2	13	3	76	38	254	No	No	No
<i>Gpr97</i>	0	0	0	0	1	4	12	9	0	48	34	258	No	No	No
<i>Ccdc135</i>	0	0	0	0	1	0	4	4	0	19	15	41	-	No	Yes
<i>Katmb1</i>	0	0	0	0	0	0	1	2	0	31	7	26	-	No	Yes?
<i>Kifc3</i>	0	0	0	0	0	3	9	1	3	53	2	81	No	Yes	Yes
<i>Cngb1</i>	0	0	0	0	2	2	16	0	1	0	0	0	No	No	Yes
<i>Cngb1</i>	0	0	15	0	3	1	16	1	1	0	0	202	-	No	Yes
<i>Tepp</i>	0	0	0	0	0	0	3	0	2	44	85	100	-	No	-
<i>Zfp319</i>	0	0	0	0	0	0	4	0	0	4	20	0	-	No	No
<i>Usb1</i>	0	0	0	0	1	1	2	2	2	55	67	79	No	No	-
<i>Mmp15</i>	0	0	0	0	0	0	8	4	0	30	19	52	-	Yes	Yes
<i>Gtl3</i>	0	0	0	0	0	0	0	0	0	3	0	8	-	No	Yes
<i>Csnk2a2</i>	0	0	0	0	0	0	0	4	0	1	15	95	-	No	Yes
<i>4933406B17Rik</i>	0	0	0	0	0	0	2	0	0	0	0	0	-	No	No
<i>Ccdc113</i>	0	0	0	0	0	0	1	0	0	5	48	46	-	No	Yes
<i>1700112L15Rik</i>	0	0	0	0	0	0	-	0	0	0	0	0	-	No	-
<i>Prss54</i>	0	0	0	0	0	1	2	0	0	30	10	204	Yes	No	-
<i>Gims3</i>	0	0	0	0	0	0	1	0	0	7	1	3	-	No	Yes
<i>Ndrg4</i>	0	0	0	0	0	0	2	2	2	60	16	91	-	No	Yes
<i>Seid6</i>	0	0	0	0	0	0	1	0	0	17	13	8	-	No	Yes?
<i>Cnot1</i>	0	0	0	0	1	0	0	2	0	0	12	41	-	No	No?
<i>4930513N10Rik</i>	0	0	0	0	0	0	2	0	0	1	1	2	-	No	No
<i>Slc38a7</i>	0	0	0	0	0	0	0	1	0	1	4	1	-	No	Yes
<i>Got2</i>	0	0	0	0	0	0	0	1	0	0	3	8	-	No	Yes

**Appendix E.** *Xkr8* electroporation results compared to all electroporated genes and control plasmids.



**Appendix F.** *Ggct* electroporation results compared to all electroporated genes and control plasmids.



**Appendix G.** The *Ggct* promoter sequences for A/J and B6/J mice strains differ by 478 base pairs, due to an insertion into the A/J strain (highlighted in yellow). All sequences are listed 5' to 3', with the transcriptional start site located at +1.

### A/J Promoter Sequence

( -1890 ) GAACTCACAGAGAACTGCCTGCCTCTGCCTCTCGAGTGATGGTATTTAAAGGTGC  
AGTCCACAATGCCAGCTTCATGTTGCTTTCTGACTGTGTCAGGATAGTCTTCTTTTATTG  
GTGACCAGATTGACTGGCTATCAGGTGAGAGAGGTCAGGTTTCCCAAATAATCATGGTCTT  
CCTGTCCAATGACTAGCAGTGAGCCTTGGGGGATAACTGAGACTCTATAAACATCCCTGTG  
ACCTGATGCTCCTGACGGGAAGTTTGGTTGCACCGGAGACAGATGTTCTAATCCCAGTACC  
CCCATTTCTGCATTTAGCCAGTATACCTCTGTTGCGCGCGCTCAACTAGCCAGGAAGAAC  
GATGCTGCAACAGGATCCTTCTGCACACGTTTATTCAGTCCTGTTTCTTCTTTCTCTATAT  
CTCCCTTGTTTATATCTCCCTTGTTTATATCTCCCTTGTTTATATATCTCCCTTGTTTATA  
TATCTCCCTTGTTTTTATATCTCCCTTGTTTTTATATCTCCCTTGTTTTTATATCTCCCC  
GAACCCTGGGCCTCTCACTCTTTTATACTCTCAGTTCCCATCCACGCACAGAAGGCCACGC  
TACCTCACCAGGCACGCAGCTTCAGCTAATCAGGGCAGCAGGGGCATATCTCCATCAAAAT  
GGATTCACCAGTATCCTGGTACACCTGCGCAGCACTCAAGATGTTTGTGTCTTATATGAGG  
AAGTCAGGTGCAAGTCATATGACTTAGCTGCAGTCCCTGGCGCCTTTGGGACTGCCGCCAC  
ACCCGCTCCCCACATACCTTTTTTTAAAAAAGCAAAGAATTGCTTCCTCATCAGCTATTTG  
GTTTTCAAAAATACAGTTGGTACTAGAAAGGCAGAACACTCATTCTTAAATACCCACTT  
TTTTAAAAGTGATGAAGTGTTAGCCACTGATGGCATGGCAATATGGTTCTCTTCTCTGTTTT  
AATTTGGTTTACTTCCTGAAGGGAATGACATACATTTAGGGATCATTTTAGAGTTTCCAGT  
CGTTCTGCTCCTAAGTTGTTCTCCCTTTGTCTAGTGAATGGTCTTTTAGGAATGACCTTG  
TTCATCTTGGGGTTCTCATTTTCTGGATTATTGTTCTTTCAAGAGGTATTTTCACTCCCAG  
CTTTGACCTAAGATTCAGTCATTTCTCCAGGAATCCTGGCACCTGTCAGTGTGGAGTTGAA  
TTTAGATTAATTTCTGAGGGCCAACGGCAGTCATTGCTCTAGACCTTCAGTTTGCTCTCCT  
ATCTTCATTTCAAGAGCAACAACATGGGTGTTTTGTGTCTGTTCTATTTTTAAAAAGAGGAAA  
TAGATTGCAACGATGAACAGAGTCAACTGGCTAGCAAATGGCATGTCCGGATCTGAACGTG  
GGAGAAAGACTACCCTGGTATGCAGTGAGGCAACTTCAGGTAGTGATCCTAAGAAAACCTTG  
TAGGATCAGCCTTCCCATTCAGGAAGGCTGAGGCAGGAGAACTGCCGCAAGATCCAGGCT  
AGGCCGACAGCAATTTGAGACTTGTCTCCTCTATAACCAGGCGCAGAGCCTACCGCACCCT  
GGTTGACCTGGGCAATCGCCACCAGGTGGGGAAAACACAGTCGCCAGTAGCCACTCTCGGG  
CTGTCCGTTAGACTCGCCAATCAGCGGCGCCTCAGGCAGGGGGCCGTACATCCGAGGGATG  
CATCCAATAGAAAAGCGACGCCAGTGGGCGGGAGGAGCTGTAGACAGGCAATCCTGGTAG  
TTAGCTCACGCCGGCAAGCCGGCAGCCAATCCTCAGCGCGCTCTCTGTGCGGCTCCGCCCG  
CCGCTCTGCACTACCGCGTGGGTGGCGGCGCACTGCTCTTTTTAGCAGCGCTAGTCCGGCT  
TCTCTG (-1)

### B6/J Promoter Sequence

( -1413 ) GAACTCACAGAGAACTGCCTGCCTCTGCCTCTCGAGTGATGGTATTTAAAGGTGC  
AGTCCACAATGCCAGCTTCATGTTGCTTTCTGACTGTGTCAGGATAGTCTTCTTTTATTG  
GTGACCAGATTGACTGGCTATCAGGTGAGAGAGGTCAGGTTTCCCAAATAATCATGGTCTT  
CCTGTCCAATGACTAGCAGTGAGCCTTGGGGGATAACTGAGACTCTATAAACATCCCTGTG  
ACCTGATGCTCCTGACGGGAAGTTTGGTTGCACCGAGAGACAGATGTTCTAATCCCAGTACC  
CCCATTTCTGCATTTAGCCAGTATACTTTTTTTTTAAAAAAGCAAAGAATTGCTTCCTCAT  
CAGCTATTTGTTTTTCAAAAATACAGTTGGTACTAGAAAGGCAGAACACTCATTCTTAA

ATACCCACTTTTTAAAAGTGATGAAGTGTTAGCCACTGATGGCATGGCAATATGGTTCTCT  
TCTCTGTTTTAATTTGGTTTACTTCCTGAAGGGAATGACATACATTTAGGGATCATTTTAG  
AGTTTCCAGTCGTTCTGCTCCTTAAGTTGTTCTCGCTTTGTCTAGTGAATGGTCTTTTAGG  
AATGACCTTGTTTCATCTTGGGGTTCTCATTTTCTGGATTATTGTTCTTTCAAGAGGTAATT  
TTCACTCCCAGCTTTGACCTAAGATTCAGTCATTTCTCCAGGAATTCTGGCACCTGTCAGT  
GTGGAGTTGAATTTAGATTAATTTCTGAGGGCCAACGGCAGTCATTGCTCTAGACCTTCAG  
TTTGCTCTCCTATCTTCATTTCAAGAGCAACAACATGGGTGTTTTGTGTCGTTCTATTTTA  
AAAAGAGGAAATAGATTGCAACGATGAACAGAGTCAACTGGCTAGCAAATGGCATGTCCGG  
ATCTGAACGTGGGAGAAAGACTACCCTGGTATGCAGTGAGGCAACTTCAGGTAGTGATCCT  
AAGAAAACCTTGTTAGGATCAGCCTTCCCATTCCAGGAAGGCTGAGGCAGGAGAAGTCCCGCA  
AGATCCAGGCTAGGCCGACAGCAATTTGAGACTTGTCTCCTCTATAACCAGGCGCAGAGCCT  
ACCGCACCACTGGTTGACCTGGGCAATCGCCGCCAGGTGGGGAAAACACAGTCGCCAGTAG  
CCACTCTCGGGCTGTCCGTTAGACTCGCCAATCAGCGGCCTCAGGCAGGGGGCCGTACA  
TCCGAGGGATGCATCCAATAGAAAAGCGACGTCAGTGGGCGGGAGGAGCTGTAGACAGGCC  
AATCCTGGTAGTTAGCTCACGCCGGCAAGCCGGCAGCCAATCCTCAGCGCGCTCTCTGTGC  
GGCTCCGCCCGCGCTCTGCACTACCGCGTGGGTGGCGGCCTGCTCTTTTTTAGCAGCG  
CTAGTCCGGCTTCTCTG (-1)